

Electronic Thesis and Dissertation Repository

10-24-2022 2:00 PM

Insight into the Stereochemistry and Mechanism of σ -Addition to Disilenes

Zahra M. Sharif, *The University of Western Ontario*

Supervisor: Baines, Kim M., *The University of Western Ontario*

A thesis submitted in partial fulfillment of the requirements for the Master of Science degree in Chemistry

© Zahra M. Sharif 2022

Follow this and additional works at: <https://ir.lib.uwo.ca/etd>

Recommended Citation

Sharif, Zahra M., "Insight into the Stereochemistry and Mechanism of σ -Addition to Disilenes" (2022). *Electronic Thesis and Dissertation Repository*. 9020. <https://ir.lib.uwo.ca/etd/9020>

This Dissertation/Thesis is brought to you for free and open access by Scholarship@Western. It has been accepted for inclusion in Electronic Thesis and Dissertation Repository by an authorized administrator of Scholarship@Western. For more information, please contact wlsadmin@uwo.ca.

Abstract

The stereochemistry of the addition of HX (X = OH, NH₂, Cl, Br, I) to the stereoisomers of 1,2-di-*tert*-butyl-1,2-bis(2,4,6-triisopropylphenyl)disilene (**3E** or **3Z**) was found to be 100 % stereospecific resulting in the *syn*-isomer, except for HCl which resulted in the *anti*-isomer. Kinetic studies on the reaction of tetramesityldisilene (**I**) with *isopropyl* amine (*i*PrNH₂) revealed that the order in both amine and disilene was 1, indicating that the proton is transferred in the rate determining step with KIE of 3.06, and that the addition is nucleophilic. Computational studies of the mechanism revealed nucleophilic addition gives the *anti*-oriented donor adduct which is independent of the substituents on the disilene. Inversion or rotation in the *anti*-donor adduct relies on the twist of the disilene. Depending on the substituents on the disilene, the rate-determining step might be inversion or proton transfer. The hydrolysis of the synthesized adducts occurs with inversion of stereochemistry.

Keywords: Disilene, σ -addition, Stereochemistry, *Syn*-oriented donor adduct, *Anti*-oriented donor adduct, Mechanistic studies, Computational studies, Inversion, Rotation, Stereospecific.

Summary for Lay Audience

Silicon, with 27.7 % abundance, is the second most abundant element on earth after oxygen and thus, it is of interest to investigate applications of silicon-based chemicals. Just like alkenes, molecules with a carbon-carbon double bond (C=C), disilenes, with a silicon-silicon double bond (Si=Si), can be synthesized. These species have been shown to be capable of reacting with and activating important small molecules such as water and ammonia. However, the understanding of the mechanism of these disilene reactions is shallow, although such an understanding is critical for the development of applications of disilene chemistry. Thus, in this work, the spatial characteristics of the addition of HX (X = OH, NH₂, Cl, Br, I) to 1,2-di-*tert*-butyl-1,2-bis(2,4,6-triisopropylphenyl)disilene (**3E** or **3Z**), were investigated. The results of these studies will be used along with mechanistic studies and computational studies, done in collaboration, to refine the understanding of the mechanisms of these fundamental reactions.

The experimental studies of the addition of HX to **3E** or **3Z** revealed that the reactions formed a single and unique product for each disilene. The reaction conditions, such as solvent, concentration of reagent, and temperature, had no influence on the outcome of the reaction. The ability to generate exclusively one product in HX additions is very advantageous. Thus, understanding the factors affecting the mechanism will allow for control of the reactivity of disilenes in future applications.

Co-Authorship Statement

Zahra Mohamad Sharif performed all synthetic experiments and the characterization work. The data were checked by Dr. Kim M. Baines.

The mechanistic studies in **Chapter 3** were performed with the guidance of Dr. Sarah L. McOnie.

The computational studies presented in **Chapter 3** were performed in collaboration with Gül Altınbaş Özpınar and Thomas Müller from Carl von Ossietzky Universität Oldenburg.

Acknowledgements

I would like to thank almighty Allah for all his blessings and this opportunity he gave me. I would like to thank all the individuals who were part of making this thesis project possible. First, I would like to thank my supervisor, Dr. Kim M. Baines, for all her guidance and support in the past few years. Dr. Kim brought the best out of me as an undergraduate and a graduate student. She guided and supported me to grow as an individual and a researcher. Thank you for your patience with me throughout the research, for being a great mentor during all the times, and a great support during the difficult times. It is an honor and a pleasure to be a part of the Baines group. Moreover, thank you to all the group members, the graduate students, Andrew T. Henry and undergraduate students Taylor Cosby and Dana Nanan for being joyful and providing me with the support, advice, and care at all times. Special thanks to Dr. Sarah McOnie, she was the best guide, support, and joy to have as a young researcher. Thank you for sharing those moments with the INOVA 600 MHz spectrometer and the Babaz dinners, you were my best mentor and older sister.

I would like to thank the Chemistry Department at The University of Western Ontario for providing us with this opportunity. Special thanks to Haidy Metwally and Aruni Chathu Pulukkody for running my ESI-MS samples. Thanks to Robert Harbottle, Benjamin Bridge, and Dr. Chris Levy for allowing me to use the equipment in the undergraduate labs. Special thanks to Paul Boyle for obtaining single crystal X-ray diffraction data and my crystal structures. Thank you to Mathew Willans, NMR facility manager, for answering my calls every time I needed help. Finally, thank you to Gül Altınbaş Özpınar and Thomas Müller from Carl von Ossietzky Universität Oldenburg for conducting the computational studies, it was great to collaborate internationally.

Special thanks to my dear best friend Mansha Nayyar, whom I consider a family and partner in crime, for being the support, guide, care and love during all the hard times and the late hours. Thank you to Jeffery Kai Yu Li and Haley Marier for pulling the late nights with me editing this work. Thank you to all of you for celebrating every step in my journey and be the best motivational spirits. Thank you to Nils Hermann Vogeler for being helpful and generous with materials I needed. Finally, I would love to thank my lovely family for being the warm arms that pushed me forward with love and kindness. Thank you to all of you for always being there at my lowest and best times. This journey would not have been possible without your love, guidance, and support.

Table of Contents

Abstract.....	ii
Summary for Lay Audience.....	iii
Co-Authorship Statement.....	iv
Acknowledgements.....	v
Table of Contents.....	vi
List of Tables.....	x
List of Figures.....	xi
List of Schemes.....	xii
List of Appendices Figures.....	xv
List of Appendices Tables.....	xvii
List of Abbreviations.....	xviii
Chapter 1.....	1
1 Introduction.....	1
1.1 Overview of Main Group Disilene Chemistry.....	1
1.1.1 Structure and Bonding in Disilenes.....	2
1.2 Reactivity of Disilenes.....	5
1.2.1 The σ -Addition in Disilenes:.....	5
1.2.2 Addition Reactions of ROH to Disilenes.....	8
1.2.3 Addition Reactions of NH ₃ to Disilenes.....	13
1.2.4 Addition Reactions of HX (X = F, Cl, Br) to Disilenes.....	18
1.3 Research Scope of the Thesis.....	20
1.4 References.....	21
Chapter 2.....	23

2	The Stereochemistry of the Addition Reactions of HX (X = OH, NH ₂ , Cl, Br, I) to Disilenes.....	23
2.1	The Addition Reactions of HX (X = NH ₂ , OH, Cl, Br, I) to 1,2-di- <i>tert</i> -butyl-1,2-bis(2,4,6-triisopropylphenyl)disilene (3Z or 3E).....	23
2.1.1	Addition Reactions of H ₂ O to <i>Z</i> or <i>E</i> -1,2-di- <i>tert</i> -butyl-1,2-bis(2,4,6-triisopropylphenyl)disilene (3Z or 3E).....	25
2.1.2	Addition Reactions of NH ₃ <i>Z</i> or <i>E</i> -1,2-di- <i>tert</i> -butyl-1,2-bis(2,4,6-triisopropylphenyl)disilene (3Z or 3E).....	27
2.1.3	Addition Reactions of HX (X = Cl, Br, I) to <i>Z</i> or <i>E</i> -1,2-di- <i>tert</i> -butyl-1,2-bis(2,4,6-triisopropylphenyl)disilene (3Z or 3E).....	30
2.2	Influence of Reaction Conditions on the Stereochemistry of the Reaction.....	33
2.3	Discussion and Conclusion of Addition of HX (X = NH ₂ , OH, Cl, Br, I) to 3E or 3Z	35
2.4	Substitution of X at Si-X in Tetrahedral Silicon Compounds.....	37
2.4.1	Nucleophilic Substitution of X at Si-X.....	37
2.4.2	Hydrolysis of Disilanes 20-27	40
2.4.3	Discussion.....	41
2.5	Experimental Details.....	42
2.5.1	General Considerations.....	42
2.5.2	Water Addition to 3Z or 3E	43
2.5.3	Ammonia Addition to 3Z or 3E	46
2.5.4	Addition of HX (X = Cl, Br, I) to 3Z or 3E	47
2.6	Experimental for The Substitution Reactions.....	52
2.7	References.....	53
	Chapter 3.....	55
3	Mechanistic Study of the Addition of Amines to Disilene.....	55
3.1	Insight into Mechanistic Studies of Nucleophilic Addition to Disilenes.....	55

3.1.1 Literature Review of the Mechanism of the Addition of Ammonia to Disilenes.....	56
3.2 Results and Discussion	59
3.2.1 VTNA of the Addition of $i\text{PrNH}_2$ to Tetramesityldisilene 1	59
3.2.2 KIE Study of the Addition of $i\text{PrN(H/D)}_2$ to Tetramesityldisilene 1	63
3.2.3 Computational Studies of the Addition of Ammonia to <i>E</i> -1,2-di- <i>tert</i> -butyl-1,2-bis(2,4,6-triisopropylphenyl)disilene 3E	65
3.2.4 Discussion of the Mechanism and Stereochemistry in the Addition of Ammonia and Amines to Disilenes	70
3.3 Experimental Details.....	71
3.3.1 Synthesis of $i\text{PrND}_2$	72
3.3.2 VTNA Experiments	72
3.3.3 KIE Experiment	73
3.3.4 Computational Methodology	73
3.4 References.....	74
Chapter 4.....	76
4 Summary, Conclusion and Future Work.....	76
4.1 Summary.....	76
4.2 Conclusion	78
4.3 Future Work.....	79
4.4 References.....	82
5 Appendices.....	83
5.1 Appendix A: Supplementary Material for Chapter 2.....	83
5.1.1 NMR Spectra Data for Compounds 18-27	83
5.2 Appendix A: ATR-IR Data for Chapter 2.....	102
5.3 Appendix A: Single Crystal X-ray Diffraction Data for Chapter 2	107

5.4 Appendix B: Supplementary Material for Chapter 3	115
Curriculum Vitae	116

List of Tables

Table 1.1: The structural parameters for compounds <i>1</i> , <i>3E</i> , <i>6E</i> and <i>9Z</i>	3
Table 1.2: Addition of H ₂ O, MeOH and EtOH to disilene <i>6E</i> in C ₆ D ₆ vs THF at rt.....	8
Table 1.3: Addition of EtOH and <i>i</i> PrOH to <i>11E</i>	9
Table 2.1: Important bond length and angles for <i>21</i> in comparison to <i>10B</i>	29
Table 2.2: Relevant ¹ H and ²⁹ Si Chemical shifts for compounds <i>22-27</i>	31
Table 2.3: Selected bond lengths and angles for compounds <i>23</i> , <i>25</i> , and <i>27</i>	31
Table 2.4: Pauling electronegativity and pK _a in water.....	42

List of Figures

- Figure 1.1:** Structural parameters for disilenes, distance (d), fold angle (θ) and twist angle (τ). 2
- Figure 1.2:** Qualitative MO model showing the formation of the *trans*-bent geometry at the silicon center in comparison to alkene. 4
- Figure 1.3:** Orbital mixing between the σ and π^* MOs resulting in *trans*-bending in disilenes. 5
- Figure 1.4:** Proposed initial interactions between water and H₂Si=SiH₂ (**14**) leading to the formation of a) nucleophilic reactant complex, C_N, or b) electrophilic reactant complex, C_E. 12
- Figure 2.1:** Molecular structure of **18**, Si-H not detected. Hydrogen atoms are omitted for clarity. Selected parameters (bond lengths in Å; bond angles in °): Si1-O1 1.7442(15), Si1-Si1¹ 2.4015(12), Si1¹-H1Si1 1.4210; O1-Si1-C1 105.92(7), O1-Si1-Si1¹ 104.32(6), H1Si1-Si1¹-C1 105.9. 26
- Figure 2.2:** Molecular structure of **21**. Hydrogen atoms are omitted for clarity. Selected parameters (bond lengths in Å; bond angles in °) are given in **Table 2.1**. 28
- Figure 2.3:** Molecular structure of a) **23**, b) **25**, and c) **27**. Hydrogen atoms are omitted for clarity. Selected parameters (bond lengths in Å; bond angles in °) are given in **Table 2.3**. 32
- Figure 3.1:** Plot of product [**2M**] versus $\Sigma[{}^i\text{PrNH}_2,]^\beta \Delta t$ when a) $\beta = 1$, b) $\beta = 2$, c) $\beta = 3$ for two concentrations of *i*PrNH₂. (Concentrations in M; average of two runs). 61
- Figure 3.2:** Plot of product [**2M**] versus $\Sigma[\text{Disilene } I]^\beta \Delta t$ when a) $\beta = 1$, b) $\beta = 2$, c) $\beta = 3$ for two concentrations of *I*. (Concentrations in M; average of two runs). 62
- Figure 3.3:** Relative free energies (in kcal/mol, at 298 K and 1 atm) with NH₃ monomer or dimer (NH₂-NH₂) given in parenthesis. Computational level used is M06-2X/6-311+G(d,p). Path A (green), Path B (red), Path C (blue). 68
- Figure 3.4:** The energy profile for the rotation about Si1-Si2 bond in **Inta 20** computed with the M06-2X/6-311+G(d,p) level. Hydrogens are omitted for clarity. 69
- Figure 3.5:** Average cone angle in for (Mes = 2,4,6-methylbenzene) substituent in disilene **1** and (Tip = 2,4,6-*isopropyl*benzene) **3E** in degrees.⁴ 70

List of Schemes

Scheme 1.1: Classic reactions of disilenes.	5
Scheme 1.2: Addition of XY molecules to disilene a) 1 , b) 3Z or 3E , c) 6Z or 6E , d) 9Z .	7
Scheme 1.3: Addition of the <i>t</i> PrOH to 3E .	8
Scheme 1.4: Pathways for the addition of alcohol to disilene 11E : a) <i>syn</i> -isomer via intramolecular transfer or b) <i>anti</i> -isomer via intermolecular transfer of the proton. R= alkyl.	10
Scheme 1.5: Addition of <i>p</i> -CH ₃ OC ₆ H ₄ OH (ArOH) to 6E in benzene or tetrahydrofuran.	10
Scheme 1.6: Mechanisms proposed for the addition of <i>p</i> -CH ₃ OC ₆ H ₄ OH to 6E .	11
Scheme 1.7: Possible pathways for the addition of water to H ₂ Si=SiH ₂ to give the <i>anti/syn</i> -isomer. The thermodynamic data of stationary points ($\Delta G^{298\text{ K}}$ in kcal/mol) was calculated using the CBS-Q method.	13
Scheme 1.8: The addition of ammonia to 9Z . The transition state $\Delta G^{298\text{ K}}$ in kcal/mol.	14
Scheme 1.9: Addition of ammonia and amines to 1 .	15
Scheme 1.10: Potential reaction pathways for the addition of NH ₃ to 1 . The relative free energies (in kcal/mol, at 298 K and 1 atm) of the species involved.	16
Scheme 1.11: Mechanistic pathway of the addition of ammonia to tetramesityldisilene 1 ($\Delta G^{298\text{ K}}$ in kcal/mol at 1 atm).	17
Scheme 1.12: Addition of HCl to disilene 6E in THF at rt via electrophilic pathway. ^a	18
Scheme 1.13: Addition of HCl and HBr to disilene 16E .	19
Scheme 1.14: Computational studies of the addition of HX to parent disilene via formation of the electrophilic complex. The thermodynamic data of stationary points ($\Delta G^{298\text{ K}}$ in kcal/mol) were calculated using the complete basis set (CBS-Q) method.	19
Scheme 2.1: Synthesis of disilene 3Z and 3E .	23
Scheme 2.2: Addition of HX (X = NH ₂ , OH, Cl, Br, I) to 3Z or 3E .	24
Scheme 2.3: Addition of water to 3Z or 3E .	25
Scheme 2.4: Addition of water to a) 3Z and b) 3E giving <i>syn</i> -isomers, 18 and 19 .	27

Scheme 2.5: Addition of ammonia to 3Z or 3E	27
Scheme 2.6: Addition of ammonia to a) 3Z and b) 3E given <i>syn</i> -products 20 and 21 .29	
Scheme 2.7: Addition of HX (X = Cl, Br, I) to 3Z or 3E	30
Scheme 2.8: Addition of HX to 3Z and 3E and the stereochemical outcome.....	33
Scheme 2.9: Reaction conditions investigated in the addition of H ₂ O and NH ₃ to 3Z and 3E	34
Scheme 2.10: Reaction conditions investigated in addition of HI and HBr to 3Z or 3E .34	
Scheme 2.11: Addition of concentrated aqueous or gaseous HCl to 3Z or 3E	35
Scheme 2.12: Addition of HX (X = OH, NH ₂ , Cl, Br, I) to 3Z and 3E	35
Scheme 2.13: Mechanism of nucleophilic substitution at silicon by; a) attack of the Nu axial to LG, b) axial attack of the Nu to a substituent then pseudorotation (Ψ), c) equatorial attack of the Nu to the LG. ¹¹ Retention or inversion of configuration is noted for each mechanism.....	38
Scheme 2.14: The addition of tritium methanol (*) to <i>x</i> -C ₁₀ H ₇ MePhSiOMe in methanol (inversion) or pentane (retention). ¹³	39
Scheme 2.15: Substitution at Si-X (X = Cl or Br) with water by S _N 2-Si.....	39
Scheme 2.16: Hydrolysis reactions of Si-X in disilanes a) 23 , b) 25 and 27 via inversion.	40
Scheme 2.17: Acid-catalyzed hydrolysis of aminodisilane 21	41
Scheme 2.18: General proposed mechanism for hydrolysis of SiX in bulky disilane including a pentacoordinate intermediate.	41
Scheme 3.1: General mechanism of electrophilic addition HX to alkenes.	55
Scheme 3.2: Addition of NH ₃ to imino(silyl)disilene 9Z ; to give disilylamine 10 . Path I) with dimer, Path II) with monomeric ammonia.	56
Scheme 3.3: Addition of NH ₃ as Path 4A) a monomer or Path 4B) a dimer to 1 . The relative free energies are in (kcal/mol in benzene, at 298 K and 1 atm). ⁵	58
Scheme 3.4: Addition reaction of ^{<i>i</i>} PrNH ₂ to 1	60
Scheme 3.5: KIE experiment of the addition of ^{<i>i</i>} PrNH ₂ or ^{<i>i</i>} PrND ₂ to 1	63
Scheme 3.6: Proposed mechanism of the addition ^{<i>i</i>} PrNH ₂ to 1	65

Scheme 3.7: The addition of NH ₃ to 3E giving the <i>syn</i> -isomer 2I	65
Scheme 3.8: Proposed paths of the addition of NH ₃ monomer and/or dimer to disilene 3E	67
Scheme 4.1: Addition of HX (X = OH, NH ₂ , Cl, Br, I) to 3Z or 3E	77
Scheme 4.2: The energetically favored pathway for the addition of ammonia or dimer to disilene 3E	78
Scheme 4.3: Synthesis of disilene 6E and 6Z	80
Scheme 4.4: Synthesis of disilene 30E and 30Z . ⁶	81
Scheme 4.5: Synthesis of digermene 31E and 31Z	81

List of Appendices Figures

- AA Figure 1** ^1H NMR spectrum (400 MHz, $\text{C}_6\text{D}_5\text{H}$) of $\text{X} = \text{OH}$, **18** from **3Z**. The signal denoted by * is trace water. Upfield signals in the spectrum are attributed to trace impurities from the synthesis of **18**. 83
- AA Figure 2** $^{13}\text{C}\{^1\text{H}\}$ NMR spectrum (100 MHz, C_6D_6) of $\text{X} = \text{OH}$, **18**. The signal denoted with * is the solvent C_6D_6 84
- AA Figure 3** ^1H - ^{29}Si gHMBC spectrum (C_6D_6) of $\text{X} = \text{OH}$, **18**. 84
- AA Figure 4** ^1H NMR spectrum (400 MHz, $\text{C}_6\text{D}_5\text{H}$) of $\text{X} = \text{OH}$, **19** from **3E**. The signal denoted by * is trace water. Upfield signals in the spectrum are attributed to trace impurities from the synthesis of **19**. 85
- AA Figure 5** $^{13}\text{C}\{^1\text{H}\}$ NMR spectrum (100 MHz, C_6D_6) of $\text{X} = \text{OH}$, **19** from **3E**. The signal denoted with * is the solvent C_6D_6 86
- AA Figure 6** ^1H - ^{29}Si gHMBC spectrum (C_6D_6) of $\text{X} = \text{OH}$, **19** from **3E**. 86
- AA Figure 7** ^1H NMR spectrum (400 MHz, $\text{C}_6\text{D}_5\text{H}$) of $\text{X} = \text{NH}_2$, **20** from **3Z**. The signal denoted by * is trace water. Upfield signals in the spectrum are attributed to trace impurities from the synthesis of **20**. 87
- AA Figure 8** $^{13}\text{C}\{^1\text{H}\}$ NMR spectrum (100 MHz, C_6D_6) of $\text{X} = \text{NH}_2$, **20** from **3Z**. The signal denoted with * is the solvent C_6D_6 87
- AA Figure 9** ^1H - ^{29}Si gHMBC spectrum (C_6D_6) of $\text{X} = \text{NH}_2$, **20** from **3Z**. 88
- AA Figure 10** ^1H NMR spectrum (400 MHz, $\text{C}_6\text{D}_5\text{H}$) of $\text{X} = \text{NH}_2$, **21** from **3E**. The signal denoted by * is trace water. Upfield signals in the spectrum are attributed to trace impurities from the synthesis of **21**. 89
- AA Figure 11** $^{13}\text{C}\{^1\text{H}\}$ NMR spectrum (100 MHz, C_6D_6) of $\text{X} = \text{NH}_2$, **21** from **3E**. The signal denoted with * is the solvent C_6D_6 89
- AA Figure 12** ^1H - ^{29}Si gHMBC spectrum (C_6D_6) of $\text{X} = \text{NH}_2$, **21** from **3E**. 90
- AA Figure 13** ^1H NMR spectrum (400 MHz, $\text{C}_6\text{D}_5\text{H}$) of $\text{X} = \text{Cl}$, **22** from **3Z**. The signal denoted by * is trace water. Upfield signals in the spectrum are attributed to trace impurities from the synthesis of **22**. 91
- AA Figure 14** $^{13}\text{C}\{^1\text{H}\}$ NMR spectrum (100 MHz, C_6D_6) of $\text{X} = \text{Cl}$, **22** from **3Z**. The signal denoted with * is the solvent C_6D_6 91
- AA Figure 15** ^1H - ^{29}Si gHMBC spectrum (C_6D_6) of $\text{X} = \text{Cl}$, **22** from **3Z**. The signal denoted with * is traces of **23** from **3E**. 92

AA Figure 16 ^1H NMR spectrum (400 MHz, $\text{C}_6\text{D}_5\text{H}$) of X = Cl, 23 from 3E . The signal denoted by * is trace water. Upfield signals in the spectrum are attributed to trace impurities from the synthesis of 23	93
AA Figure 17 $^{13}\text{C}\{^1\text{H}\}$ NMR spectrum (100 MHz, C_6D_6) of X = Cl, 23 from 3E . The signal denoted with * is the solvent C_6D_6	93
AA Figure 18 ^1H - ^{29}Si gHMBC spectrum (C_6D_6) of X = Cl, 23 from 3E	94
AA Figure 19 ^1H NMR spectrum (400 MHz, $\text{C}_6\text{D}_5\text{H}$) of X = Br, 24 from 3Z . The signal denoted by * is trace water. The signal denoted ** is traces of 25 from 3E	95
AA Figure 20 $^{13}\text{C}\{^1\text{H}\}$ NMR spectrum (100 MHz, C_6D_6) of X = Br, 24 from 3Z . The signal denoted with * is the solvent C_6D_6	95
AA Figure 21 ^1H - ^{29}Si gHMBC spectrum (C_6D_6) of X = Br, 24 from 3Z . The signal denoted * is traces of 25 from 3E	96
AA Figure 22 ^1H NMR spectrum (400 MHz, $\text{C}_6\text{D}_5\text{H}$) of X = Br, 25 from 3E . The signal denoted by * is trace water.....	97
AA Figure 23 $^{13}\text{C}\{^1\text{H}\}$ NMR spectrum (100 MHz, C_6D_6) of X = Br, 25 from 3E . The signal denoted with * is the solvent C_6D_6	97
AA Figure 24 ^1H - ^{29}Si gHMBC spectrum (C_6D_6) of X = Br, 25 from 3E	98
AA Figure 25 ^1H NMR spectrum (400 MHz, $\text{C}_6\text{D}_5\text{H}$) of X = I, 26 from 3E . The signal denoted by * is trace water. Upfield signals in the spectrum are attributed to trace impurities from the synthesis of 26	99
AA Figure 26 $^{13}\text{C}\{^1\text{H}\}$ NMR spectrum (100 MHz, C_6D_6) of X = I, 26 from 3E . The signal denoted with * is the solvent C_6D_6	99
AA Figure 27 ^1H - ^{29}Si gHMBC spectrum (C_6D_6) of X = I, 26 from 3E . The signal denoted * is attributed to the SiI attentively.	100
AA Figure 28 ^1H NMR spectrum (400 MHz, $\text{C}_6\text{D}_5\text{H}$) of X = I, 27 from 3E . The signal denoted by * is trace water. Upfield signals in the spectrum are attributed to trace impurities from the synthesis of 27	101
AA Figure 29 $^{13}\text{C}\{^1\text{H}\}$ NMR spectrum (100 MHz, C_6D_6) of X = I, 27 from 3E . The signal denoted with * is the solvent C_6D_6	101
AA Figure 30 ^1H - ^{29}Si gHMBC spectrum (C_6D_6) of X = I, 27 from 3E	102
AA Figure 31 ATR-IR X = OH, 18 from 3Z	102
AA Figure 32 ATR-IR X = OH, 19 from 3E	103

AA Figure 33 ATR-IR X = NH ₂ , 20 from 3Z	103
AA Figure 34 ATR-IR X = NH ₂ , 21 from 3E	104
AA Figure 35 ATR-IR X = Cl, 22 from 3Z	104
AA Figure 36 ATR-IR X = HCl, 23 from 3E	105
AA Figure 37 ATR-IR X = Br, 24 from 3Z	105
AA Figure 38 ATR-IR X = Br, 25 from 3E	106
AA Figure 39 ATR-IR X = I, 27 from 3E	106
AA Figure 40 ATR-IR X = I, 26 from 3Z	107
AB Figure 1 ² H { ¹ H} NMR spectrum (92 MHz, C ₆ D ₆) of 29	115

List of Appendices Tables

AA Table 1 Summary of crystal data for 18	107
AA Table 2 Summary of crystal data for 21	109
AA Table 3 Summary of crystal data for 23	110
AA Table 4 Summary of crystal data for 25	111
AA Table 5 Summary of crystal data for 27	113

List of Abbreviations

°	degrees
~	approximately
Δ	change
δ	chemical shift
Σ	sum
Ψ	pseudorotation
θ	fold angle
τ	twist angle
{ ¹ H}	proton decoupled
¹ H- ¹ H gCOSY	proton-proton gradient correlation spectroscopy
¹ H- ¹³ C gHMBC	proton-carbon gradient heteronuclear multiple bond coherence
¹ H- ¹³ C gHSQC	proton-carbon gradient heteronuclear single-quantum correlation
¹ H- ²⁹ Si gHMBC	proton-silicon gradient heteronuclear multiple bond correlation
Å	angstrom, 10 ⁻¹⁰ m
ACN	acetonitrile
Ar	Aryl group
ATR	attenuated total reflectance
[B]	Reactant concentration
br	broad
BPO	dibenzoyl peroxide
C	Celsius
C _N	nucleophilic complex
C _E	electrophilic complex
calc	calculated
CBS	complete basis set

d (NMR)	doublet
DCM	dichloromethane
Dip	2,6-diisopropylphenyl
E	energy
ESI-MS	electrospray ionization-mass spectrometry
Equiv	molar equivalents
Et	ethyl
FMO	frontier molecular orbital
g	grams
G	Gibb's free energy
g/mol	grams per mole
hrs	hours
Hz	hertz
HOMO	highest occupied molecular orbital
<i>i</i>	<i>ipso</i>
i (kinatic)	initial
IR	infrared
<i>i</i> Pr	isopropyl
<i>J</i>	Coupling constant
K	Kelvin
kcal/mol	kilocalorie per mole
KIE	Kinetic isotopic effect
kJ	kilojoules
LG	leaving group
LUMO	lowest unoccupied molecular orbital
<i>m/z</i>	mass to charge ratio
<i>m</i> (NMR)	<i>meta</i>

m (ATR-IR)	medium
m.p.	melting point
Mes	2,4,6-trimethylphenyl
MHz	megahertz
Me	methyl
mg	milligram
min	minute
mL	millilitre
mol	moles
mmol	millimoles
mole %	molar percent
MO	molecular orbital
Nu	nucleophilic
Naph	Napthalene
NBS	N-Bromosuccinimide
NMR	nuclear magnetic resonance
Ni ^t Bu	Bis(<i>tert</i> -butyl)imidazolin-2-imino
<i>o</i>	<i>ortho</i>
<i>p</i>	<i>para</i>
[P]	product concentration
Pr	propyl
ppm	parts per million
R	alkyl
RC	reactant complex
rds	rate determining step
rt	room temperature
s (ATR-IR), (NMR)	strong, singlet

sept (NMR)	septet
Si ^t Bu ₃	triter ^t butylsilyl, supersilyl
t (NMR)	triplet
t	time
^t Bu	<i>tert</i> -butyl
THF	tetrahydrofuran
Tbt	Tbt = 2,4,6- tris[bis(trimethylsilyl)methyl]phenyl
Tip	2,4,6-triisopropylphenyl
TMS	trimethylsilyl
TLC	thin layer chromatography
w (ATR-IR)	weak
VTNA	visual time normalization analysis
X	element, or halide

Chapter 1

1 Introduction

1.1 Overview of Main Group Disilene Chemistry

Small molecules are important in industrial application which demands further studies in activation and functionalization of these molecules. Addition reactions to reactive molecules allow the activation of small molecules by breaking their strong covalent bonds. For decades, the activation of these molecules were done using transition metal catalysis.¹ However, recently Disilenes, compounds with silicon-silicon double bonds, have shown to activate small molecules such as ammonia and dihydrogen by σ -addition.² Disilenes are one of the fundamental classes of compounds in silicon chemistry.³ The synthesis of disilenes was thought to be impossible due to the “Double-Bond Rule” which stated that elements with a principal quantum number greater than 3, such as silicon, do not effectively participate in π -bonding.^{4,5} However, the first stable disilene, tetramesityldisilene *I* (mesityl = 2,4,6-trimethylphenyl), was isolated in 1981 by West and coworkers.⁶ The key to the stability of *I* is the bulky aryl substituents that stabilize the molecule.⁴ The synthesis of *I* sparked interest in the field and the synthesis of many other stable disilene derivatives were achieved. Detailed investigations of the structures, bonding, and reactivity of these novel compounds and preliminary mechanistic studies were carried out.^{7, 8, 9} The field was less active in the first decade of the new millennium, until 2010, when Power and coworkers drew an analogy between the reactivity of low valent main group compounds and the reactivity of transition metals, and the relevance to bond activation and catalysis.¹⁰ Since then, a resurgence in interest in the chemistry of low valent main group compounds has occurred. Disilenes have been part of this renaissance in main group chemistry; they have recently been shown to activate the σ -bond of small molecules, such as NH_3 ^{11, 12} and H_2 .¹³ Despite the ability of disilenes to activate σ -bonds, very little is known about the stereochemistry of the addition. An understanding of the chemistry of σ -addition reactions is important to enable their further development in applications.

The focus of this thesis is to study the stereochemistry of the addition of NH_3 , H_2O , and HX ($\text{X} = \text{Cl}, \text{Br}, \text{I}$) to disilenes. In addition, experiments designed to enhance the understanding of the mechanism of amine addition and preliminary studies of the stereochemistry of substitution reactions of functionalized silanes will be discussed. An understanding of structure and bonding

is important for understanding the reactivity, and thus, the structure and bonding of disilenes are reviewed.

1.1.1 Structure and Bonding in Disilenes

Unlike alkenes which are planar, disilenes typically have a *trans*-bent geometry around the Si=Si double bond. The bulk and the electronic nature of the substituents influence the bond distance (d in Å) of the Si=Si bond, the fold angle (θ in deg) between the Si-Si axis, the R-Si-R plane, and the twist angle (τ in deg), which is the angle between the substituents about the Si-Si vector (Figure 1.1).¹⁴

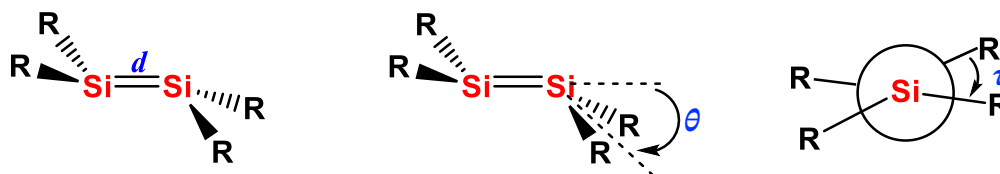


Figure 1.1: Structural parameters for disilenes, distance (d), fold angle (θ) and twist angle (τ).¹⁴

The typical Si=Si bond length is between 2.14-2.29 Å, the fold (*trans*-bending) angle is around 0-14 ° and the degree of twisting is usually between 0-25 °. However, in some derivatives, such as compound **9Z**, the bond length and twist angle are not in the typical range, which is attributed to the bulk and electronic effects of the substituents.¹³ Selected bond lengths, bond angles, and twist angles of compounds **1**, **3E**, **6E** and **9Z** are shown in **Table 1.1** as these compounds will be the focus of this research.¹⁴

Table 1.1: The structural parameters for compounds *I*, *3E*, *6E* and *9Z*.

Disilenes	Bond distance (<i>d</i>)/Å	Fold angle (θ)/°	Twist angle (τ)/°	Products of addition
Mes ₂ Si=SiMes ₂ (<i>I</i>) ^{4, 14} Mes: 2,4,6-trimethylphenyl	2.160	(Si _I) = 12 (Si _{II}) = 14	3	2
^t BuTipSi=SiTip ^t Bu (<i>3E</i>) ¹⁵ Tip: 2,4,6-triisopropylphenyl	2.157	0	0	4 or 5
^t BuMesSi=SiMes ^t Bu (<i>6E</i>) ^{4, 14}	2.143	0	0	6 or 7
(TMS) ₃ SiNI ^t BuSi=SiNI ^t BuSi(TMS) ₃ (<i>9Z</i>) ¹³ NI ^t Bu = (HCN ^t Bu) ₂ C=N TMS = Si(CH ₃) ₃	2.312	(Si _I) = 37.89 (Si _{II}) = 39.03	23.1	8

In comparison to the 12 % decrease in bond length upon the formation of a double bond in alkenes, only an 8-9 % decrease in the Si-Si bond length is observed in disilenes.¹⁴ Nonetheless, there is a significant π -bond component in these double bonds.¹⁴ Planar disilenes such, as *3E* and *6E*, which have zero twist and fold angles do exist. The planarity about the Si=Si is likely due to the extreme bulk of the 2,4,6-triisopropylphenyl-substituent in *3E* or the 2,4,6-trimethylphenyl substituent in *6E* and the *tert*butyl substituents. Disilene *9Z* exhibits a large twist angle and significant pyramidalization at both central silicon atoms due to both the steric bulk and electronics of the substituents.¹³ Substituents containing electronegative groups (i.e. O or N) have been found to increase the degree of twisting over substituents containing electropositive groups (i.e. Si).¹³ In addition, solvation of the aromatic substituents in disilenes can affect the degree of *trans*-bending and twisting at the Si=Si bond.¹⁶ For example, different degrees of bending and twisting angles were observed for disilene *I*. When crystallized from tetrahydrofuran (THF) ($\theta = 0^\circ$, $\tau = 13^\circ$) or from toluene ($\theta = 18^\circ$, $\tau = 12^\circ$), disilene *I* exhibits different bending and twisting angles.^{14, 16}

The unique *trans*-bent geometry of disilenes is attributed to the bonding interaction between two monomeric divalent species. Two bonding models have been proposed to explain the formation of the *trans*-bent disilene.¹⁷ The first model uses Molecular Orbital (MO) theory to illustrate how silylenes dimerize to form the double bond in disilenes. The planar geometry of

alkenes is attributed to a covalent interaction between singly occupied MOs in the ground state and the triplet state of a carbene (**Figure 1.2A**). However, silylenes, the heavier analogue of carbenes, have a singlet ground state. The covalent interaction between the singlet ground states of two silylenes results in Pauli repulsion between doubly occupied n -orbitals (**Figure 1.2B**) preventing bond formation. The formation of a planar disilene, as in alkenes, would require a large amount of energy to overcome the singlet-triplet energy gap (ΔE_{ST}). Instead, disilenes prefer to form a donor-acceptor type bond (**Figure 1.2C**). The lone pair of the silylene donates electron density into the empty p -orbital on the other silylene which minimizes steric bulk and electronic repulsion resulting in the formation of the *trans*-bent disilene.¹⁷

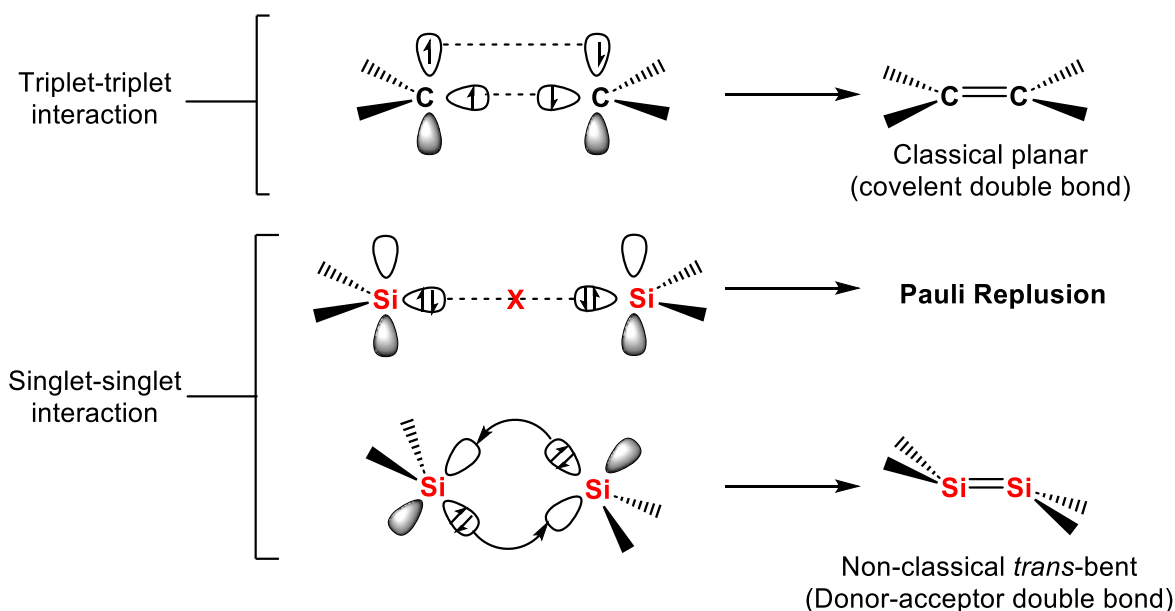


Figure 1.2: Qualitative MO model showing the formation of the *trans*-bent geometry at the silicon center in comparison to alkene.¹⁷

The second bonding model proposed to explain the *trans*-bent geometry in disilenes involves orbital mixing between the σ^* and π MOs and the σ and π^* MOs. The major contributor to the orbital mixing is the σ^* and π of the Si double bond, while the contribution from the σ - π^* combination is significantly less. The strong interaction between the energies of the σ^* and π MOs increases down group 14 as the gap between the σ and π^* MOs decreases and there is more mixing, thus, increasing the *trans*-bending of the molecule (**Figure 1.3**).

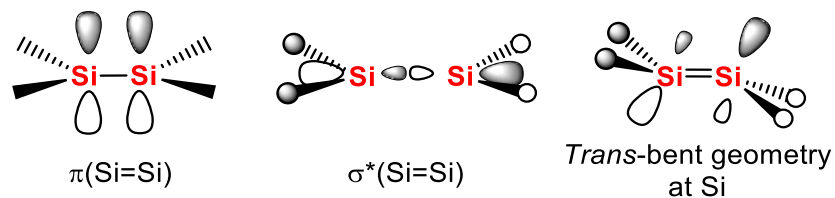
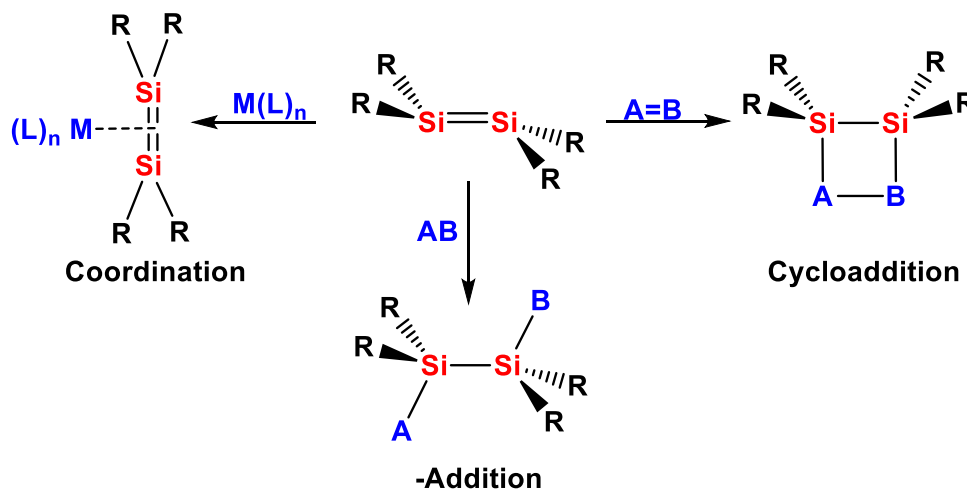


Figure 1.3: Orbital mixing between the σ and π^* MOs resulting in *trans*-bending in disilenes.^{14,17}

1.2 Reactivity of Disilenes

Disilenes have been studied extensively to understand the reactivity of the π -bond. Reactions at the periphery of the disilene framework have also been studied.³⁻⁵ Some of the classic reactions of the disilenes π -bond are σ -addition, cycloadditions, and coordination chemistry (**Scheme 1.1**).^{3, 4, 18}

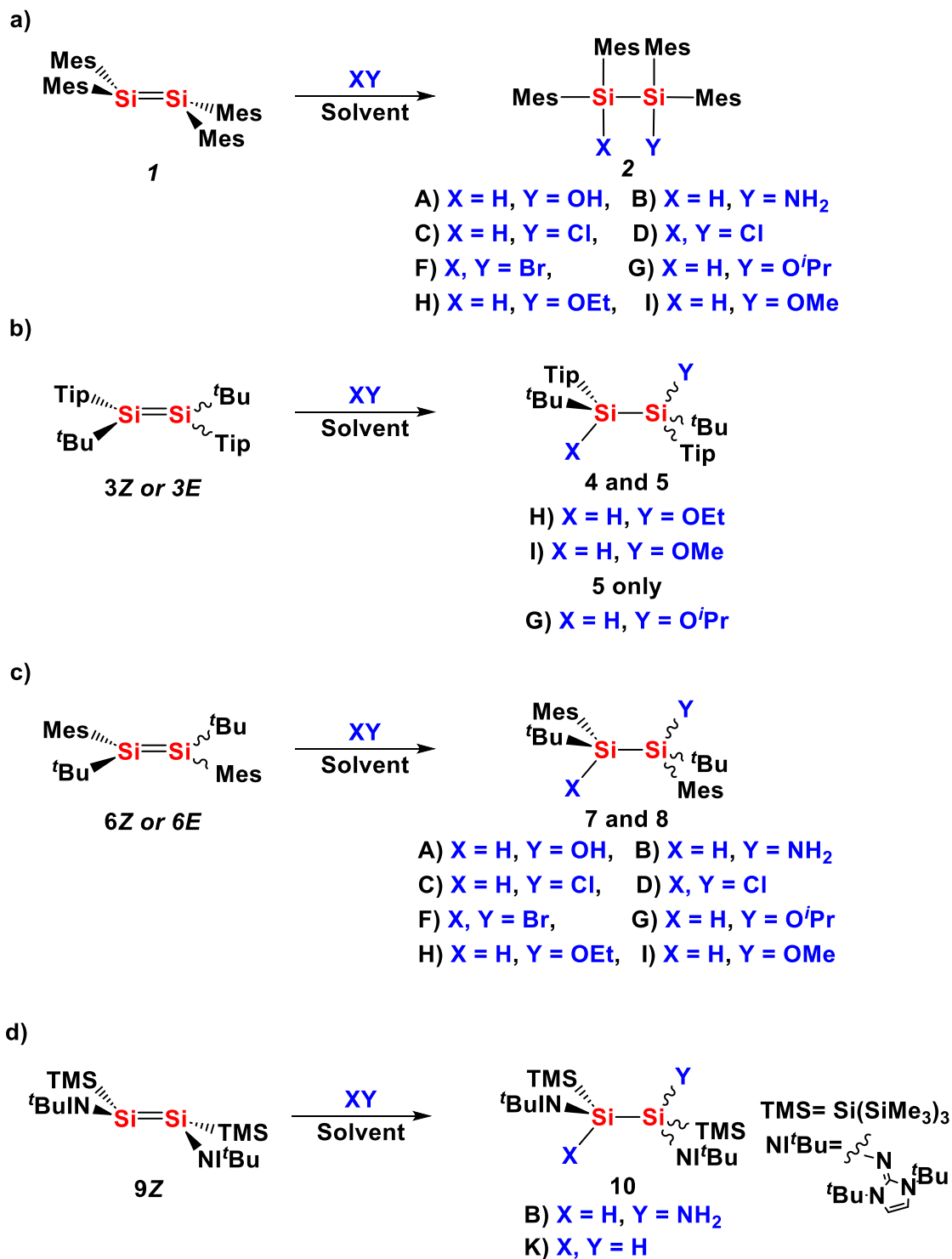


Scheme 1.1: Classic reactions of disilenes.^{3, 4, 18}

1.2.1 The σ -Addition in Disilenes:

The σ -addition across the double bond of disilenes takes place with a wide array of compounds ranging from water to chlorine (**Scheme 1.2**).^{3-8, 12-14} More recently, disilenes have shown to activate the σ -bond in small molecules, such as NH_3 and H_2 , reactivity typically

associated with transition metal chemistry.¹⁰ The higher reactivity of disilenes compared to alkenes is due to the small energy gap between the high-lying HOMO, and the low-lying LUMO allowing reactivity with small molecules. The functionalization of small molecules by disilenes holds great potential; however, more in depth understanding of the stereochemistry and mechanism of these reactions is required.¹⁰ Despite the large scope of reagents investigated (**Scheme 1.2**), very little is known about the stereochemistry of these disilene reactions and their associated mechanisms. The focus of this work is to investigate the σ -addition of H₂O, NH₃, and HX (X = Cl, Br, I) to disilene 1,2-di-*tert*-butyl-1,2-bis(2,4,6-triisopropylphenyl)disilene **3Z** and **3E** and study the stereochemistry of the reactions and the mechanisms of reaction using computational and kinetic studies. Before discussing the results, what is currently known about these reactions is discussed.



Scheme 1.2: Addition of XY molecules to disilene a) 1, b) 3Z or 3E, c) 6Z or 6E, d) 9Z.^{3-7, 12-14}

1.2.2 Addition of ROH to Disilenes

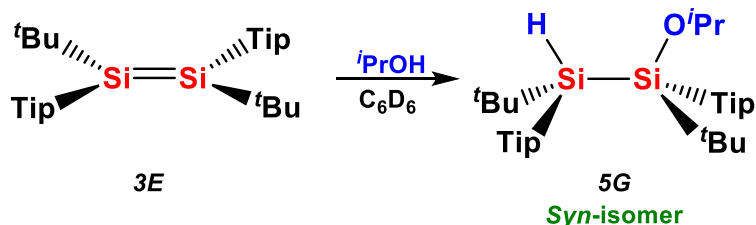
The addition of alcohols to alkenes proceeds through an electrophilic addition. However, the addition of alcohols to disilenes has been found to be nucleophilic.⁸ West and coworkers did extensive studies of the addition of ROH (R = H, Me, Et, *i*Pr) to several disilenes (**Scheme 1.2a, b, c**).^{6,7}

The products were identified by ¹H Nuclear Magnetic Resonance (NMR) spectroscopy as a single diastereomer or a mixture of diastereomers depending on the solvent. Different ratios of diastereomers are observed in the reaction of 1,2-di-*tert*-butyl-1,2-bis(2,4,6-trimethylphenyl)disilene **6E** with H₂O, MeOH or EtOH in THF (**Table 1.2**). However, the stereochemistry of the specific diastereomers was not identified. In contrast, the addition of MeOH and EtOH to **6E** in C₆D₆ were 100 % stereospecific. The addition of *i*PrOH, EtOH and MeOH to **3E** or **3Z** in C₆D₆ were also 100 % stereospecific giving **4G**, **4H**, **4I** and **5G**, **5H**, **5I**, respectively, (**Scheme 1.2b**). The addition reactions of alcohols to **3E** or **3Z** in THF were not reported.⁷

Table 1.2: Addition of H₂O, MeOH and EtOH to disilene **6E** in C₆D₆ vs THF at rt. ^a at 50 °C.

Disilene	Alcohol	Isomer ratio of A:B in C ₆ D ₆	Isomer ratio of A:B in THF
6E	H ₂ O	-	50:50
	MeOH	100:0	50:50
	EtOH	100:0	96:4
50:50 ^a			

The stereochemistry of the addition of *i*PrOH to **3E** in C₆D₆ was determined by single crystal X-ray diffraction to be the *syn*-isomer **5G** (**Scheme 1.3**).



Scheme 1.3: Addition of the *i*PrOH to **3E**.⁷

From this result, it was assumed that stereospecific addition reactions of alcohols to disilenes in C₆D₆ gave the *syn*-isomer as there is no other isomer formed. Thus, the second diastereomer observed in the reactions with THF, is therefore, the *anti*-isomer which is formed due to the effect of the solvent polarity on stabilizing the reactive species within the reaction, allowing intermolecular transfer of proton from a second equivalent of the alcohol leading to the *anti*-isomer.

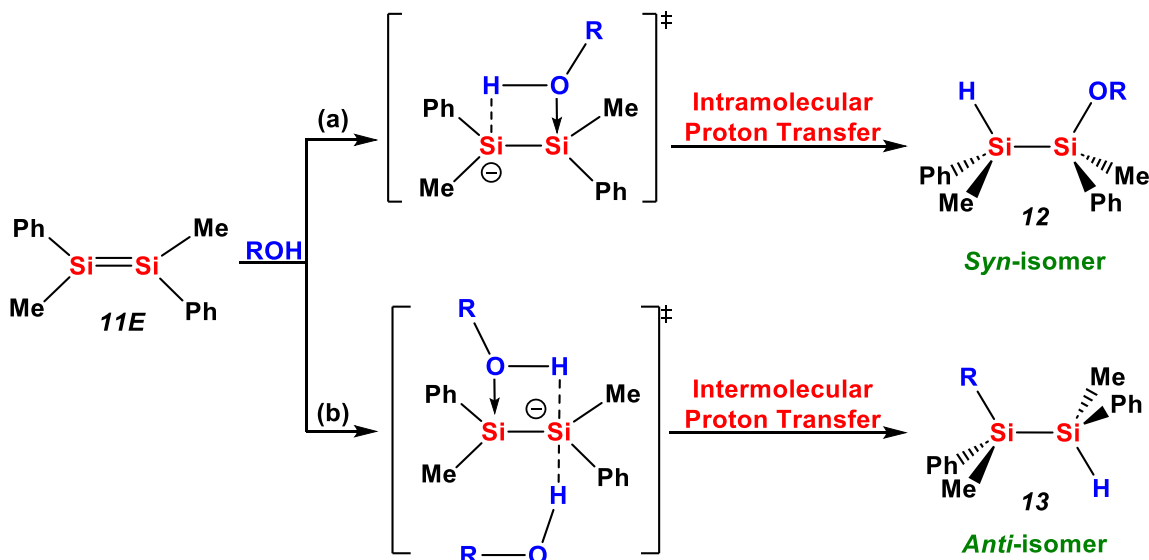
The influence of the concentration of alcohol on the stereochemistry of the addition reaction was studied by Sekiguchi, Maruki, and Sakurai.¹⁹ They investigated the addition of EtOH and ⁱPrOH to *E*-1,2-dimethyl-1,2-diphenyldisilene **11E** in hexane at different concentrations (**Table 1.3**).¹⁹ At higher alcohol concentrations, a greater proportion of the *anti*-isomer was formed.

Table 1.3: Addition of EtOH and ⁱPrOH to **11E**.¹⁹

Disilene	Alcohol	Concentration (M)	<i>Syn (12): Anti (13)</i>
11E	EtOH	0.85	92:8
	EtOH	5.65	51:49
	ⁱ PrOH	1.31	>99:<1
	ⁱ PrOH	4.33	89:11

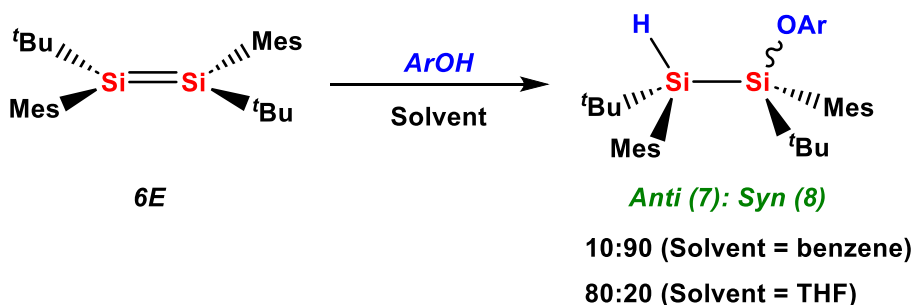
The following mechanism was proposed to account for the formation of *anti*-product at higher concentrations.¹⁹ The first step is proposed to be the nucleophilic addition of the alcohol to the disilene which was also identified as the rate determining step (rds) based on the following evidence.^{8, 19} First, the addition of alcohols to phenyl-substituted disilenes is very rapid, and thus, the disilene is believed to react prior to isomerization. Second, the reaction rate decreases as the bulk of the alcohol increases (EtOH > ⁱPrOH >> ^tBuOH). This contrasts with what would be expected in an electrophilic addition where the bulk of the substituents is expected to not influence the rate of the reaction. Third, a Kinetic Isotopic Effect (KIE) study of addition of deuterated ethanol to **11E** or **11Z** gave a $k_H/k_D \sim 1.0$, which is not a *primary* deuterium isotope effect indicating that the proton is not transferred in the rds of the reaction.^{8, 19} Together, these facts strongly indicate that the rate determining step must be the nucleophilic addition where the alcoholic oxygen attacks the unsaturated silicon center. The second step in alcohol addition to disilene is proposed to be

transfer of the proton through an intramolecular transfer (**Scheme 1.4a**) giving the *syn*-isomer, or through an intermolecular proton transfer from a second equivalent of alcohol giving the *anti*-isomer, and thus a ratio of *syn:anti* isomers were observed (**Scheme 1.4b**).⁷



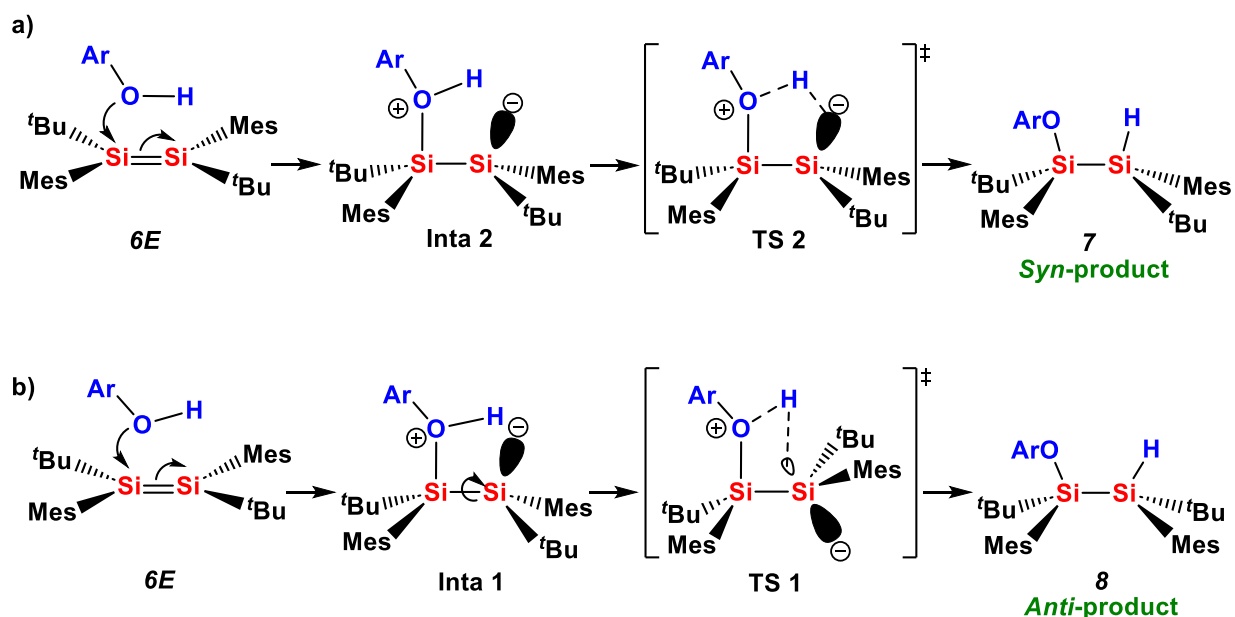
Scheme 1.4: Pathways for the addition of alcohol to disilene **11E**: a) *syn*-isomer via intramolecular transfer or b) *anti*-isomer via intermolecular transfer of the proton. ⁸ R= alkyl.

Apeloig and coworkers further studied the mechanism of the addition of alcohols to disilene using phenols. The addition of 4-methoxyphenol (*p*-CH₃OC₆H₄OH), to **6E** (**Scheme 1.5**) was investigated. Reaction in benzene gave a ratio of 10:90, and the reaction in tetrahydrofuran gave 80:20 of the *anti:syn* isomers **7** and **8**, respectively.²⁰



Scheme 1.5: Addition of *p*-CH₃OC₆H₄OH (ArOH) to **6E** in benzene or tetrahydrofuran.²⁰

It was observed that the stereochemistry of the addition is independent of the concentration of the $p\text{-CH}_3\text{OC}_6\text{H}_4\text{OH}$, ruling out the intermolecular proton transfer pathway proposed by Sakurai and West previously.⁶ Thus, Apeloig and coworkers proposed a different mechanism for the formation of the *anti*-adduct. The formation of the *syn*-oriented donor adduct as in transition state 2 (TS 2) undergoes rotation around the Si-Si and then fast proton transfer in intermediate 2 (Inta 2) to the backside of the Si bearing a negative charge leading to the formation of the *anti*-isomer (Scheme 1.6a). Apeloig proposed the same mechanism as previously proposed by Sakurai for the formation of the *syn*-isomer **8** (Scheme 1.6b). Notably, Apeloig did not consider the *trans*-bent geometry of the disilene, the energy barrier for the formation of the *syn*-donor adduct, nor the rotation barrier of the Si-Si bond in the intermediate donor adduct in their mechanistic proposal (Scheme 1.6).²⁰



Scheme 1.6: Mechanisms proposed for the addition of $p\text{-CH}_3\text{OC}_6\text{H}_4\text{OH}$ to **6E**.^{7, 20}

Computationally, the mechanism of the addition of water to the parent disilene has also been examined using density functional theory (DFT).²¹ Two pathways were proposed to account for the *syn*- and *anti*-isomer observed in alcohol addition. The π^* (LUMO) of the disilene was proposed to interact with the lone pair of the HOMO (n) on the oxygen to give a nucleophilic complex (C_N) (Figure 1.4a) or the O-H σ^* (LUMO) of water with the π (HOMO) of the disilene to form the electrophilic complex (C_E) (Figure 1.4b).²¹

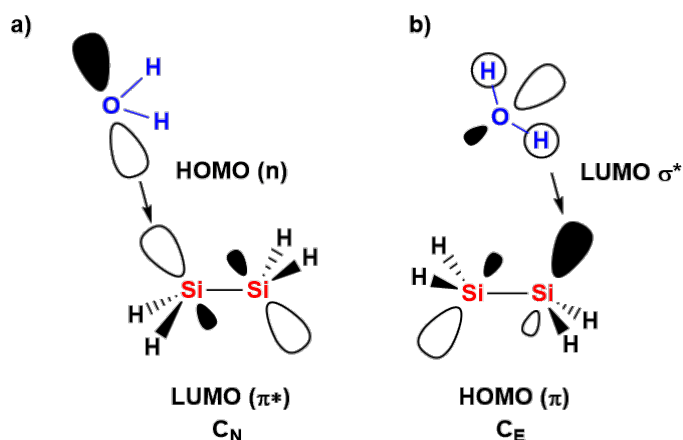
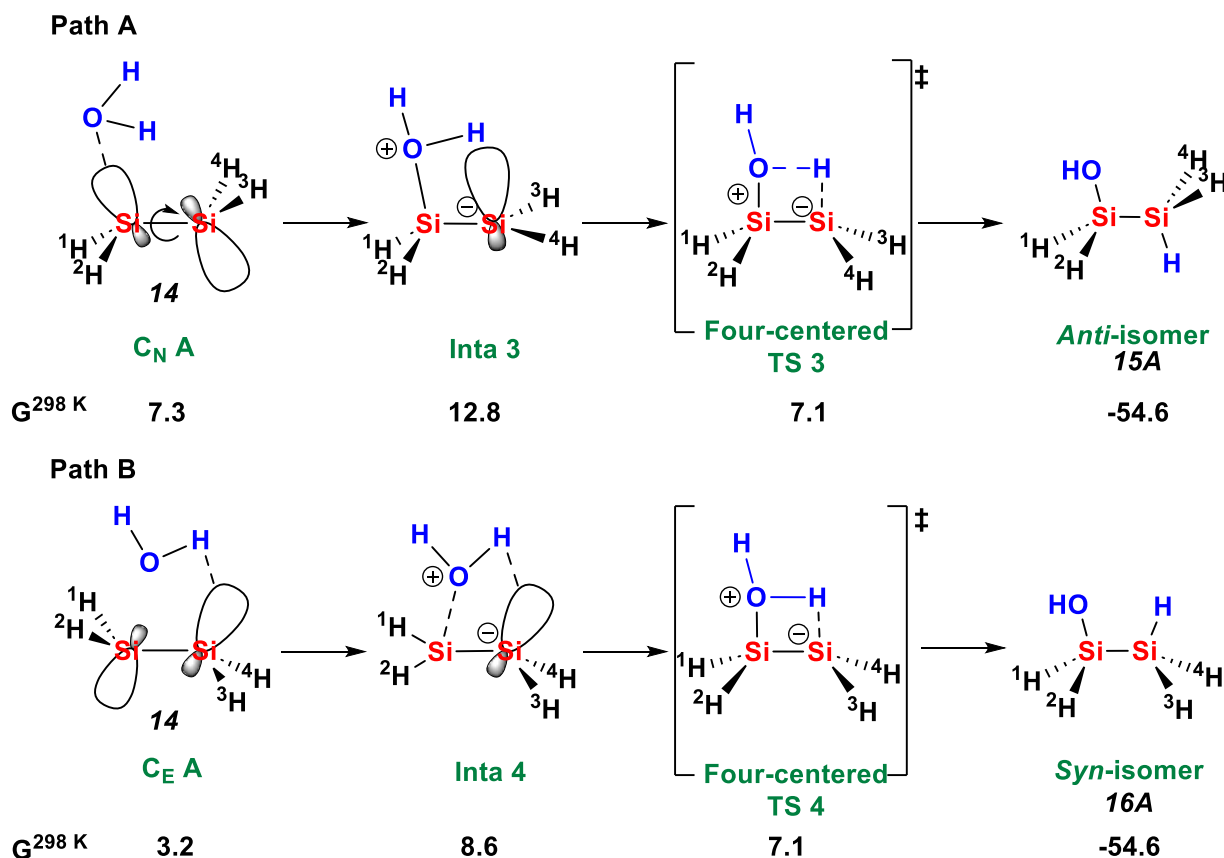


Figure 1.4: Proposed initial interactions between water and $\text{H}_2\text{Si}=\text{SiH}_2$ (**14**) leading to the formation of a) nucleophilic reactant complex, C_N , or b) electrophilic reactant complex, C_E .²¹

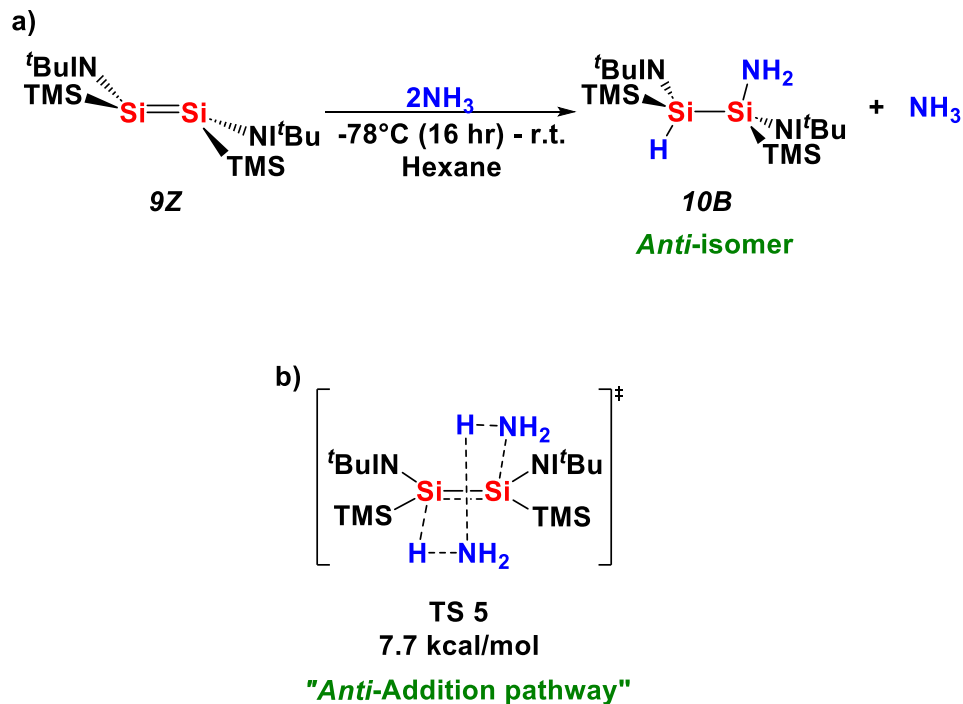
The authors proposed that the stereochemistry of the product is governed by the nature of the initial reactant complex between H_2O and the parent disilene.²¹ The pathway from the nucleophilic reactant complex, C_N , leads to the *anti*-isomer **15A** (Scheme 1.7a). The pathway from the electrophilic reactant complex, C_E , leads to the *syn*-isomer **16A** (Scheme 1.7b). The energy barrier in the two reaction pathways were 5.16 kcal/mol for **Path A**, and 2.92 kcal/mol for **Path B**. Since **Path B** has a lower energy barrier and lower transition state energy thus, the formation of the *syn*-isomer was proposed to be favored (Scheme 1.7).^{21b}



Scheme 1.7: Possible pathways for the addition of water to $H_2Si=SiH_2$ to give the *anti/syn*-isomer. The thermodynamic data of stationary points ($\Delta G^{298\text{ K}}$ in kcal/mol) was calculated using the CBS-Q method.²¹

1.2.3 Addition Reactions of NH_3 to Disilenes

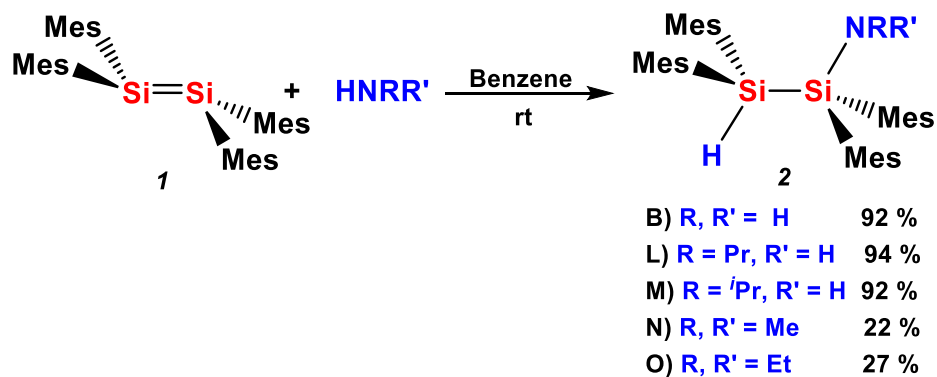
The addition of ammonia to (*Z*)-imino(silyl)disilene **9Z**, a disilene with a highly *trans*-bent and twisted structure ($\theta = 37.86$ and 39.03° , $\tau = 23.1^\circ$), has been studied by Inoue and coworkers (**Scheme 1.8**).¹² The addition of ammonia to **9Z** in hexanes at a low temperature formed the *anti*-isomer adduct **10B**, stereospecifically (**Scheme 1.8**).¹² The mechanism of the addition of ammonia and dimeric ammonia to disilene **9Z** was also studied computationally. A low energy barrier for the *anti*-transition state (TS 5 = 7.7 kcal/mol) involving two ammonia molecules was found, leading to the formation of the *anti*-isomer (**Scheme 1.8**).¹⁰



Scheme 1.8: a) Addition of ammonia to **9Z**, b) The transition state $\Delta G^{298\text{ K}}$ in kcal/mol.¹⁰

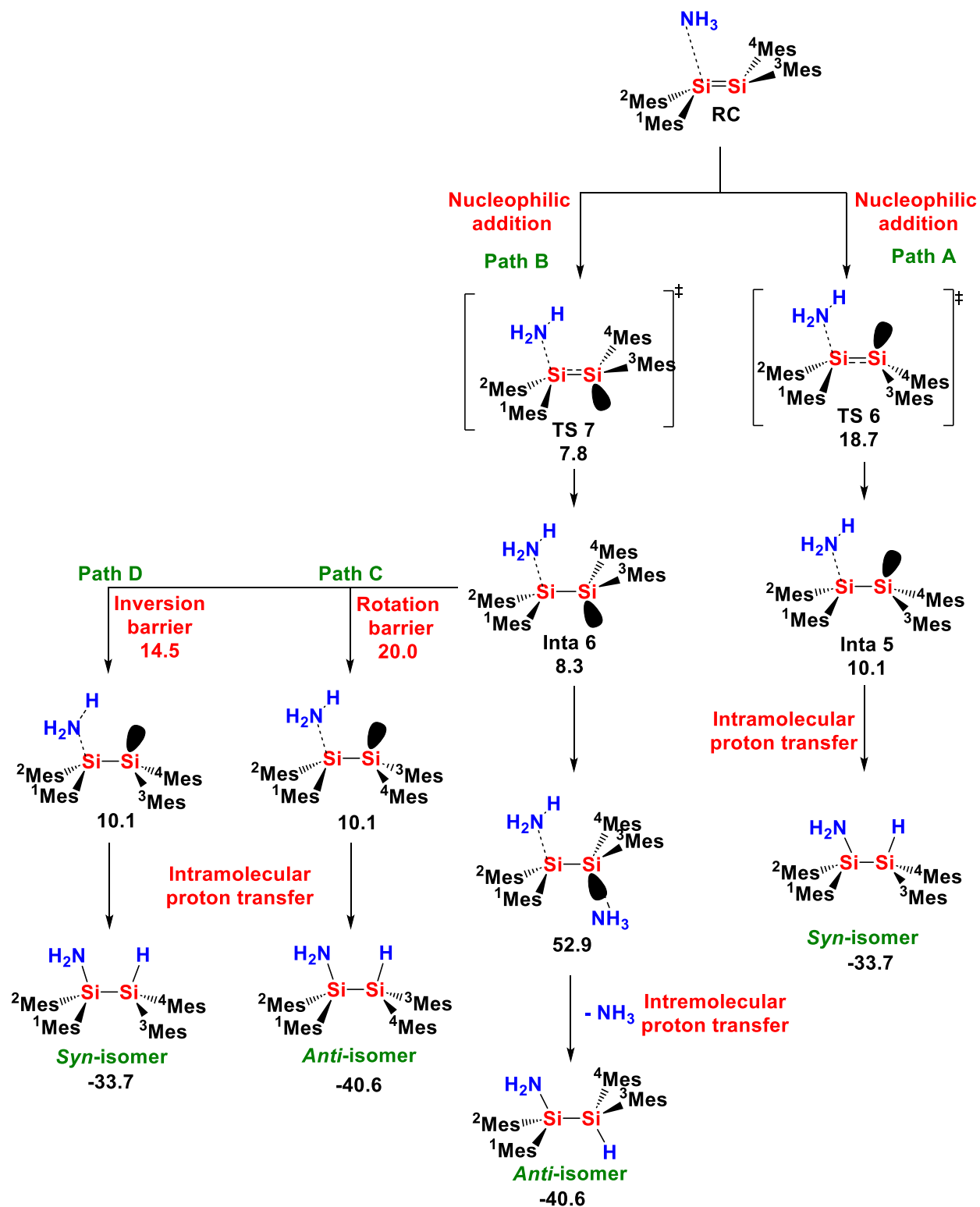
The stereospecific formation of the *anti*-isomer **10B** in the addition of ammonia to **9Z** (**Scheme 1.8**), is in contrast with the stereoselective addition of water and alcohols to disilenes, where the formation of the *syn*-isomer is favored over the *anti*-isomer.

Baines, Ozpinar and coworkers investigated the addition of ammonia and amines to disilene **1**, experimentally and computationally. Experimentally, good to excellent yields of the disilylamine were obtained (**Scheme 1.9**).¹¹



Scheme 1.9: Addition of ammonia and amines to **1**.¹¹

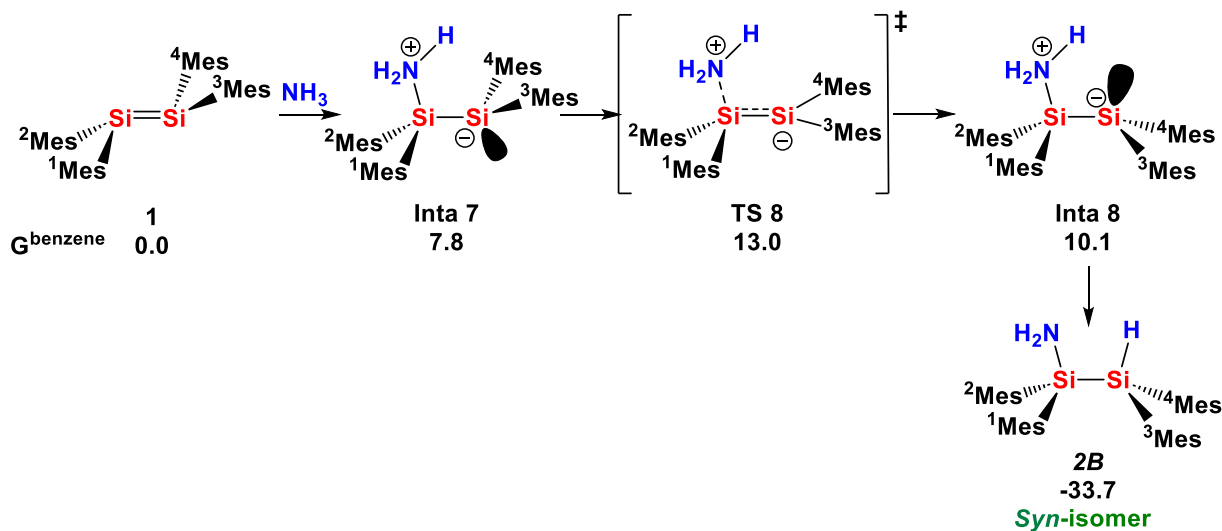
Four reaction pathways were investigated for the addition of NH_3 to **1**. Nucleophilic addition of NH_3 to **1** forming; 1) a *syn*-oriented donor adduct **TS 6** followed by *syn*-intra molecular transfer of proton **Inta 5** leading to the *syn*-isomer (**Path A, Scheme 1.10**). 2) Formation of an *anti*-oriented donor adducts **TS 7**, intermolecular transfer of proton from a second molecule of ammonia (**Inta 6**) forming the *anti*-isomer (**Path B, Scheme 1.10**). 3) Formation of the *anti*-oriented donor adduct (**TS 7**) followed by rotation, and *syn*-intramolecular transfer of the proton leading to the *anti*-isomer (**Path C, Scheme 1.10**), or 4) formation of the *anti*-oriented donor adduct followed by inversion at the silicon bearing the lone pair, then *syn*-intramolecular transfer of the proton forming the *syn*-isomer (**Path D, Scheme 1.10**).¹¹



Scheme 1.10: Potential reaction pathways for the addition of NH_3 to **I**. The relative free energies (in kcal/mol, at 298 K and 1 atm) of the species involved.¹¹

Based on the relative energies of the species involved in the reaction pathways examined, the following insights were gained: a) the *anti*-oriented donor adduct (**TS 7** = 7.8 kcal/mol) is energetically more preferred over the *syn*-oriented donor adduct (**TS 6** = 18.7 kcal/mol), b) the inversion barrier (14.5 kcal/mol) is lower in energy than the rotation barrier (20.0 kcal/mol) at the Si with the lone pair, c) intermolecular transfer of a proton is energetically not favorable in non-polar solvents, d) the electronic and/or the bulk of the substituents evidently affects the stereochemical outcome of the reactions, particularly their influence on the barrier of rotation and/or inversion at the Si-Si bond.¹¹

Computational studies of the addition of ammonia to tetramesityldisilene (**I**) indicated the preferential formation of the *syn*-isomer. The addition occurs in three distinct steps: formation of the *anti*-ammonia-disilene donor adduct **Inta 7**, inversion at the β -silicon to give **Inta 8**, followed by intramolecular *syn*-transfer of the proton to give the *syn*-isomer **2B** (**Scheme 1.11**).¹¹



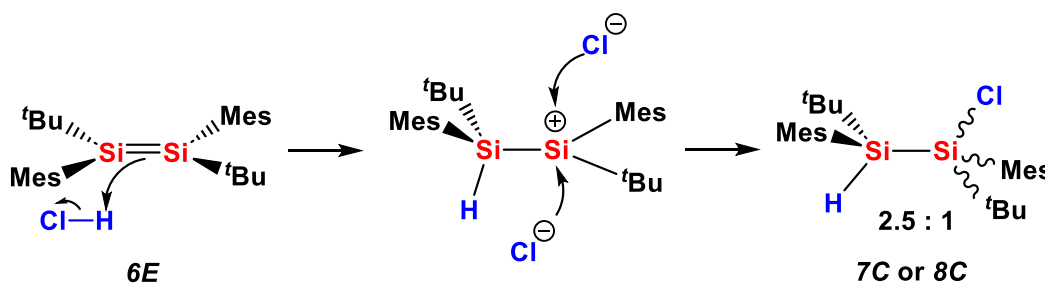
Scheme 1.11: Mechanistic pathway of the addition of ammonia to tetramesityldisilene **I** ($\Delta G^{298\text{ K}}$ in kcal/mol at 1 atm).¹¹

The *anti*-isomer can be formed in one of two ways: 1) protonation of the *anti*-donor adduct in **Inta 7** by a second molecule of ammonia, or 2) rotation about the Si-Si bond to give the *syn*-conformation of **Inta 8** followed by intramolecular *syn*-transfer of the proton. The pathway with rotation about the Si-Si bond was shown to have a high activation energy barrier of 20 kcal/mol,

making it unfavorable. Furthermore, intramolecular *syn*-transfer of a proton is energetically more favored ($\Delta G = 13.2$ kcal/mol) compared to intermolecular transfer ($\Delta G = 47.8$ kcal/mol).¹¹

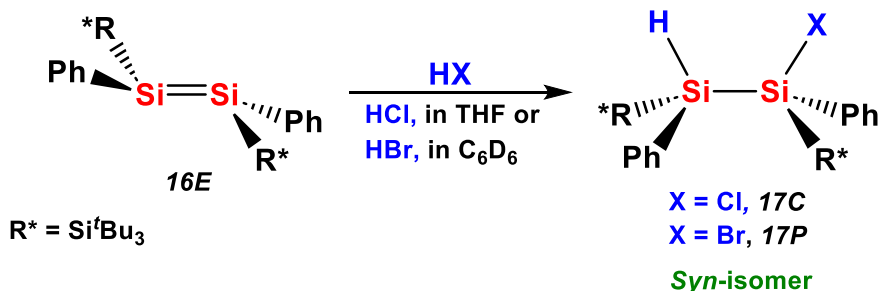
1.2.4 Addition of HX (X = F, Cl, Br) to Disilenes

The addition of HCl to disilene **1** and **6E** was examined by West and coworkers.⁴ Two isomeric products were observed upon the addition of HCl to **6E**. However, the individual isomers were not identified (**Scheme 1.12**).^{6a} The mechanism of the addition was hypothesized to be analogous to the addition of HCl to alkenes, that is, electrophilic addition forming a silylenium cation followed by the addition of chloride. The high acidity of HCl can lead to the electrophilic addition of HCl to disilene resulting in the formation of the planar silylenium cation, which accounts for the observed mixture of diastereomeric chlorodisilanes. On those bases, the chloride can attack from either face of the cation leading to the formation of a mixture (**Scheme 1.12**).^{6a}



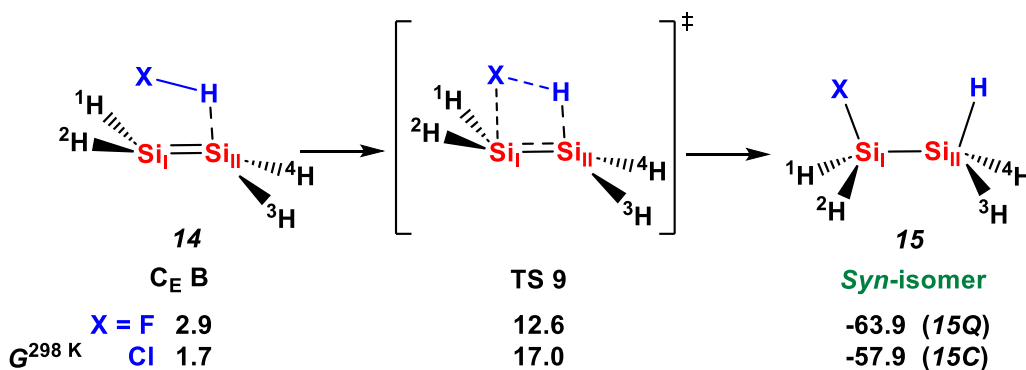
Scheme 1.12: Addition of HCl to disilene **6E** in THF at rt via electrophilic pathway.^{6a}

The addition of HCl and HBr to *E*-1,2-supersilyl-1,2-phenyldisilene **16E** (supersilyl = Si^tBu₃) was also examined.²² Disilene **16E** has a bond length of 2.182 Å, with fold and twist angles of $\theta = 35^\circ$ and $\tau = 3^\circ$.^{22, 23} In the addition of HCl to **16E** in THF, the formation of a single diastereomer was observed and identified by single crystal X-ray diffraction to be the *syn*-isomer. On this basis, the addition of HBr to **16E** in C₆D₆, which also formed a single diastereomer, was proposed to give the *syn*-isomer as observed in the addition of HCl (**Scheme 1.13**).²²



Scheme 1.13: Addition of HCl and HBr to disilene **16E**.²²

The addition of HF and HCl to $\text{H}_2\text{Si}=\text{SiH}_2$ was examined computationally to understand the stereochemistry of the addition of hydrogen halides to disilenes.²⁴ The addition of HX (X = F, Cl) was found to approach the disilene to form an electrophilic complex $\text{C}_E \mathbf{B}$ similar to the one observed in the addition of water to the parent disilene (**Scheme 1.14**). The addition of HX to the disilene occurs via a four-center transition state. No pathway involving the formation of nucleophilic reactant complex was located which was attributed to the strong acidic character of HF and HCl and suggested that the formation of the *anti*-isomer is not possible. Based on the computations, the selective formation of *syn*-product is predicted (**Scheme 1.14**).²⁴



Scheme 1.14: Computational studies of the addition of HX to parent disilene via formation of the electrophilic complex. The thermodynamic data of stationary points ($\Delta G^{298 \text{ K}}$ in kcal/mol) were calculated using the complete basis set (CBS-Q) method.²⁴

As only a few examples of the addition of hydrogen halides to disilenes have been reported, the influence of the substituents, the reaction conditions and the reagent acidity (pK_a) on the stereochemistry is relatively unknown. Investigations into the mechanism of hydrogen halide

addition to disilenes with known stereochemistry will enhance the understanding of this reaction and the stereochemical implications of each elementary step.

1.3 Research Scope of the Thesis

The formation of the *anti*-isomer in **10B** from the addition of ammonia to disilene **9Z**¹² was observed experimentally and computationally by Inoue and coworkers. However, recent computational work by Baines and Ozpinar and coworkers predicts the formation of a *syn*-isomer **2B** in the addition of ammonia to disilene **1**.¹¹ In addition, the stereochemistry of the addition of water to disilenes **6E** was found to be 50 % stereospecific experimentally. Whereas the calculations regarding the addition of water to H₂Si=SiH₂ (**14**) by Kira and Veszpremi and coworkers predicts preferential formation of the *syn* isomer.²¹ Notably, there has only been one experimental study on each of the stereochemistry of the addition of water or ammonia to a disilene. Moreover, experimental studies of the addition of hydrogen halides to disilenes gave conflicting results. In one case, a diastereomeric mixture was formed, in the only other study the reactions were stereospecific.²² The objective of this research is to provide further insights into the stereochemistry of these fundamental σ -additions reactions of disilenes by examining the addition of water, ammonia, and hydrogen halides to a stereoisomeric pair of disilenes.

The disilene chosen for this work is 1,2-di-*tert*-butyl-1,2-bis(2,4,6-triisopropylphenyl)disilene (**3Z** and **3E**). Disilene **3** was selected as each isomer can be isolated cleanly. Herein, the stereochemistry of the addition of water, ammonia and HX (X = Cl, Br, I) to **3Z** or **3E** and the effect of reaction conditions such as solvent, reagent concentration and temperature on the stereochemistry of the reaction was investigated. In addition, mechanistic studies using kinetic analyses, specifically Variable Time Normalization Analysis (VTNA) and Kinetic Isotopic Effect (KIE) studies, for the reaction of tetramesityl disilene with *isopropyl* amine (^{*i*}PrNH₂) were carried out to further understand the mechanism of the addition of amines to disilenes. Finally, the stereochemistry of the hydrolysis reaction on the disilane HX adducts was studied.

1.4 References

1. a) G. W. Margulieux, M. J. Bezdek, Z. R. Turner, P. J. Chirik, *J. Am. Chem. Soc.*, 2017, **139**, 6110-6113, b) J. Hoover, *Science*, 2016, **354**, 707-708.
2. F. Hanusch, L. Groll, S. Inoue, *Chem. Sci.*, 2021, **12**, 2001-2015.
3. a) A. Rammo, D. Scheschkewitz, *Chem. Eur. J.*, 2018, **24**, 6866-6885, b) T. Matsuo, N. Hayakawa, *Sci. Technol. Adv. Mater.*, 2018, **19**, 108-129, c) G. Raabe, J. Michl, *Chem. Rev.* 1985, **85**, 419-509, d) R. West, *Angew. Chem. Int. Ed.*, 1987, **26**, 1201-1211, e) N. C. Norman, *Polyhedron*, 1993, **12**, 2431-2446.
4. F. Hanusch, L. Groll, S. Inoue, *Chem. Sci.*, 2021, **12**, 2001-2015.
5. L. E. Gusel'nikov and N. S. Nametkin, *Chem. Rev.*, 1979, **79**, 529-577.
6. a) M. J. Fink, M. J. Michalczyk, K. J. Haller, R. West, J. Michl, *Organometallics*, 1984, **3**, 793-800, b) R. West, M. J. Fink, J. Michl, *Science*, 1981, **214**, 1343-1344.
7. J. Budaraju, D. R. Powell, R. West, *Main Group Metal Chemistry*, 1996, **19**, 531-537.
8. H. Sakurai, Mechanism and Structures in Alcohol Addition Reactions of Disilenes and Silenes. *The Chemistry of Organic Silicon Compounds*. John Wiley & Sons, Ltd. 1998; 15, pp 827-855.
9. T. L. Morkin, T. R. Owens, W. J. Leigh, Kinetic Studies of the Reactions of Si = C and Si = Si Bonds. *PATAI's Chemistry of Functional Groups*, John Wiley & Sons, Ltd. 2009; 1, pp 1-78.
10. a) P. P. Power, *Nature*, 2010, **463**, 171-177, b) C. Weetman, *Chem. Eur. J.*, 2021, **27**, 1941-1954.
11. S. L. McOnie, G. A. Özpınar, J. L. Bourque, T. Müller, K. M. Baines, *Dalton Trans.*, 2021, **50**, 17734-17750.

12. D. Wendel, T. Szilvási, D. Henschel, P. J. Altmann, C. Jandl, S. Inoue, B. Rieger, *Angew. Chem. Int. Ed.*, 2018, **57**, 14575-14579.
13. D. Wendel, T. Szilvási, C. Jandl, S. Inoue, B. Rieger, *J. Am. Chem. Soc.*, 2017, **139**, 9156-9159.
14. M. Kira, *Proc. Jpn. Acad. Ser. B.*, 2012, **88**, 167-191.
15. R. S. Archibald, Y. V. Winkel, A. J. Millevolte, J. M. Desper, R. West, *Organometallics*, 1992, **11**, 3276-3281.
16. M. J. Fink, M. J. Michalczyk, K. J. Haller, R. West, J. Michl, *J. Chem. Soc., Chem. Commun.*, 1983, **18**, 1010-1011.
17. Lee, V. Y.; Sekiguchi, A. *Organometallic Compounds of Low-Coordinate Si, Ge, Sn and Pb: From Phantom Species to Stable Compounds*; John Wiley & Sons Ltd: Chichester, 2010.
18. S. Ishida, T. Iwamoto, *Coordination Chemistry Reviews*, 2016, **314**, 34-63.
19. A. Sekiguchi, I. Maruki and H. Sakurai, *J. Am. Chem. Soc.*, 1993, **115**, 11460-11466.
20. Y. Apeloig, M. Nakash, *Organometallics*, 1998, **17**, 1260-1265.
21. a) M. Takahashi, T. Veszpremi, M. Kira, *Organometallics* 2004, **23**, 5768-5778, b) M. Takahashi, T. Veszpremi, B. Hajgató, M. Kira, *Organometallics* 2000, **19**, 4660-4662.
22. N. Wiberg, W. Niedermayer, K. Polborn, *Z. Anorg. Allg. Chem.*, 2002, **628**, 1045-1052.
23. N. Wiberg, W. Niedermayer, K. Polborn, P. Mayer, *Chem. Eur. J.*, 2002, **8**, 2730-2739.
24. B. Hajgató, M. Takahashi, M. Kira, T. Veszpremi, *Chem. Eur. J.*, 2002, **8**, 2126-2133.

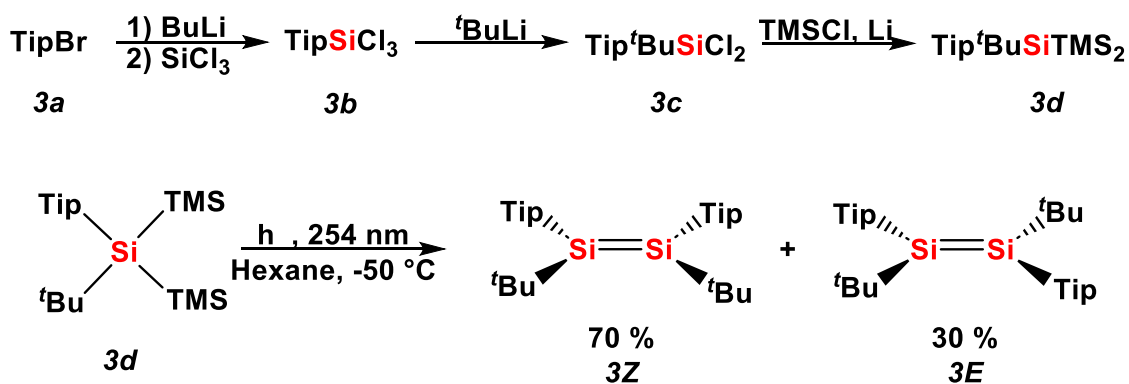
Chapter 2

2 The Stereochemistry of the Addition of HX (X = OH, NH₂, Cl, Br, I) to Disilenes

2.1 The Addition of HX (X = NH₂, OH, Cl, Br, I) to 1,2-di-*tert*-butyl-1,2-bis(2,4,6-triisopropylphenyl)disilene (**3Z** or **3E**)

Disilenes have shown to activate small molecules such as ammonia, water, and dihydrogen.¹ Understanding the mechanism behind these reactions is important for future applications. The stereochemistry of the product can be used to have an insight into the mechanism and the reactive species involved in the reaction. Thus, in this chapter the stereochemistry of the addition of HX (X = NH₂, OH, Cl, Br, I) to 1,2-di-*tert*-butyl-1,2-bis(2,4,6-triisopropylphenyl)disilene (**3E** or **3Z**) will be investigated to further understand the mechanism.

To study the stereochemistry of the addition of a reagent to disilene, it is necessary to be able to synthesize the *E* and *Z* isomers of a disilene as easily and to be able to separate the two isomers purely. Disilene **3Z** and **3E** were chosen to use in this study as they were synthesized previously with a reliable method to separate the two isomers.² Photolysis of Tip^{*t*}BuSiTMS₂ (TMS = Si(CH₃)₃) in hexane at -50 °C gave **3Z** and **3E** in a ratio of 70:30 (Scheme 2.1).^{2a}

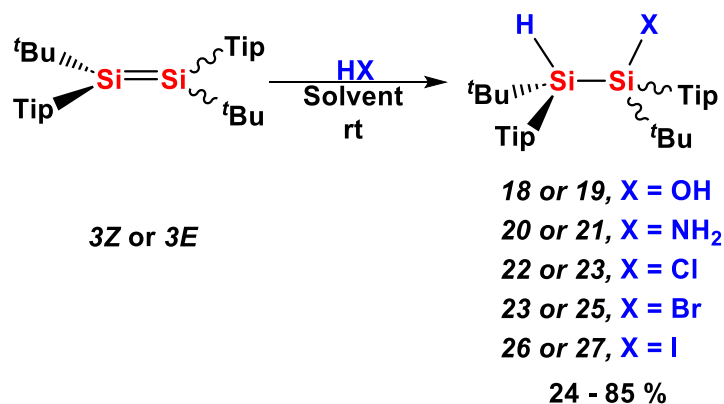


Scheme 2.1: Synthesis of disilene **3Z** and **3E**.²

Disilene **3E** precipitates as a yellow solid from the reaction mixture at -50 °C, the solid was removed by filtration and washed with hexane to remove traces of **3Z** giving pure **3E**. Disilene **3Z** remains in solution. After multiple precipitations and filtration of **3E** traces, the necessary purity

of **3Z** can be achieved following solvent removal by vacuum. The purity of each disilene was assessed by ^1H and ^{29}Si NMR spectroscopy and was found to be $> 95\%$ pure. For all subsequent reactions, disilene **3Z** or **3E** was placed in tetrahydrofuran (THF), benzene or hexane, and the solution was stirred until the disilene was completely dissolved.

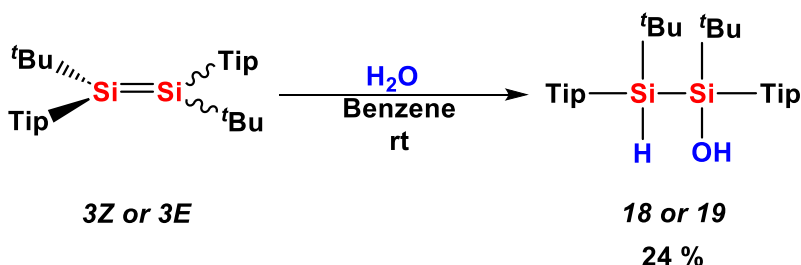
The addition of water to both disilene **3Z** and **3E** was conducted following the same procedure. Water (0.1 M in THF) was added to a solution of disilene **3Z** or **3E** to give products **18** or **19**, respectively. A solution of ammonia (0.4 M in THF) was added to a solution of **3Z** or **3E**, to give compounds **20** or **21**, respectively. Finally, the addition of HX (X = Cl, Br, I) to **3Z** or **3E** was conducted by the direct addition of the commercially available hydrogen halide solution to the disilene solution. Concentrated aqueous HCl (12.0 M) was added to the solution of the disilene to form either compounds **22** or **23**. A solution of HBr (48 % M in H_2O) was added to the solution of the disilene to form either compounds **24** or **25**. Similarly, solution of HI (57 % M in H_2O) was added to the solution of disilene to form either compounds **26** or **27** (Scheme 2.2). The decolorization of the disilene solutions indicate that the reaction was completed. All reactions were conducted at room temperature under an inert atmosphere using a glovebox or a Schlenk line, and the purification of the product, if needed, was performed using thin layer chromatography (TLC).



Scheme 2.2: Addition of HX (X = NH₂, OH, Cl, Br, I) to **3Z** or **3E**.

2.1.1 Addition of H₂O to *Z* or *E*-1,2-di-*tert*-butyl-1,2-bis(2,4,6-triisopropylphenyl)disilene (**3Z** or **3E**)

The addition of water to **3Z** or **3E** in benzene gave product **18** or **19**, respectively. Both reactions were 100 % stereospecific. The crude product yields were 50-70 %. Additional purification was necessary and resulted in low isolated yields (**Scheme 2.3**).



Scheme 2.3: Addition of water to **3Z** or **3E**.

The electrospray ionization mass spectrum (ESI-MS) of **18** revealed a signal at m/z 594.4891 which is consistent with the formula C₃₈H₆₇OSi₂ [M+H⁺] for **18**. Similarly, the ESI-MS of **19** revealed a signal at m/z 617.4564 which is consistent with the formula C₃₈H₆₆ONaSi₂ [M+Na⁺]. In each case, the ESI-MS revealed the formation of the 1:1 adduct between the disilene and water.

The attenuated total reflectance-infrared (ATR-IR) spectra of **18** and **19** were obtained. Signals at 3688 cm⁻¹ and 3690 cm⁻¹ were observed and were assigned to the -OH stretching vibration, respectively. The signal at 2170 cm⁻¹ and 2115 cm⁻¹ for **18** and **19**, respectively, were assigned to an Si-H stretching vibration.

NMR spectroscopy was used to quickly assess the progress of the reaction and to easily distinguish the different isomers. Compounds **18** and **19** exhibit ¹H signals with chemical shifts (δ) at 4.95 and 5.02 ppm, respectively, which were assigned to the SiH moiety. Two ²⁹Si chemical shifts were evident in the ¹H-²⁹Si gHMBC NMR spectra for **18** and **19** (²⁹Si δ = -33.1 and 14.4, -33.3 and 15.1) which were assigned to the SiH and SiOH moieties. The ¹H and ¹³C NMR spectra showed two different environments of Tip and ^tBu groups in each case. Broad signals at 1.69 and 1.77 ppm for **18** and **19**, respectively, were assigned to the -OH group and, accordingly, the signals disappeared upon the addition of D₂O to the NMR sample.

To identify the stereochemistry of the products, crystallographic data were obtained for one isomer. Crystals of **18** were obtained from **3Z** by slow evaporation of hexane giving colourless prisms after three weeks. The bond lengths and angles of **18** fall within normal ranges and are comparable to those of Mes^tBuSiH-SiⁱPrMes^tBu **7G**,³ a structurally related hydroxydisilane. The disorder observed in the -OH moiety and the -H atom is likely due to the bulk of the Tip and ^tBu groups which makes it difficult to find the SiH, and thus, approximate positions were obtained from difference Fourier maps (**Figure 2.1**). However, the disorder does not affect the assignment of stereochemistry.

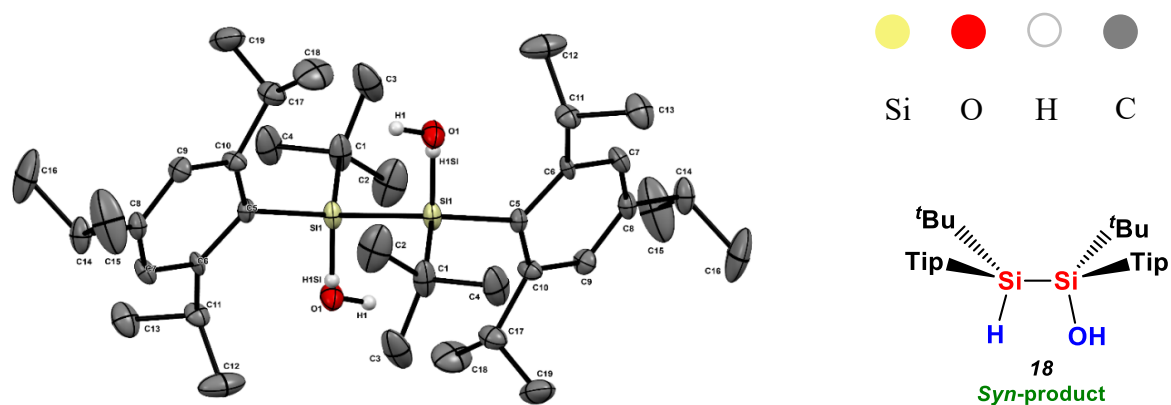
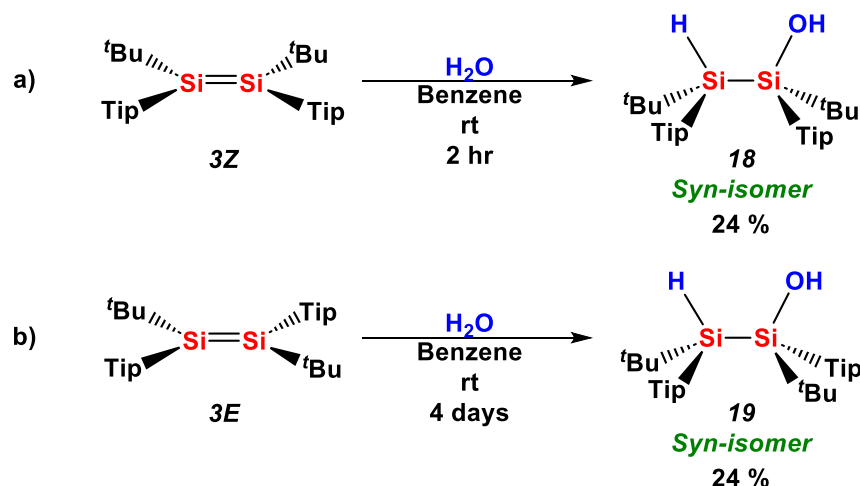


Figure 2.1: Molecular structure of **18**, Si-H not detected. Hydrogen atoms are omitted for clarity. Selected parameters (bond lengths in Å; bond angles in °): Si1-O1 1.7442(15), Si1-Si1¹ 2.4015(12), Si1¹-H1Si1 1.4210; O1-Si1-C1 105.92(7), O1-Si1-Si1¹ 104.32(6), H1Si1-Si1¹-C1 105.9.

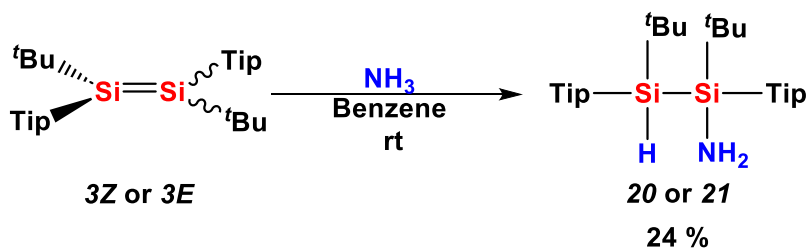
Despite the disorder in the molecular structure of **18**, the stereochemistry indicates the formation of *syn*-isomer from the addition of H₂O to **3Z**. Based on this evidence and as the ¹H and ²⁹Si NMR spectra indicate formation of two different isomers, **19** must also be the *syn*-diastereomer derived from the addition of H₂O to **3E** (**Scheme 2.4**).



Scheme 2.4: Addition of water to a) $3Z$ and b) $3E$ giving *syn*-isomers, 18 and 19 .

2.1.2 Addition of NH_3 *Z* or *E*-1,2-di-*tert*-butyl-1,2-bis(2,4,6-triisopropylphenyl)disilene ($3Z$ or $3E$)

The addition of ammonia to $3Z$ or $3E$ in benzene yields product 20 or 21 , respectively. Both reactions were 100 % stereospecific. The crude products yields were between 80-95 %. Additional purification was conducted by TLC using silica gel plates to give low isolated yields (**Scheme 2.5**).



Scheme 2.5: Addition of ammonia to $3Z$ or $3E$.

ESI-MS of 20 and 21 revealed signals at m/z 594.4891 and m/z 594.4887, respectively, which are consistent with the formula $C_{38}H_{68}NSi_2 [M+H^+]$. In each case, the ESI-MS revealed the formation of the 1:1 adduct between the disilene and ammonia.

The ATR-IR spectra were obtained of **20** and **21**. The broad signals at 3412 cm^{-1} and 3422 cm^{-1} were assigned to the $-\text{NH}_2$ group, respectively. The absorptions at 2179 cm^{-1} and 2113 cm^{-1} for **20** and **21**, respectively, were assigned to the Si-H stretching vibration.

The ^1H chemical shifts at 4.95 and 5.08 ppm were assigned to the SiH groups of **20** and **21**, respectively. Two signals were evident in the ^1H - ^{29}Si gHMBC NMR spectra of **20** or **21** (^{29}Si $\delta = -31.0$ and -2.3 , -34.8 and -0.71), and were assigned to the SiH and SiNH₂ groups, respectively. The ^1H and ^{13}C NMR spectra showed evidence for two different environments of Tip and *t*Bu substituents. Broad signals at 0.66 and 0.95 ppm in the ^1H NMR spectra of **20** and **21**, respectively, were assigned to $-\text{NH}_2$ group and, accordingly, the signals disappeared upon the addition of D_2O to the NMR sample.

To identify the stereochemistry of the products, crystallographic data were obtained for one isomer. Crystals of **21** were obtained from **3E** by slow evaporation of hexane giving colourless prisms after three weeks. The bond lengths and angles of **21** fall within the normal ranges and are comparable to those of **10B**, a structurally related aminodisilane.⁴ The disorder observed in the $-\text{NH}_2$ moiety and the $-\text{H}$ atom is likely due to the bulk of the Tip and *t*Bu groups which makes it difficult to observe the Si-H. Thus, approximate positions were obtained from difference Fourier maps (**Figure 2.2**). The disorder does not affect the stereochemical assignment.

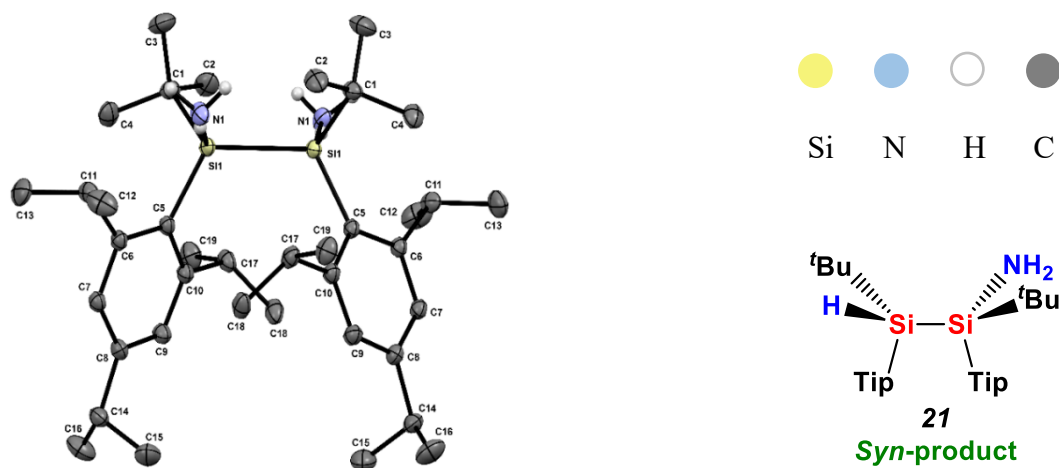


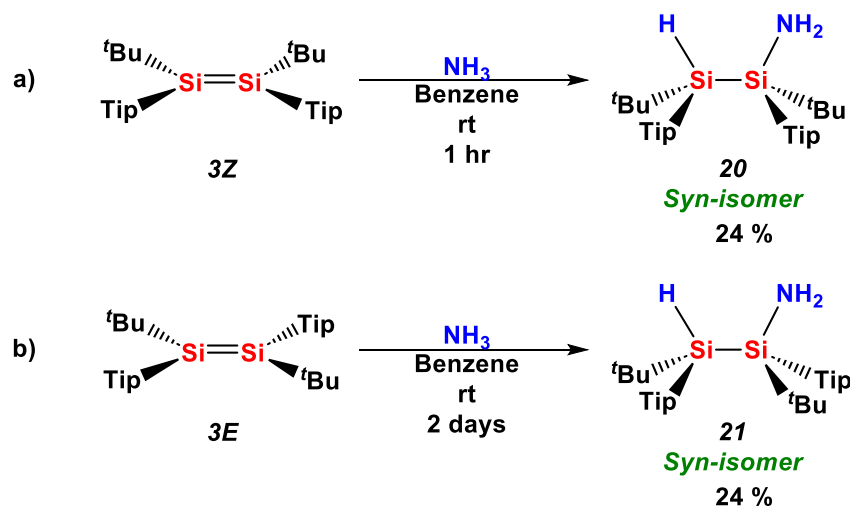
Figure 2.2: Molecular structure of **21**. Hydrogen atoms are omitted for clarity. Selected parameters (bond lengths in Å; bond angles in °) are given in **Table 2.1**.

The bond lengths and angles of **21** were compared to those of aminodisilane **10B** synthesized by Inoue and coworkers (Table 2.1).⁴ Despite the different substituents, there is no significant difference in the Si-N and Si-Si bond lengths and the N-Si-Si bond angles between **21** and **10B**. However, there is a significant difference in N1-Si1-C5 bond angles which can be attributed to the difference in the bulk of the substituents and their electronic effect.

Table 2.1: Important bond length and angles for **21** in comparison to **10B**.⁴

Atoms	Bond length (Å)		Atoms	Angle (°)	
	21	10B		21	10B
Si1-N7	1.744(2)	1.7497(15)	N1-Si1-C5	112.65(9)	100.0
Si1-Si1 ¹	2.423(8)	2.3984(6)	N1-Si1-Si1 ¹	100.01(8)	101.3
Si1 ¹ -H1Si1	1.4278	1.58	Si-Si-H	-	100.5

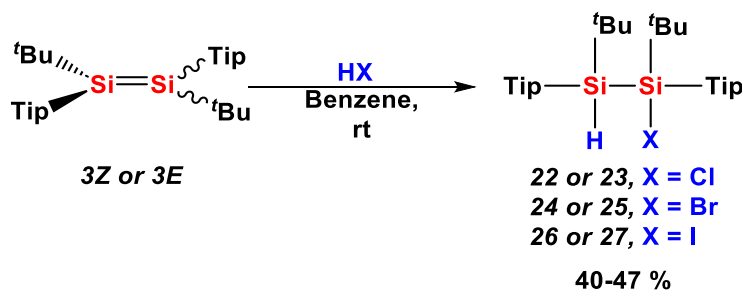
Despite the disorder in the molecular structure of **21**, the stereochemistry indicates the formation of *syn*-isomer from the addition of NH₃ to **3E**. Based on this evidence and as the ¹H and ²⁹Si NMR spectra indicate formation of two different isomers, **20** must be the *syn*-diastereomer derived from the addition of NH₃ to **3Z** (Scheme 2.6).



Scheme 2.6: Addition of ammonia to a) **3Z** and b) **3E** given *syn*-products **20** and **21**.

2.1.3 Addition of HX (X = Cl, Br, I) to *Z* or *E*-1,2-di-*tert*-butyl-1,2-bis(2,4,6-triisopropylphenyl)disilene (**3Z** or **3E**)

The addition of HX to **3Z** or **3E** in benzene yielded single isomers in each case; decolorization of the reaction mixture occurred within 5-10 min. In each reaction, only a single product was obtained in relatively high yields. The products were precipitated and washed with acetonitrile to remove excess acid; purification with TLC was conducted on products requiring further purification (**Scheme 2.7**).



Scheme 2.7: Addition of HX (X = Cl, Br, I) to **3Z** or **3E**.

ESI-MS of **22** or **23** revealed signals at m/z 635.4194 or m/z 635.4182, respectively, which are consistent with the formula $\text{C}_{38}\text{H}_{65}\text{NaClSi}_2$ [$\text{M}+\text{Na}^+$]. ESI-MS of **26** or **27** revealed signals at m/z 727.3524 and m/z 727.3547, respectively, which are consistent with the formula $\text{C}_{38}\text{H}_{65}\text{NaISi}_2$ [$\text{M}+\text{Na}^+$]. ESI-MS of **24** and **25** revealed signals at m/z 679.3700 and m/z 679.3700, respectively, which are consistent with the formula $\text{C}_{38}\text{H}_{65}\text{NaBrSi}_2$. In each case, the ESI-MS revealed the formation of the 1:1 adduct between the disilene and HCl, HBr, or HI.

The ATR-IR spectra of **22**, **23**, **24**, **25**, **26** and **27** were obtained. The signals at 2211, 2135, 2098, 2110, 2112, 2096 cm^{-1} were assigned to the SiH stretching vibration, respectively.

The ^1H chemical shifts (δ) of the SiH group and the ^{29}Si chemical shifts for the SiH and the SiX are listed in **Table 2.2**. The ^1H NMR and ^{13}C NMR spectroscopy showed two different Tip and ^tBu groups in each compound.

Table 2.2: Relevant ^1H and ^{29}Si Chemical shifts for compounds **22-27**.

Compound		^1H NMR	^{29}Si Chemical Shifts	
		SiH (δ)	SiH (δ)	SiX (δ)
X = Cl	22, 23	4.99, 5.21	-29.5, -34.8	21.3, 22.8
X = Br	24, 25	5.13, 5.28	-28.9, -35.1	17.8, 18.4
X = I	26, 27	5.33, 5.37	-26.4, -35.5	~ 5 , -0.4

To identify the stereochemistry of the products, crystallographic data were obtained for one compound in each pair of isomers. Crystals of **23**, **25**, and **27** were obtained by slow evaporation from a solution of hexane and acetonitrile giving colourless prisms (**Figure 2.3**).

The identity of X has little influence on the structure of the halodisilanes, other than on the Si-X bond length. As expected, the Si-X bond length increases with the size of the halogen (Cl < Br < I). However, the Si1-Si2, Si1-C(^tBu), Si1-C(Tip) bond lengths change by less than 1 % (Si1-Si2 \approx 2.4091(8) Si1-C(^tBu) \approx 1.933(12), Si1-C(Tip) \approx 1.9124(10)). Selected bond lengths (in Å) and bond angles (in $^\circ$) are given in **Table 2.3**.

Table 2.3: Selected bond lengths and angles for compounds **23**, **25**, and **27**.

Compound	Bond length (Å)		Bond Angle ($^\circ$)	
23	Si1-C11	2.113(7)	C1-Si1-C11	104.66(5)
	Si1-Si2 ¹	2.399(7)	C11-Si1-Si2	100.83(2)
	Si2-H2	1.391(16)	Si1-Si2-H2	100.06(6)
25	Si1A-Br1A	2.275(2)	C1A-Si1A-Br1A	105.0(2)
	Si1A-Si2A	2.416(7)	Br1A-Si1A-Si2A	98.29(2)
	Si2A-H2A	1.000	Si1A-Si2A-HI2A	103.3
27	Si1-I1	2.522(7)	C1-Si1-I1	106.67(5)
	Si1A-Si2A	2.423(9)	I1-Si1-Si2	98.06(2)
	Si2-H2	1.000	Si1-Si2-H2	103.2(6)

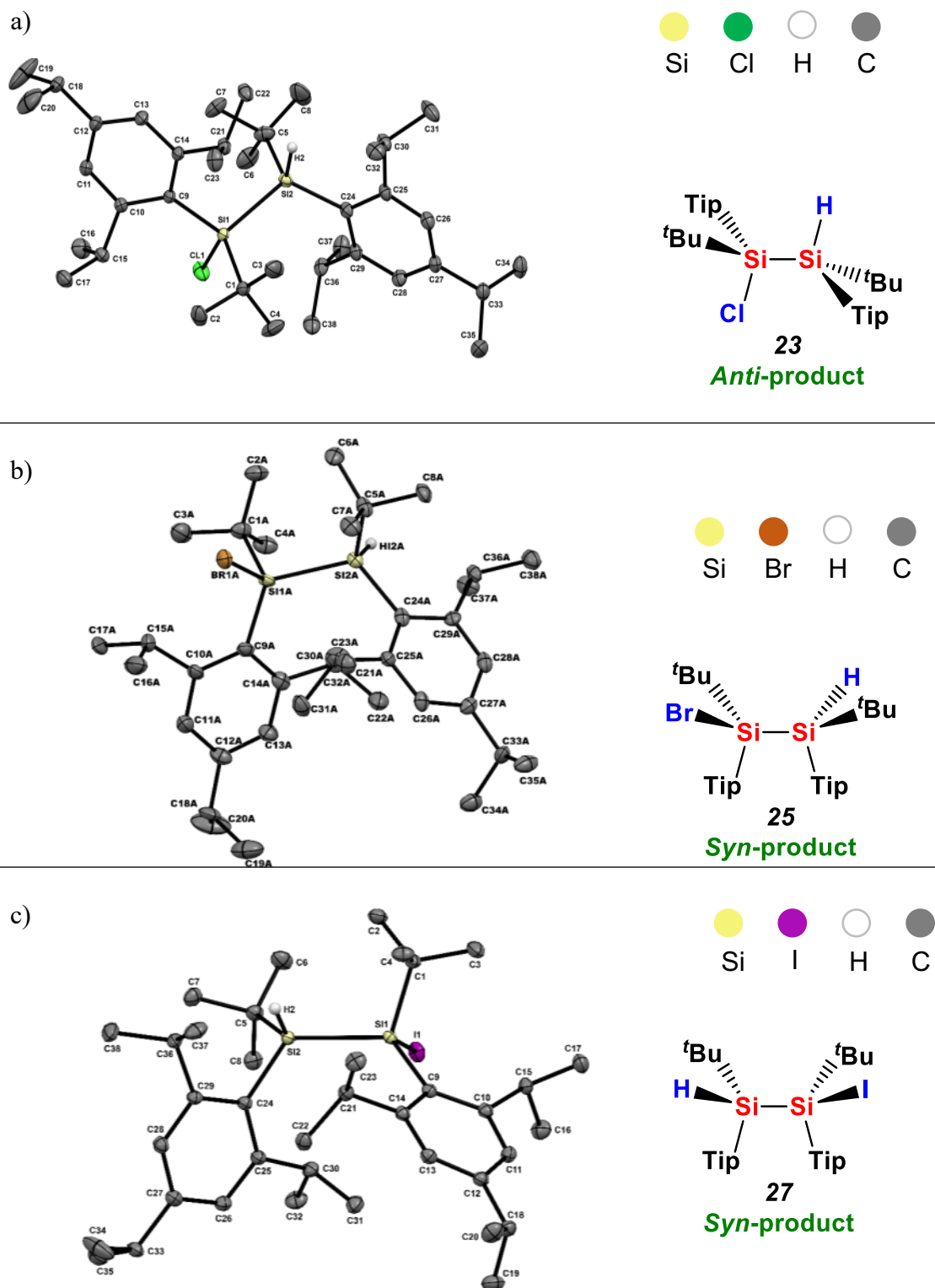
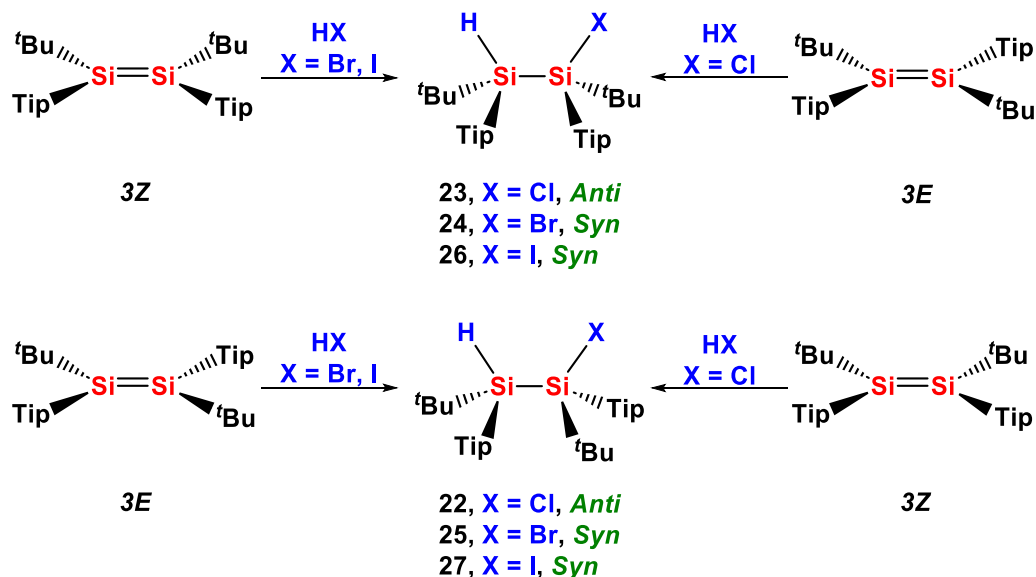


Figure 2.3: Molecular structure of a) 23, b) 25, and c) 27. Hydrogen atoms are omitted for clarity. Selected parameters (bond lengths in Å; bond angles in °) are given in **Table 2.3**.

The addition of HCl to disilene **3E** gave the *anti*-isomer. In contrast, the addition of HBr and HI to **3E** gave the *syn*-isomer. Each of these reactions were 100 % stereospecific and, given that the ^1H and ^{29}Si NMR spectroscopy data indicated the formation of the two isomeric products in the addition of HX to disilene **3Z** and **3E**, **22** must be the *anti*-diastereomer from the addition of HCl to **3Z**, and **24** and **26** are the *syn*-diastereomer for the addition of HBr and HI to **3Z**, respectively (Scheme 2.8).

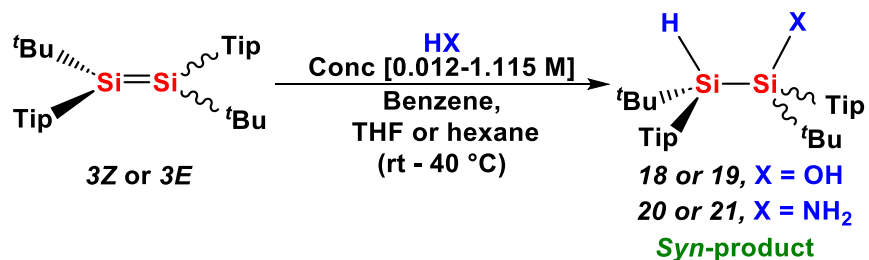


Scheme 2.8: Addition of HX to **3Z** and **3E** and the stereochemical outcome.

2.2 Influence of Reaction Conditions on the Stereochemistry of the Reaction

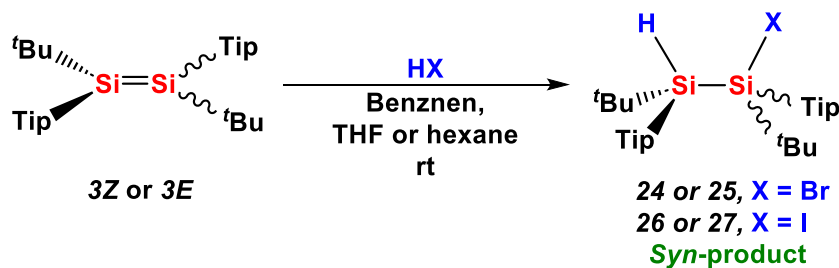
The conditions of the reactions for the addition of reagents to **3Z** or **3E** were altered to observe the influence of solvents, such as benzene, THF and hexane, temperature (rt to 40 °C) and concentration of reagents (0.012, 0.023, 0.115, 1.15 M) on the stereochemistry of the addition reaction. Other solvents such as dichloromethane, chloroform, acetonitrile, and benzonitrile were attempted. However, disilenes **3Z** and **3E** are reactive toward chlorinated solvents as observed previously with tetramesityldisilene **1**.⁵ Polar solvents such as acetonitrile ($\epsilon = 0.460$), and benzonitrile ($\epsilon = 0.333$),⁶ did not solubilize **3Z** and **3E**, and thus, were not investigated further.

The addition of H₂O and NH₃ to disilenes **3Z** and **3E** in tetrahydrofuran was 100 % stereospecific. The temperature of the reaction was increased (rt to 40 °C) in benzene or THF; no effect on the stereochemistry was observed. Different concentrations of H₂O and NH₃ (0.012, 0.023, 0.115, 1.15 M) ranging from 2 equivalents to 100 equivalents of reagent, were also examined. All reactions of the addition of H₂O or NH₃ to **3Z** or **3E** were 100 % stereospecific giving the *syn*-adduct under all conditions examined (**Scheme 2.9**).



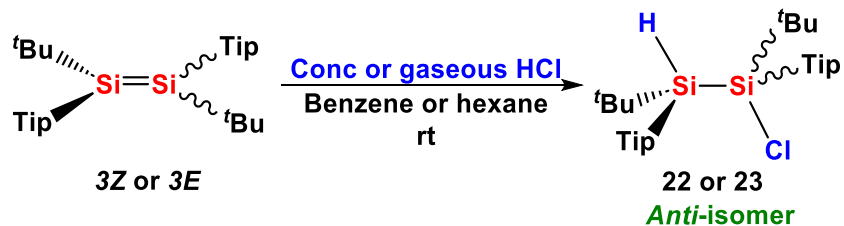
Scheme 2.9: Reaction conditions investigated in the addition of H₂O and NH₃ to **3Z** and **3E**.

In the addition of hydrogen halides to **3Z** and **3E**, the solvents examined were benzene, THF and hexane. All reactions were 100 % stereospecific giving the *syn*-isomer in the addition of HBr and HI; the *anti*-isomer was observed in the addition of HCl (**Scheme 2.10**).



Scheme 2.10: Reaction conditions investigated in addition of HI and HBr to **3Z** or **3E**.

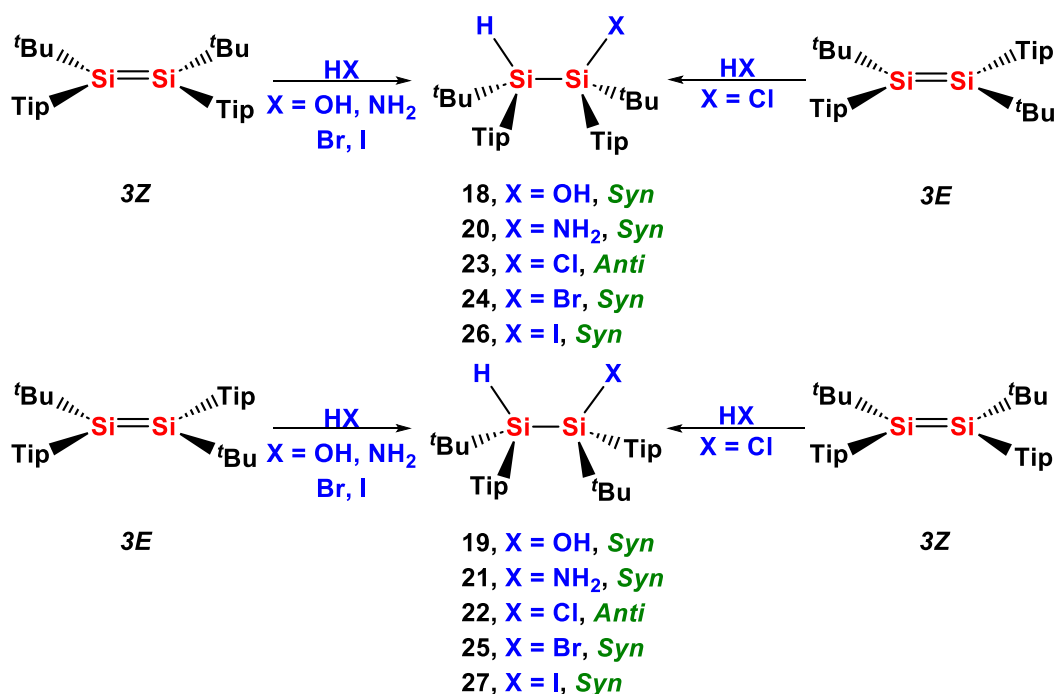
Furthermore, the addition of HCl to **3Z** and **3E** was conducted using concentrated aqueous HCl as the reagent, or gaseous HCl in hexane. The *anti*-isomer was formed using either reagent as indicated by ¹H-²⁹Si gHMBC NMR spectrum (**Scheme 2.11**). Further insight into the mechanism of the reaction is required to understand the stereochemical outcome of the HCl addition and why it varies from that of HBr and HI.



Scheme 2.11: Addition of concentrated aqueous or gaseous HCl to **3Z** or **3E**.

2.3 Discussion and Conclusion of Addition of HX (X = NH₂, OH, Cl, Br, I) to **3E** or **3Z**

The addition of ammonia, water, hydrobromic acid and hydroiodic acid to disilene **3Z** or **3E** under all conditions examined resulted in the exclusive formation of the *syn*-isomer. Interestingly, the addition of hydrochloric acid under the conditions examined gave the *anti*-isomer, and all reactions were 100 % stereospecific (**Scheme 2.12**).



Scheme 2.12: Addition of HX (X = OH, NH₂, Cl, Br, I) to **3Z** and **3E**.

The effect of solvent, temperature, and concentration of the reagent were studied. However, there was no effect on the stereochemistry of the reaction. Increasing the temperature from rt to 40 °C reduced the reaction time and lead to the formation of more impurities. Increasing the concentration of water or ammonia from 0.012-1.15 M only reduced the reaction time and did not affect the stereochemical outcome of the reaction.

These results contrast with the results of West and coworkers who reported that the addition of water to **6E** in THF was 50 % stereospecific forming a 1:1 mixture the diastereomers.³ Also, West and coworkers did not study the addition of water to *Z*-isomer (**6Z**) nor **3E** or **3Z**. It is difficult to understand the difference in the formation of the 1:1 diastereomer mixture observed in the addition of water to **6E** compared to that for **3E** and **3Z**, even though, disilenes **3E** and **6E** are both planar in geometry. After an attempt to synthesis and purify **6E**, isolating isomer **6Z** or **6E** was not possible as both isomers remained in solution. Thus, we hypothesized that disilene **6E** and was contaminated with **6Z**, resulting in the formation of a mixture of diastereomers.

In addition, the results of the addition of NH₃ to **3E** and **3Z** are in contrast with what Inoue and coworkers observed,⁴ regarding the sole formation of the *anti*-product **10B** in the addition of ammonia to **9Z** in hexane.

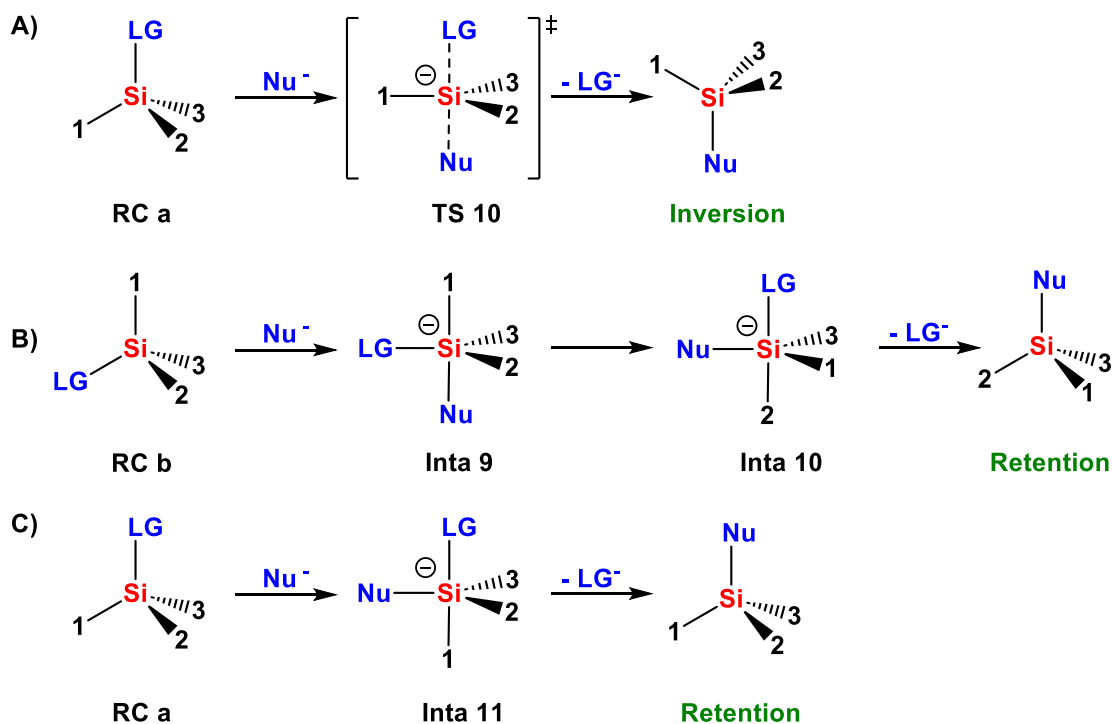
In conclusion, the addition of HX to disilene **3Z** or **3E** were all 100 % stereospecific giving the *syn*-isomer, except for HCl addition giving the *anti*-isomer. The reaction conditions did not influence the stereochemical outcome of the reactions. From these results, it can be concluded that no planar silicon is formed along the reaction pathway, and that any silicon with a lone pair generated throughout the reaction pathway must have a significant barrier to inversion. These conclusions, made on the basis of the stereochemistry of the reactions, must be taken into consideration in the formulation of the reaction mechanism which is considered in the next chapter.

2.4 Substitution of X at Si-X in Tetrahedral Silicon Compounds

2.4.1 Nucleophilic Substitution of X at Si-X

The substitution at the silicon center in silicon-containing compounds has been investigated since the 1960s.⁷ The stereochemistry of the substitution was explored to understand the mechanism of substitution and to compare it to substitution reactions at carbon centers.^{7, 8} Sommer,⁹ Prince,¹⁰ Corriu,¹¹ and coworkers have extensively investigated the nucleophilic substitution at the silicon center in organosilicon compounds.

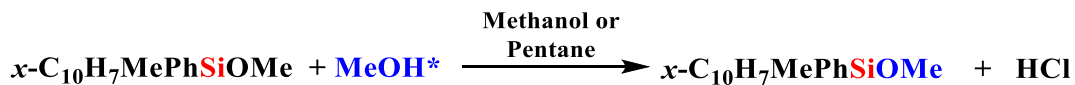
Three reaction pathways have been proposed for nucleophilic substitution at silicon: A) a pathway, similar to an S_N2 substitution in carbon, where the nucleophile approaches opposite to the leaving group (**TS 10**) resulting in inversion of configuration with or without the formation of a pentacoordinate intermediate, B) axial attack of the nucleophile to a substituent forming a pentacoordinate silicon intermediate **Inta 9** followed by pseudorotation (Ψ) to give **Inta 10** and then departure of the LG giving retention of configuration. C) Equatorial approach of the nucleophile between two substituents and formation of pentacoordinate silicon intermediate (**Inta 11**) where the LG is in an axial position followed by departure of the leaving group to give retention of configuration (**Scheme 2.13**).¹²



Scheme 2.13: Mechanism of nucleophilic substitution at silicon by; a) attack of the Nu axial to LG, b) axial attack of the Nu to a substituent then pseudorotation (Ψ), c) equatorial attack of the Nu to the LG.¹¹ Retention or inversion of configuration is noted for each mechanism.

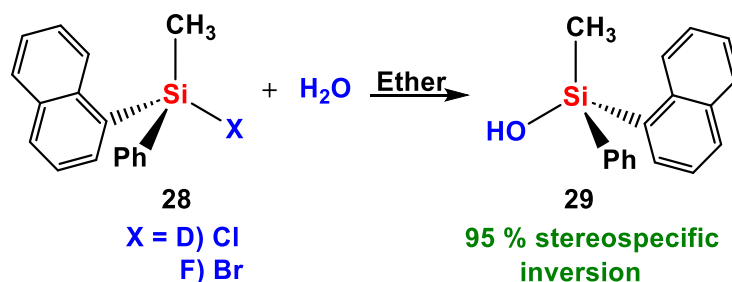
Recent computational studies have shown that the formation of a stable pentacoordinate intermediates during nucleophilic substitution at silicon is favored for silicon centers with bulky substituents. Studies have also shown that electronegative substituents at silicon favor a single step substitution mechanism.¹³

The strength of the leaving group can influence the reaction stereochemistry. The reactions with a good leaving group such as $-\text{Cl}$, $-\text{OCOR}$, which have a conjugate acid with a pK_a smaller than 5, predominantly favor inversion of configuration. However, a poor leaving group such as $-\text{H}$, $-\text{OCH}_3$, or $-\text{OH}$, whose conjugate acids have a pK_a larger than 10, the stereochemical outcome depends on other factors such as reaction conditions (i.e. solvent polarity or temperature). Inversion of configuration is more likely in polar solvents, and retention is more likely in non-polar solvents such as pentane (**Scheme 2.14**).¹⁴



Scheme 2.14: The addition of tritium methanol (*) to $x\text{-C}_{10}\text{H}_7\text{MePhSiOMe}$ in methanol (inversion) or pentane (retention).¹³

The substitution of silyl halides in R_3SiX ($\text{X} = \text{Cl}, \text{Br}$) with water in ether resulted in inversion of configuration (**Scheme 2.15**).¹⁵ Due to the good leaving group and the bulky substituents the reaction was proposed to proceed by an $\text{S}_{\text{N}}2\text{-Si}$ mechanism where the water molecules attacks from the axial to give a pentacoordinate intermediate, followed by expulsion of the leaving group X, resulting in inversion.

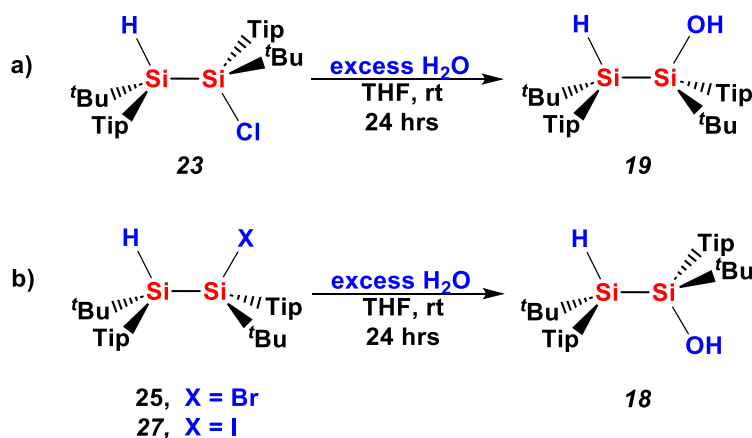


Scheme 2.15: Substitution at Si-X ($\text{X} = \text{Cl}$ or Br) with water by $\text{S}_{\text{N}}2\text{-Si}$.¹⁵

With the identification of the stereochemistry of compounds **20-27**, it is possible to examine the stereochemistry of the hydrolysis of bulky amine and halide derivatives of 1,2-di-*tert*-butyl-1,2-bis(2,4,6-triisopropylphenyl)disilanes. Based on previous work, it is hypothesized that inversion at the silicon center Si-X ($\text{X} = \text{Cl}, \text{Br}, \text{I}$) will be observed. To our knowledge, the stereochemistry of the hydrolysis of silylamines has not been studied. Given that the NH_2 group is a poor leaving group (LG), it is hypothesized that retention of configuration may be observed. To this end, the hydrolysis of functionalized disilenes **20-27** is investigated.

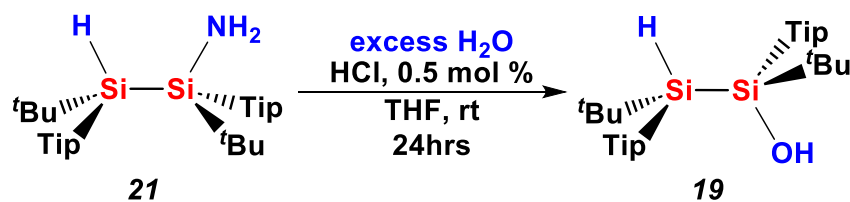
2.4.2 Hydrolysis of Disilanes **20-27**

The hydrolysis of 1,2-di-*tert*-butyl-1,2-bis(2,4,6-triisopropylphenyl)aminodisilane **21** and 1,2-di-*tert*-butyl-1,2-bis(2,4,6-triisopropylphenyl)halodisilanes **23**, **25**, **27** and their diastereomers, were conducted in THF at room temperature under ambient atmosphere. The reactions were monitored by ^1H NMR spectroscopy and had 100 % conversion for all derivatives. The products were identified by comparing the ^1H NMR data of the product of those synthesized by addition of H_2O to **3E** or **3Z**. For the halosilanes, inversion of configuration at the halosilanes was observed (**Scheme 2.16**). The results are aligned with Sommer and coworkers as they also observed inversion in the hydrolysis of **28D/F** (**Scheme 2.15**) complexes.¹⁵



Scheme 2.16: Hydrolysis reactions of Si-X in disilanes a) **23**, b) **25** and **27** via inversion.

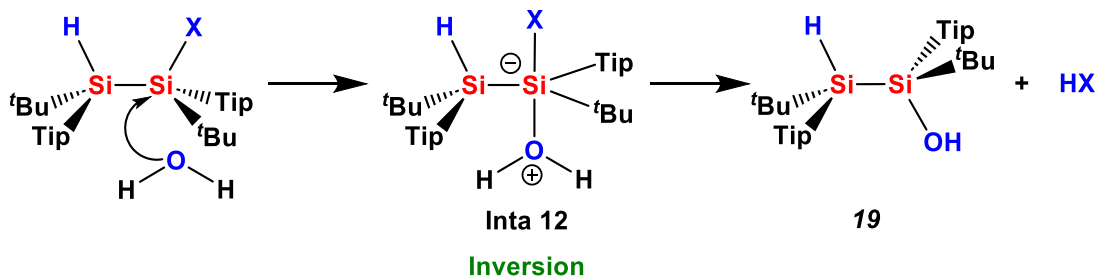
The hydrolysis of aminodisilane **21** in THF at rt did not proceed after 48 hrs. The reaction was also investigated with the addition of 0.5-5.0 mole % of NaOH to investigate if the reaction is base catalyzed; however, no hydrolysis was observed after 24 hrs. Alternatively, 0.5 mole % of HCl was added to determine if the reaction is acid catalyzed. The reaction proceeded after 24 hrs giving 100 % conversion to **18**, stereospecifically. Once again, inversion of configuration was observed (**Scheme 2.17**). The result of this reaction indicates the importance of a good leaving group.¹⁵ Catalyzing the reaction by the addition of an acid allows the conversion of a poor leaving group, $-\text{NH}_2$, into a good leaving group, $-\text{NH}_3^+$ leading to hydrolysis. The loss of a good leaving group results in inversion of configuration at the silicon center.



Scheme 2.17: Acid-catalyzed hydrolysis of aminodisilane **21**.

2.4.3 Discussion

On the basis of the results, the hydrolysis of **23** gave **18**, and the hydrolysis of **21**, **25** and **27** gave **19** providing clear evidence for inversion at the silicon center in all reactions (**Scheme 2.18**).



Scheme 2.18: General proposed mechanism for hydrolysis of SiX in bulky disilane including a pentacoordinate intermediate.

As reported by Sommer, when the leaving group is good, that is, when the electronegativity is low and pKa of the conjugate acid is less than 5,¹² inversion of configuration is predominant (**Table 2.4**), and that is what is observed for X = Cl, Br, I. The amino group -NH₂ is a bad leaving group (pKa of NH₃ is > 35) which is why it requires an acid catalyst to allow the reaction to proceed after the formation of good leaving group such as -NH₃⁺. The pKa of NH₄⁺ is 9.0 which should be a reasonable approximation for the [H₃NSi]⁺ species formed under acidic conditions with the disilylamines. For -NH₃⁺ as a leaving group, the stereochemical outcome may depend on other factors such as solvent polarity or temperature. Under the reaction conditions investigated here, THF as the solvent at room temperature, inversion of configuration was observed.

Table 2.4: Pauling electronegativity and pKa in water.¹⁶

Bond Si-X	Electronegativity of X	pKa in water (kcal/mol) ¹⁵
Si-F	3.98	3.2
Si-Cl	3.16	-2.2
Si-N	3.04	9.2
Si-Br	2.96	-4.7
Si-I	2.66	-5.2

The observed outcomes of these reactions are consistent with the observations of Sommer, a good leaving group leads to inversion of configuration and not retention. The bulky substituents in **20-27** may also influence the attack of the nucleophile to the silicon center. Retention requires the nucleophile to approach equatorial to the LG, and to overcome a pseudorotational (Ψ) barrier which could be large due to the bulky substituents.

2.5 Experimental Details

2.5.1 General Considerations

All reactions were conducted under an inert atmosphere of dried argon using Schlenk line techniques, or under an atmosphere of nitrogen in an MBraun glovebox. Glassware was dried prior to use by heating at 120 °C in a Lindberg/Blue M, Gravity Oven model number: G01390C-1, for approximately 20 hrs.

Dried solvents were obtained from an Innovative Technologies 400-5 Solvent Purification System. Solvents were stored over activated 4 Å molecular sieves before use, except for ACN which was stored over 3 Å molecular sieves. A stock solution of 0.1 M of water in THF was prepared and degassed under an atmosphere of argon. Ammonia, HCl, HBr, HI were purchased (0.4 M NH₃ solution in THF, Conc 12 M HCl, 47 wt % HBr in water, 57 wt % HI in water), from Sigma Aldrich. The synthesis of TipSiCl₃, Tip^tBuSiCl₂, **3Z** and **3E** Tip^tBuSi=SiTip^tBu were conducted following the literature procedures.^{17a-c}

¹H, ¹³C {¹H}, ¹H-¹H gCOSY, ¹H-¹³C gHMBC, ¹H-²⁹Si gHMBC and ¹H-¹³C gHSQC NMR spectra were recorded in C₆D₆ on a Bruker 400 MHz NMR spectrometry operating at a frequency of

400.13 MHz for ^1H and 100.61 MHz for ^{13}C . The chemical shift for the ^{29}Si were all extracted from the ^1H - ^{29}Si gHMBC. ^1H NMR spectra were referenced to $\text{C}_6\text{D}_5\text{H}$ (7.16 ppm), the ^{13}C was referenced to C_6D_6 (128.06 ppm); ^{29}Si NMR spectra were referenced to external TMS. Attenuated total reflection-infrared (ATR-IR) spectra were collected on a Bruker Alpha II spectrometer and the data were analyzed using the OPUS software package. Melting points were recorded on a Gallenkamp melting point apparatus.

Mass spectrometry data were obtained by Dr. Haidy Metwally and Dr. Aruni Chathu Pulukkody using electrospray ionization mass spectrometry (ESI-MS) on a Bruker microOTOF 11 or a Waters Synapt HMS spectrometer. A solution of the samples was infused into the electro-sprayer using a syringe pump; samples were diluted using methanol. NaI was routinely used as an iodizing agent, enabling the observance of several $[\text{M}+\text{Na}]^+$ species in the ESI-MS spectrum.

X-ray measurements were done by Dr. Paul D. Boyle using Bruker Kappa Axis Apex2 diffractometer at a temperature of 110 K. The samples were mounted on a Mitegen polyimide micromount with a small amount of Paratone N oil. Frame integration was performed using SAINT.¹⁸ The resulting raw data were scaled, and absorption corrected using a multi-scan averaging of symmetry equivalent data using SADAB,¹⁹ TWINABS.²⁰ for **27**, The COSET program was used to derive the possible twin laws for **25**. The structures were solved by using a dual space methodology using the SHELXT. The structure was refined using the SHELXL program from the SHELX suite of crystallographic software programs.²¹ All non-hydrogen atoms were obtained from the initial solution. The hydrogen atoms were introduced at idealized positions and were allowed to ride on the parent atom. The structural models were fit to the data using full matrix least-squares based on F^2 . The calculated structure factors included corrections for anomalous dispersion from the usual tabulation. The structures were refined using the SHELXL program from the SHELXTL suite of crystallographic software.²¹ Graphic plots were produced using the Mercury program.²²

2.5.2 Water Addition to **3Z** or **3E**.

Disilene **3Z** or **3E** (0.040 g, 0.069 mmol) was dissolved in benzene or THF (3 mL) to give a clear orange or yellow solution, respectively. A solution of water in THF (6.93 mL of 0.100 M

solution, 0.693 mmol) was added via syringe and stirred at room temperature for 3 days until the mixture became clear and colourless. The solvent was removed *in vacuo*. The products were purified on silica gel plates by Thin Layer Chromatography (TLC) using hexane:dichloromethane (70:30) as the eluent. Crystals of **17** were obtained via slow evaporation from hexane.

X = OH, 18 from **3Z**: Yield: 0.01 g, 24.0 %, white solid, M.P.: 135.8-139.0 °C, ^1H NMR (400 MHz, C_6D_6) δ : 1.14 (s, 9H, $^t\text{BuSiH}$), 1.15 (s, 9H, $^t\text{BuSiOH}$), 1.19 (d, $J = 8$ Hz, 9H, $^i\text{Pr-CH}_3$), 1.24 (d, $J = 8$ Hz, 6H, $^i\text{Pr-CH}_3$), 1.29, 1.30, 1.32 (each d, $J = 8$ Hz, 9H total, $^i\text{Pr-CH}_3$), 1.398, 1.402 (each d, $J = 6, 7$ Hz respectively, 6H total, $^i\text{Pr-CH}_3$), 1.46 (d, $J = 8$ Hz, 3H, $^i\text{Pr-CH}_3$), 1.63 (d, $J = 8$ Hz, 3H, $^i\text{Pr-CH}_3$), 1.69 (s, 1H, OH), 2.76, 2.80 (each sept, $J = 8$ Hz, 2H total, $o\text{-}^i\text{Pr-CH}$), 3.15 (sept, $J = 8$ Hz, 1H, $p\text{-}^i\text{Pr-CH}$), 3.46 (sept, $J = 8$ Hz, 1H, $p\text{-}^i\text{Pr-CH}$), 3.95 (d sept, $J = 1.6, 8$ Hz, 1H, $o\text{-}^i\text{Pr-CH}$), 4.09 (sept, $J = 8$ Hz, 1H, $o\text{-}^i\text{Pr-CH}$), 4.95 (d, $J = 1.6$ Hz, 1H, SiH), 7.12 (d, $J = 1.6$ Hz, 1H, $m\text{-ArH}$), 7.15 (δ extracted from $^1\text{H-}^{29}\text{Si}$ gHMBC spectrum, $m\text{-ArH}$), 7.26 (d, $J = 1.6$ Hz, 2H, $m\text{-ArH}$).

$^{13}\text{C}\{^1\text{H}\}$ NMR (101 MHz, C_6D_6) δ : 22.02, 22.94 ($^t\text{Bu-C}$), 23.99, 24.06, 24.07, 24.11, 24.56, 25.12, 25.42, 25.46, 25.77, 25.82, 27.39, 28.87 ($^i\text{Pr-CH}_3$), 29.19, 31.40 ($^t\text{Bu-CH}_3$), 32.24, 34.08 ($o\text{-}^i\text{Pr-CH}$), 34.54, 34.56 ($p\text{-}^i\text{Pr-CH}$), 35.30, 37.36 ($o\text{-}^i\text{Pr-CH}$), 120.88, 121.33, 122.35, 123.06 (Ar, $m\text{-CH}$), 129.54 (Ar, $i\text{-CSiH}$), 132.00 (Ar, $i\text{-CSiOH}$), 150.41, 150.50 (Ar, $p\text{-C}$), 155.27, 156.36, 156.87, 157.90 (Ar, $o\text{-C}$).

$^1\text{H-}^{29}\text{Si}$ HMBC NMR (400 MHz, C_6D_6) δ : -33.1 (SiH), 14.4 (SiOH).

ATR-IR (cm^{-1}): 3688 (w, -OH), 2960 (m), 2861 (m), 2170 (w, SiH), 1457 (m), 789 (s), 441 (s).

High resolution ESI-MS (negative ion) m/z $\text{C}_{38}\text{H}_{65}\text{OSi}_2$ $[\text{M-H}^-]$ calc. 593.4574, found 593.4575.

X = OH, 19 from **3E**:^a Yield: 0.01 g, 24.0 %, white solid, M.P.: 136.2-139.1 °C, ¹H NMR (400 MHz, C₆D₆) δ: 0.61 (d, *J* = 8 Hz, 3H, ^{*i*}Pr-CH₃), 0.77 (d, *J* = 8 Hz, 3H, ^{*i*}Pr-CH₃), 1.15, 1.16, 1.175 (each d, *J* = 8 Hz, 12H total, ^{*i*}Pr-CH₃), 1.23 (d, *J* = 6 Hz, 3H, ^{*i*}Pr-CH₃), 1.27, 1.28 (each d, *J* = 8 Hz, 6H total, ^{*i*}Pr-CH₃), 1.30, 1.31 (each s, ^{*t*}Bu, 18H total), 1.33 (d, *J* = 7 Hz, 3H, ^{*i*}Pr-CH₃), 1.36 (d, *J* = 7 Hz, 3H, ^{*i*}Pr-CH₃), 1.38 (d, *J* = 6 Hz, 3H, ^{*i*}Pr-CH₃), 1.77 (s, 1H, OH), 2.71, 2.77 (each sept, *J* = 8 Hz, 3H total, 2x *p*- and 1x *o*-^{*i*}Pr-CH), 3.16 (sept, *J* = 8 Hz, 1H, *o*-^{*i*}Pr-CH), 3.73 (d sept, *J* = 1.6, 8 Hz, 1H, *o*-^{*i*}Pr-CH), 3.93 (sept, *J* = 8 Hz, 1H, *o*-^{*i*}Pr-CH), 5.02 (d, *J* = 1.6 Hz, 1H, SiH), 6.96 (d, *J* = 1.6 Hz, 1H, *m*-ArH), 6.98 (d, *J* = 1.6 Hz, 1H, *m*-ArH), 7.16 (δ extracted from ¹H-²⁹Si gHMBC spectrum, *m*-ArH), 7.18 (d, *J* = 1.6 Hz, 1H, *m*-ArH).

¹³C {¹H} NMR (101 MHz, C₆D₆) δ: 21.57, 22.77 (^{*t*}Bu-C), 23.94 (2C, ^{*i*}Pr-CH₃), 24.10, 24.13, 24.16, 24.38, 24.45, 24.89, 25.01, 26.73, 27.61, 27.90 (^{*i*}Pr-CH₃), 29.75, 31.88 (^{*t*}Bu-CH₃), 32.43, 34.27 (*o*-^{*i*}Pr-CH), 34.46, 34.62 (*p*-^{*i*}Pr-CH), 36.31, 37.64 (*o*-^{*i*}Pr-CH), 121.40, 121.52, 122.50, 122.94 (Ar, *m*-CH), 129.87 (Ar, *i*-CSiH), 132.03 (Ar, *i*-CSiOH), 150.17, 150.37 (Ar, *p*-C), 155.10, 156.08, 156.26, 157.25 (Ar, *o*-C).

¹H-²⁹Si HMBC NMR (400 MHz, C₆D₆) δ: -33.3 (SiH), 15.1 (SiOH).

ATR-IR (cm⁻¹): 3690 (w, -OH), 2954 (m), 2857 (m), 2115 (w, SiH), 1455 (m), 775 (s).

High resolution ESI-MS (positive ion) *m/z* for C₃₈H₆₆NaOSi₂ [M+Na⁺] calc. 617.4544, found 617.4564.

^a There is evidence of an unknown impurity in the ¹H NMR spectrum of **19**.

2.5.3 Ammonia Addition to **3Z** or **3E**.

Disilene **3Z** or **3E** (0.040 g, 0.069 mmol) was dissolved in benzene or THF (3 mL) to give a clear orange or yellow, respectively. A solution of ammonia in THF (1.73 mL of 0.4 M solution, 0.693 mmol) was added via syringe and stirred at room temperature for up to 2 days until the mixture was clear and colourless. The solvent was removed *in vacuo*. The product was purified by TLC using a silica gel plate and cyclohexane as the eluent. Products **18** and **21** were crystallized by slow evaporation of a hexane solution.

X = NH₂, 20 from **3Z** : Yield: 0.01 g, 24.0 %, white solid, M.P.: 135.9-141.5 °C, ¹H NMR (400 MHz, C₆D₆) δ: 0.66 (s, 2H, NH₂), 0.98 (d, *J* = 8 Hz, 3H, ^{*i*}Pr-CH₃), 1.15 (s, 9H, ^{*t*}BuSiH), [1.18 (s, ^{*t*}BuSiNH₂), 1.19 (d, *J* = 8 Hz, ^{*i*}Pr-CH₃) 15H total], 1.22 (d, *J* = 8 Hz, 3H, ^{*i*}Pr-CH₃), 1.254, 1.257, 1.28 (each d, *J* = 8 Hz, 9H total, ^{*i*}Pr-CH₃), 1.31 (d, *J* = 7 Hz, 3H, ^{*i*}Pr-CH₃), 1.34 (d, *J* = 6 Hz, 3H, ^{*i*}Pr-CH₃), 1.45, 1.47 (each d, *J* = 7 Hz, 6H total, ^{*i*}Pr-CH₃), 1.63 (d, *J* = 6 Hz, 3H, ^{*i*}Pr-CH₃), 2.77, 2.82 (each sept, *J* = 8 Hz, 2H total, *p*-^{*i*}Pr-CH), 3.07 (sept, *J* = 8 Hz, 1H, *o*-^{*i*}Pr-CH), 3.66 (sept, *J* = 8 Hz, 1H, *o*-^{*i*}Pr-CH), 3.79 (sept, *J* = 8 Hz, 1H, *o*-^{*i*}Pr-CH), 4.03 (d sept, *J* = 1.6, 8 Hz, 1H, *o*-^{*i*}Pr-CH), 4.94 (d, *J* = 1.6 Hz, 1H, SiH), 7.11 (d, *J* = 1.6 Hz, 1H, *m*-ArH), 7.16 (δ extracted from ¹H-²⁹Si gHMBC spectrum, *m*-ArH), 7.27 (d, *J* = 1.6 Hz, 1H, *m*-ArH).

¹³C{¹H} NMR (101 MHz, C₆D₆) δ: 21.67, 22.59 (^{*t*}Bu-C), 24.03, 24.07, 24.11, 24.17, 24.96, 25.10, 25.35, 25.52, 25.72, 26.05, 26.39, 29.16 (^{*i*}Pr-CH₃), 30.09, 31.45 (^{*t*}Bu-CH₃), 32.73, 34.13 (*o*-^{*i*}Pr-CH), 34.53, 34.55 (*p*-^{*i*}Pr-CH), 34.81, 37.52 (*o*-^{*i*}Pr-CH), 120.69, 121.36, 122.19, 122.87 (Ar, *m*-CH), 130.37 (Ar, *i*-CSiH), 133.18 (Ar, *i*-CSiNH₂), 150.0 (2C, Ar, *p*-C), 155.41, 155.99, 156.69, 157.56 (Ar, *o*-C).

¹H-²⁹Si HMBC NMR (400 MHz, C₆D₆) δ: -31.0 (SiH), -2.3 (SiNH₂).

ATR-IR (cm⁻¹): 3412 (w, SiNH₂), 2960 (m), 2919 (m), 2179 (w, SiH), 1459 (m), 876 (m), 439 (s).

High resolution ESI-MS (positive ion) *m/z* for C₃₈H₆₈NSi₂ [M+H⁺] calc. 594.4885, found 594.4891.

X = NH₂, 2I from **3E** : Yield: 0.01 g, 24.0 %, white solid, M.P.: 136.9-141.5 °C, ¹H NMR (400 MHz, C₆D₆) δ: 0.45 (d, *J* = 8 Hz, 3H, ^{*i*}Pr-CH₃), 0.68 (d, *J* = 8 Hz, 3H, ^{*i*}Pr-CH₃), 0.95 (br s, 2H, NH₂), 1.15, 1.157, 1.161 (each d, *J* = 8 Hz, 12H total, ^{*i*}Pr-CH₃), [1.26 (d, *J* = 8 Hz, ^{*i*}Pr-CH₃), 1.275 (^{*i*}Pr-CH₃), 1.28 (s, ^{*t*}BuSiNH₂), 1.29 (s, ^{*t*}BuSiH), 24H total], 1.31 (d, *J* = 7 Hz, 3H, ^{*i*}Pr-CH₃), 1.38, 1.39, 1.42 (each d, *J* = 7 Hz, 9H total, ^{*i*}Pr-CH₃), [2.70 (sept, *J* = 8 Hz, *p*-^{*i*}Pr-CH), 2.72 (sept, *J* = 8 Hz, *p*-^{*i*}Pr-CH), 2.77 (sept, *J* = 8 Hz, *o*-^{*i*}Pr-CH), 3H total], 3.20 (sept, *J* = 8 Hz, 1H, *o*-^{*i*}Pr-CH), 3.67 (sept, *J* = 8 Hz, 1H, *o*-^{*i*}Pr-CH), 3.89 (d sept, *J* = 1.6, 8 Hz, 1H, *o*-^{*i*}Pr-CH), 5.08 (d, *J* = 1.6 Hz, 1H, SiH), 6.96 (d, *J* = 1.6 Hz, 2H, *m*-ArH), 7.14 (δ extracted from ¹H-²⁹Si gHMBC spectrum, *m*-ArH), 7.19 (d, *J* = 1.6 Hz, 1H, *m*-ArH).

¹³C{¹H} NMR (101 MHz, C₆D₆) δ: 22.14, 22.27 (^{*t*}Bu-C), 23.94, 23.97, 24.09, 24.12, 24.19, 24.40, 24.73, 25.11, 25.26, 26.50, 27.07, 27.67 (^{*i*}Pr-CH₃), 30.41, 32.22 (^{*t*}Bu-CH₃), 32.91, 34.21 (*o*-^{*i*}Pr-CH), 34.35, 34.62 (*p*-^{*i*}Pr-CH), 36.39, 37.61 (*o*-^{*i*}Pr-CH), 121.59, 121.72, 122.61, 122.74 (Ar, *m*-CH), 130.47 (Ar, *i*-CSiH), 133.24 (Ar, *i*-CSiNH₂), 149.55, 150.12 (Ar, *p*-C), 155.28, 156.04, 156.11, 157.53 (Ar, *o*-C).

¹H-²⁹Si HMBC NMR (400 MHz, C₆D₆) δ: -34.8 (SiH), -0.7 (SiNH₂).

ATR-IR (cm⁻¹): 3422 (w, SiNH₂), 2954 (s), 2857 (m), 2113 (m, SiH), 1455 (m), 771 (s), 441 (s).

High resolution ESI-MS (positive ion) *m/z* for C₃₈H₆₈NSi₂ [M+H⁺] calc. 594.4885, found 594.4887.

2.5.4 Addition of HX (X = Cl, Br, I) to **3Z** or **3E**

Disilene **3Z** or **3E** (0.040 g, 0.069 mmol) was dissolved in benzene or THF (3 mL) to give a clear orange or yellow solution, respectively. A solution of concentrated HCl (0.02 mL of 12 M solution in H₂O, 0.693 mmol) or HBr (0.04 mL of 0.47 M solution, 0.693 mmol), or HI (0.03 mL, 0.57 M solution, 0.693 mmol) was added via syringe into the mixture and stirred at room temperature for 30 min until the mixture became clear and colourless. The solvent was removed *in vacuo*. The product was isolated by washing the white solid with acetonitrile; further purification

was not necessary. Crystals of compounds **23**, **25**, and **27** were obtained via slow evaporation of THF from a mixture of THF and acetonitrile.

X = Cl, 22 from **3Z**: Yield: 0.01 g, 47.0 %, white solid, ^1H NMR (400 MHz, C_6D_6) δ : 1.11 (s, 9H, $^t\text{BuSiH}$), [1.185 (s, $^t\text{BuSiCl}$), 1.18-1.24 (overlapping d, $^i\text{Pr-CH}_3$), 27H total], 1.35 (d, $J = 8$ Hz, 3H, $^i\text{Pr-CH}_3$), 1.37 (d, $J = 8$ Hz, 3H, $^i\text{Pr-CH}_3$), 1.43 (d, $J = 8$ Hz, 3H, $^i\text{Pr-CH}_3$), 1.49 (d, $J = 8$ Hz, 3H, $^i\text{Pr-CH}_3$), 1.53 (d, $J = 8$ Hz, 3H, $^i\text{Pr-CH}_3$), 1.66 (d, $J = 8$ Hz, 3H, $^i\text{Pr-CH}_3$), 2.769, 2.776 (each sept, $J = 8$ Hz, 2H total, p - $^i\text{Pr-CH}$), 3.29 (sept, $J = 8$ Hz, 1H, o - $^i\text{Pr-CH}$), 3.50 (sept, $J = 8$ Hz, 1H, o - $^i\text{Pr-CH}$), 3.86 (sept, $J = 8$ Hz, 1H, o - $^i\text{Pr-CH}$), 4.16 (sept, $J = 8$ Hz, 1H, o - $^i\text{Pr-CH}$), 4.99 (s, 1H, SiH), 7.14 (d, $J = 1.6$ Hz, 1H, m -ArH), 7.21 (d, $J = 1.6$ Hz, 1H, m -ArH), 7.25 (d, $J = 1.6$ Hz, 1H, m -ArH). Sample contaminated with ~15 % of **23**.

$^{13}\text{C}\{^1\text{H}\}$ NMR (101 MHz, C_6D_6) δ : 23.56, 23.93, 23.99, 24.03, 24.04, 24.65, 24.78, 25.43, 25.86, 25.98, 26.21 (br s), 27.29 (br s), 29.68, 30.24 ($^i\text{Pr-CH}_3$ and ^tBuC), 29.12, 31.26 (^tBu), 33.52, 34.08 (o - $^i\text{Pr-CH}$), 34.46, 34.53 (p - $^i\text{Pr-CH}$), 36.46, 37.65 (o - $^i\text{Pr-CH}$), 120.97, 121.71, 122.21, 123.71 (Ar, m -CH), 128.71 (Ar, i -CSiH), 129.29 (Ar, i -CSiCl), 150.48, 151.34 (Ar, p -C), 156.05, 156.26 (Ar, o -C), 156.6 (δ extracted from ^1H - ^{13}C gHMBC spectrum, Ar, o -C) 158.63 (Ar, o -C).

^1H - ^{29}Si HMBC NMR (400 MHz, C_6D_6) δ : -29.5 (SiH), 21.3 (SiCl).

ATR-IR (cm^{-1}): 2957 (s), 2926 (m), 2864 (m), 1459 (m), 875 (m), 494 (s), 436 (s).

High resolution ESI-MS m/z for $\text{C}_{38}\text{H}_{65}\text{NaClSi}_2$ [$\text{M}+\text{Na}^+$] calc. 635.4206, found 635.4194.

X = Cl, 23 from **3E**: Yield: 0.01 g, 47.0 %, white solid, M.P.: 157.2-160.3 $^\circ\text{C}$, ^1H NMR (400 MHz, C_6D_6) δ : 0.32 (br d, $J = 8$ Hz, 3H, $^i\text{Pr-CH}_3$), 0.59 (d, $J = 8$ Hz, 3H, $^i\text{Pr-CH}_3$), 1.105, 1.110 (each br d, $J = 7, 8$ Hz respectively, 6H total, $^i\text{Pr-CH}_3$), 1.15 (d, $J = 8$ Hz, 6H, $^i\text{Pr-CH}_3$), 1.19 (br d, $J = 8$ Hz, 3H, $^i\text{Pr-CH}_3$), 1.32 (d, $J = 8$ Hz, 6H, $^i\text{Pr-CH}_3$), [1.35, 1.36 (br s, $^t\text{BuSiH}$, $^t\text{BuSiCl}$, respectively), 1.37 ($^i\text{Pr-CH}_3$), 1.39 (d, $J = 8$ Hz, $^i\text{Pr-CH}_3$), 24H total], 1.58 (d, $J = 8$ Hz, 3H, $^i\text{Pr-CH}_3$), 2.61, 2.65, 2.69 (each sept, $J = 8$ Hz, 3H total, 2 p -, o - $^i\text{Pr-CH}$), 3.32 (sept, $J = 8$ Hz, 1H, o - $^i\text{Pr-CH}$), 3.89 (d sept, $J = 1.6, 8$ Hz, 1H, o - $^i\text{Pr-CH}$), 4.21 (br sept, $J = 8$ Hz, 1H, o - $^i\text{Pr-CH}$), 5.21 (d, $J = 1.6$ Hz, 1H,

SiH), 6.92 (br d, $J = 1.6$ Hz, 1H, *m*-ArH), 6.95 (d, $J = 1.6$ Hz, 1H, *m*-ArH), 7.19 (d, $J = 1.6$ Hz, 2H, *m*-ArH).

$^{13}\text{C}\{^1\text{H}\}$ NMR (101 MHz, C_6D_6) δ : 23.61, 23.65, 23.76, 23.90, 23.94, 24.16, 24.24, 24.28, 24.70, 25.02, 25.32, 26.73, 27.13, 27.73 (*i*Pr-CH₃ and *t*Bu-C), 30.24, 31.46 (*t*Bu-CH₃), 33.16, 34.12 (*o*-*i*Pr-CH), 34.29, 34.61 (*p*-*i*Pr-CH), 37.29, 38.03 (*o*-*i*Pr-CH), 121.92, 122.14, 122.87, 124.06 (Ar, *m*-CH), 128.59 (Ar, *i*-CSiH), 129.19 (Ar, *i*-CSiCl), 150.69, 150.84 (Ar, *p*-C), 155.25, 156.11, 156.82, 157.89 (Ar, *o*-C).

^1H - ^{29}Si HMBC NMR (400 MHz, C_6D_6) δ : -34.8 (SiH), 22.8 (SiCl).

ATR-IR (cm^{-1}): 2960 (s), 2933 (m), 2864 (m), 2135 (w, SiH), 1721 (m), 1463 (m), 496 (s).

High resolution ESI-MS m/z for $\text{C}_{38}\text{H}_{65}\text{NaClSi}_2$ [$\text{M}+\text{Na}^+$] calc. 635.4206, found 635.4182.

X = Br, 24 from **3Z**: Yield: 0.01 g, 40 %, white solid, M.P.: 132.5-134.2 °C, ^1H NMR (400 MHz, C_6D_6) δ : 1.14 (s, 9H, *t*Bu-SiH), [1.18 (d, $J = 8$ Hz, *i*Pr-CH₃), 1.19 (d, $J = 8$ Hz, *i*Pr-CH₃), 1.21 (d, $J = 8$ Hz, *i*Pr-CH₃), 1.22 (d, $J = 8$ Hz, *i*Pr-CH₃), 1.26 (s, *t*BuSiBr), 27H total, 2d for *i*PrCH₃ not visible], 1.35 (d, $J = 8$ Hz, 6H, *i*Pr-CH₃), 1.43 (d, $J = 8$ Hz, 3H, *i*Pr-CH₃), [\sim 1.50 (*i*Pr-CH₃), 1.51 (d, $J = 8$ Hz, *i*Pr-CH₃), 6H total], 1.65 (d, $J = 8$ Hz, 3H, *i*Pr-CH₃), 2.76, 2.77 (each sept, $J = 8$ Hz, 2H total, *p*-*i*Pr-CH), 3.25 (br s, 1H, *o*-*i*Pr-CH), 3.57 (sept, $J = 8$ Hz, 1H, *o*-*i*Pr-CH), 3.90 (sept, $J = 8$ Hz, 1H, *o*-*i*Pr-CH), 4.27 (sept, $J = 8$ Hz, 1H, *o*-*i*Pr-CH), 5.13 (s, 1H, SiH), [7.13 (d, $J = 1.6$ Hz, *m*-ArH), 7.14 (d, $J = 1.6$ Hz, *m*-ArH), 2H total], 7.20 (d, $J = 1.6$ Hz, 1H, *m*-ArH), 7.25 (d, $J = 1.6$ Hz, 1H, *m*-ArH).

$^{13}\text{C}\{^1\text{H}\}$ NMR (101 MHz, C_6D_6) δ : 23.90, 23.99, 24.01, 24.03, 24.09 (br s), 24.15, 24.24 (br s), 24.42 (br s), 24.95 (br s), 25.31, 26.07, 26.17, 27.03 (br s), 29.74 (*i*Pr-CH₃ and *t*BuC), 29.64, 31.22 (*t*Bu-CH₃), 34.15, 34.20 (*o*-*i*Pr-CH), 34.44, 34.52 (*p*-*i*Pr-CH), 36.49, 37.98 (each br s, *o*-*i*Pr-CH), 120.95, 121.70, 122.34, 123.91 (Ar, *m*-CH), 127.60 (δ extracted from ^1H - ^{13}C gHMBC spectrum, Ar, *i*-CSiH), 129.49 (Ar, *i*-CSiBr), 150.42, 151.39 (Ar, *p*-C), 156.09, 156.29 (2C), 158.93 (Ar, *o*-C).

^1H - ^{29}Si HMBC NMR (400 MHz, C_6D_6) δ : -28.9 (SiH), 17.8 (SiBr).

ATR-IR (cm^{-1}): 2951 (s), 2862 (m), 2098 (w), 1464 (m), 451 (s), 412 (m).

High resolution ESI-MS m/z for $\text{C}_{38}\text{H}_{65}\text{NaBrSi}_2$ [$\text{M}+\text{Na}^+$] calc. 679.3728, found 679.3700.

X = Br, 25 from **3E**: Yield: 0.01 g, 43.0 %, white solid, M.P.: 147.1-150.1 °C, ^1H NMR (400 MHz, C_6D_6) δ : 0.29 (br s, 3H, $^i\text{Pr-CH}_3$), 0.63 (d, $J = 8$ Hz, 3H, $^i\text{Pr-CH}_3$), 1.10 (d, $J = 7$ Hz, 6H, $^i\text{Pr-CH}_3$), 1.15 (d, $J = 8$ Hz, 6H, $^i\text{Pr-CH}_3$), 1.20 (br s, 3H, $^i\text{Pr-CH}_3$), [1.31 (δ extracted from ^1H - ^1H COSY, br s, $^i\text{Pr-CH}_3$), 1.33 (d, $J = 8$ Hz, $^i\text{Pr-CH}_3$), 1.36 (s, $^t\text{BuSiH}$), 1.37 (s, $^t\text{BuSiBr}$), 1.36, 1.39 (δ extracted from COSY, $^i\text{Pr-CH}_3$), 26H total], 1.57 (br s, 3H, $^i\text{Pr-CH}_3$), [2.6 (br s, o - $^i\text{PrCH}$), 2.64 (sept, $J = 8$ Hz, p - $^i\text{Pr-CH}$), 2.70 (sept, $J = 8$ Hz, o - $^i\text{Pr-CH}$), 3H total], 3.42 (sept, $J = 8$ Hz, 1H, o - $^i\text{Pr-CH}$), 3.90 (d sept, $J = 1.6, 8$ Hz, 1H, o - $^i\text{Pr-CH}$), 4.42 (br s, 1H, o - $^i\text{Pr-CH}$), 5.28 (d, $J = 1.6$ Hz, 1H, SiH), [6.93 (br s, m -ArH), 6.96 (d, $J = 1.6$ Hz, m -ArH), 2H total], 7.19 (d, $J = 1.6$ Hz, 1H, m -ArH), (m -ArH)^b.

$^{13}\text{C}\{^1\text{H}\}$ NMR (101 MHz, C_6D_6) δ : 23.73, 23.89 (3C), 24.17, 24.18, 24.32, 24.51, 24.99, 25.24 (br s)^c below, 25.32, 26.80, 26.89 (br s), 27.70 (br s) ($^i\text{Pr-CH}_3$ and ^tBuC), 30.26 ($^t\text{Bu-CH}_3$), 31.50 ($^t\text{Bu-CH}_3$), 33.46 (br s, o - $^i\text{Pr-CH}$), 34.01 (o - $^i\text{Pr-CH}$), 34.22, 34.61 (p - $^i\text{Pr-CH}$), 37.54, 38.32 (o - $^i\text{Pr-CH}$), 122.17 (br s, Ar, m -CH)^c, 122.26, 122.99, 124.28 (Ar, m -CH), 128.74 (Ar, i -CSiH), (i -CSiBr)^c, 150.76, 150.84 (Ar, p -C), 155.43 (br s, Ar, o -C)^c, 156.09, 156.89, 158.13 (br s, Ar, o -C)^c.

^1H - ^{29}Si HMBC NMR (400 MHz, C_6D_6) δ : -35.1 (SiH), 18.4 (SiBr).

^b Unable to locate

^c Tentative assignment

ATR-IR (cm⁻¹): 2955 (s), 2862 (m), 2110 (w, Si-H), 1601 (w), 1461 (s), 1360 (w), 840 (m), 768 (s), 453 (s).

High resolution ESI-MS m/z for C₃₈H₆₅NaBrSi₂ [M+Na⁺] calc. 679.3728, found 679.3700.

X = I, 26 from **3Z**: Yield: 0.01g, 40 %, white solid, ¹H NMR (400 MHz, C₆D₆) δ: 0.9 (br s, ^tBuSiI), [1.184 (d, $J = 7$ Hz, ⁱPr-CH₃), 1.189 (s, ^tBu), 1.19 (d, $J = 7$ Hz, ⁱPr-CH₃), 1.211 (d, $J = 7$ Hz, ⁱPr-CH₃), 1.214 (d, $J = 7$ Hz, ⁱPr-CH₃), 27H total (including 2 broad signals not clearly evident)], 1.32 (d, $J = 7$ Hz, ⁱPr-CH₃), [1.44 (d, $J = 7$ Hz, ⁱPr-CH₃), 1.4 (br s, ⁱPr-CH₃), 6H total], 1.57 (br d, $J = 7$ Hz, 3H, ⁱPr-CH₃), 1.6, 1.8 (each br s, 6H total, ⁱPr-CH₃), 2.67 (sept, $J = 7$ Hz, p -ⁱPr-CH), 3.11 (br s, 1H, o -ⁱPr-CH), 3.67 (br s, 1H, o -ⁱPr-CH), 3.97 (br s, 1H, o -ⁱPr-CH), 4.46 (br s, 1H, o -ⁱPr-CH), 5.33 (s, 1H, SiH), 7.10 (br s, 1H, m -ArH), 7.18 (br s, m -ArH), 7.26 (br d, 1H, $J = 2$ Hz, m -ArH). Sample is contaminated with ~ 10 % of the water adduct **18**. Large unidentified signal at 1.37 ppm in the ¹H NMR spectrum.

¹³C{¹H} NMR (101 MHz, C₆D₆) δ: 23.15, 23.58, 23.87, 23.99, 24.01, 24.03, 25.06, 25.3 (br s), 26.2 (br s), 30.24, 30.5 (br s), 31.21 (ⁱPr-CH₃, ^tBu, ^tBuC, 2 signals not located), 34.17 (o -ⁱPr-CH), 34.40, 34.51 (p -ⁱPr-CH), 35.3 (br s, o -ⁱPrCH), 37.8 (δ extracted from ¹³C-¹H HSQC spectrum, o -ⁱPrCH), 38.50 (br s, o -ⁱPrCH), 121.02 (br s, Ar, m -CH), 121.67, 122.67 (Ar, m -CH), 124.14 (br s, Ar, m -CH), 126.10 (Ar, i -CSiH), 130.3 (Ar, i -CSiI, δ extracted from ¹H-¹³C HMBC spectrum), 150.38, 151.27 (Ar, p -C), 155.4 (δ extracted from ¹³C-¹H HMBC spectrum, Ar, o -C), 156.36 (Ar, o -C), 159.05 (br s, Ar, o -C), (Ar, o -C)^d.

¹H-²⁹Si HMBC NMR (400 MHz, C₆D₆) δ: -26.4 (SiH), ~ 5 (SiI)^c.

ATR-IR (cm⁻¹): 2955 (s), 2854 (s), 2112 (SiH, w), 1457 (m), 1362 (m), 1034 (s), 783 (s), 441 (m).

High resolution ESI-MS m/z for C₃₈H₆₅NaISi₂ [M+Na⁺] calc. 727.3562, found 727.3524.

X = I, 27 from **3E**: Yield: 0.01g, 40 %, white solid, M.P.: 167.1-168.9 °C, ¹H NMR (400 MHz, C₆D₆) δ: 0.68 (d, $J = 8$ Hz, 3H, ⁱPr-CH₃), 1.09 (d, $J = 8$ Hz, 6H, ⁱPr-CH₃), 1.15 (d, $J = 8$ Hz, 6H,

¹H NMR (400 MHz, C₆D₆) δ: 1.24 (br s, ⁱPr-CH₃), 1.35 (d, *J* = 8 Hz, ⁱPr-CH₃), 1.360 (d, *J* = 8 Hz, ⁱPr-CH₃), 1.363 (s, ^tBuSiH), 1.385 (s, ^tBuSiH), 1.387 (d, *J* = 8 Hz, ⁱPr-CH₃), 1.53 (br s, ⁱPr-CH₃), 39H total], [2.6 (br s, *o*-ⁱPr-CH₃), 2.62, 2.70 (each sept, *J* = 8 Hz, *p*-ⁱPr-CH), 3H total], 3.50 (sept, *J* = 8 Hz, 1H, *o*-ⁱPr-CH), 3.90 (d sept, *J* = 1.6, 8 Hz, 1H, *o*-ⁱPr-CH), 4.67 (br s, 4H, *o*-ⁱPr-CH), 5.37 (d, *J* = 1.6 Hz, 1H, SiH), 6.96 (d, *J* = 1.6 Hz, *m*-ArH), 7.20 (d, *J* = 1.6 Hz, 1H, *m*-ArH), (2x *m*-ArH)^c.

¹³C {¹H} NMR (101 MHz, C₆D₆) δ: 23.68, 23.69, 23.83, 23.89, 24.18, 24.40, 25.32, 25.33, 25.49, 26.19 (4 *o*-CH₃, 4 *p*-CH₃, 2 ^tBuC), 27.45 (ⁱPr-CH₃), could not locate 3 remaining *o*-CH₃, 30.24, 31.65 (^tBu-CH₃), 33.89 (*o*-ⁱPr-CH), 34.14, 34.61 (*p*-ⁱPr-CH), 39.08 (*o*-ⁱPr-CH), (2x *o*-ⁱPr-CH),^b 122.33 (Ar, *m*-CH), 122.6 (Ar, *m*-CH, δ extracted from the ¹H-¹³C HMBC spectrum), 123.14 (Ar, *m*-CH), 124.5 (Ar, *m*-CH, δ extracted from the ¹H-¹³C HMBC spectrum), 129.22 (Ar, *i*-CSiH), (*i*-C),^b 150.73, 150.83 (Ar, *p*-C), 156.06, 156.76 (Ar, *o*-C), (2x *o*-C)^b.

¹H-²⁹Si HMBC NMR (400 MHz, C₆D₆) δ: -35.5 (S-H), -0.4 (SiH).

ATR-IR (cm⁻¹): 2959 (s), 2865 (m), 2137 (w, SiH), 1463 (m), 814 (m), 496 (s).

High resolution ESI-MS *m/z* for C₃₈H₆₅NaISi₂ [M+Na⁺] calc. 727.3562, found 727.3547.

2.6 Experimental for The Substitution Reactions

The hydrolyses of compounds **23**, **25**, **27** were conducted under ambient conditions. Disilane **23**, **25**, or **27** of (0.020 g, ~ 0.030 mmol) was dissolved in THF (3 mL), water (0.5 mL, xs) was added. The mixture was left to stir for 24 hrs. The solvent was removed under vacuum and the white solid was washed with acetonitrile and dried under vacuum to give a white solid (**18** or **19**, yield of ~ 0.018 g ~ 52, 55, and 59 % respectively). The ¹H NMR spectrum of the crude material indicated 100 % conversion to **18** or **19** with 100 % stereospecificity.

The hydrolysis of compound **21** was done under ambient conditions. Disilane **21** (0.020 g, 0.030 mmol) was dissolved in THF (3 mL) and water (0.5 mL, xs) was added. For the reactions in acidic conditions, 0.5 mol % of HCl. The mixture was allowed to stir for 24 hrs, and then the solvent was removed under vacuum. The white solid was washed with acetonitrile and dried under vacuum,

giving white solid (**18**, 0.010 g, yield: 67.0 %). The ¹H NMR spectrum of the crude material indicated 100 % conversion with 100 % stereospecificity of the inversion giving product **18**. The reaction was attempted with 0.5-5.0 NaOH, 0 % conversion was observed.

2.7 References

1. a) R. West, *Angew. Chem. Int. Ed.*, 1987, **26**, 1201-1211, b) D. Wendel, T. Szilvási, D. Henschel, P. J. Altmann, C. Jandl, S. Inoue, B. Rieger, *Angew. Chem. Int. Ed.*, 2018, **57**, 14575-14579, c) D. Wendel, T. Szilvási, C. Jandl, S. Inoue, B. Rieger, *J. Am. Chem. Soc.*, 2017, **139**, 9156-9159.
2. a) R. S. Archibald, Y. V. Winkel, A. J. Millevolte, J. M. Desper, R. West, *Organometallics*, 1992, **11**, 3276-3281, b) N. Kramer, C. Jöst, A. Mackenroth, L. Greb, *Chem. Eur. J.*, 2017, **23**, 17764-17774, c) C. N. Smit, F. Bickelhaupt, *Organometallics*, 1987, **6**, 1156-1163.
3. M. J. Fink, M. J. Michalczyk, K. J. Haller, R. West, J. Michl, *Organometallics*, 1984, **3**, 793-800.
4. D. Wendel, T. Szilvási, D. Henschel, P. J. Altmann, C. Jandl, S. Inoue, B. Rieger, *Angew. Chem. Int. Ed.*, 2018, **57**, 14575-14579.
5. S. L. McOnie, G. A. Özpınar, J. L. Bourque, T. Müller, K. M. Baines, *Dalton Trans.*, 2021, **50**, 17734-17750.
6. C. Reichardt, *Solvents and Solvent Effects in Organic Chemistry*, Wiley-VCH Publishers, S. Murov, Ltd. 2003; 3rd ed.
7. L. H. Sommer, *Stereochemistry, Mechanism and Silicon*. *McGraw-Hill Series in Advanced Chemistry*, McGraw Hill, Inc. 1965; 64, pp 1-189.
8. J. E. Baines, C. Eaborn, *J. Chem. Soc.*, 1956, **17**, 1436-1441.

9. L. H. Sommer, *Intra-sci. Chem. Rep.*, 1973, **7**, 1-44.
10. R. H. Prince, *Int. Rev. Sci., Inorg. Chem. Ser. One.*, 1972, **9**, 353-393.
11. R. J. P. Corriu, C. Guerin, J. J. E. Moreau, *Top. Stereochem.*, 1984, **15**, 43-121.
12. J. A. Deiters, R. R. Holmes, *J. Am. Chem. Soc.*, 1987, **109**, 1686-1692.
13. A. P. Bento, F. M. Bickelhaupt, *J. Org. Chem.*, 2007, **72**, 2201-2207 2201.
14. R. Baker, R. W. Bott, C. Eaborn, P. W. Jones, *J. Organometallic Chem.*, 1963, **1**, 37-42.
15. L. H. Sommer, *Angew. Chem.*, 1962, **74**, 176-182.
16. F. G. Bordwell, *Acc. Chem. Res.*, 1988, **21**, 456, 463.
17. a) R. S. Archibald, Y. V. Winkel, A. J. Millevolte, J. M. Desper, R. West, *Organometallics*, 1992, **11**, 3276-3281, b) N. Kramer, C. Jöst, A. Mackenroth, L. Greb, *Chem. Eur. J.*, 2017, **23**, 17764-17774. c) C. N. Smit, F. Bickelhaupt, *Organometallics*, 1987, **6**, 1156-1163.
18. Bruker-AXS, SAINT version 2013.8, 2013, Bruker-AXS, Madison, WI 53711, USA.
19. Bruker-AXS, SADABS version 2012.1, 2012, Bruker-AXS, Madison, WI 53711, USA.
20. Bruker-AXS, TWINABS version 2012.1, 2012, Bruker-AXS, Madison, WI 53711, USA.
21. M. G. Sheldrick, *Acta Cryst.* 2015, **C71**, 3-8.
22. F. C. Macrae, J. I. Bruno, A. J. Chisholm, R. P. Edington, P. McCabe, E. Pidcock, L. Rodriguez-Monge, R. Taylor, J. van de Streek, A. P. Wood, *J. Appl. Cryst.*, 2008, **41**, 466-470.

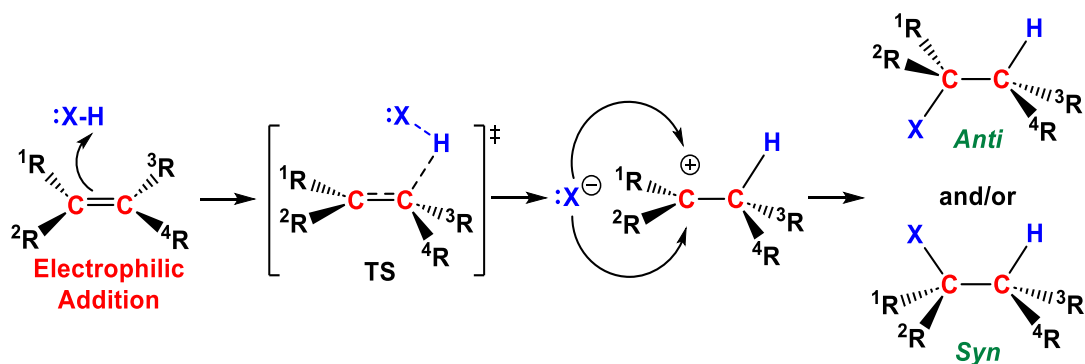
Chapter 3

3 Mechanistic Study of the Addition of Amines to Disilene

3.1 Insight into Mechanistic Studies of Nucleophilic Addition to Disilenes

Extensive computational, experimental, and kinetic studies have been conducted to understand the mechanism of the σ -addition of water and alcohols ROH (R = alkyl) to disilenes.^{1, 2} However, not much was known about the mechanism of the addition of NH₃ or amines to disilenes until recently.^{3, 4}

The stereochemistry of a reaction is a key piece of information used in the elucidation of mechanism. For example, the addition of HX to either stereoisomer of *E* or *Z* alkene results in the formation of 2 diastereomers, often in a 1:1 ratio. The formation of the diastereomeric mixture is key evidence in the formulation of the accepted mechanism of electrophilic addition of HX to the alkene involving a planar carbocationic intermediate. The nucleophile, X⁻, adds to the planar carbocationic intermediate from either face resulting in the formation of a diastereomeric mixture (Scheme 3.1).



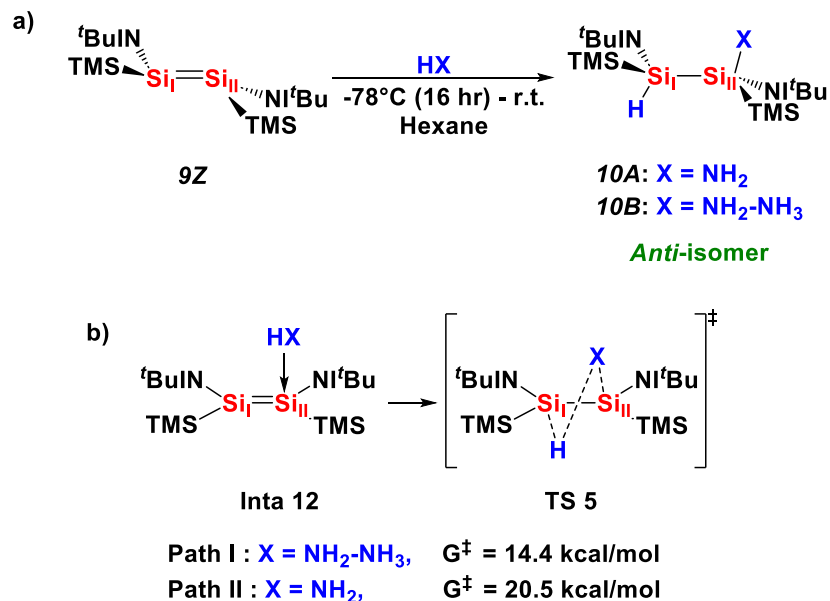
Scheme 3.1: General mechanism of electrophilic addition HX to alkenes.

In this chapter, studies directed towards understanding the mechanism of addition of amines to disilenes will be presented and discussed. Experimental kinetic studies including Variable Time Normalization Analysis (VTNA) and Kinetic Isotopic Effect (KIE) experiments of the addition of *isopropyl* amine (*i*PrNH₂) to tetramesityldisilene (*I*) were performed. In addition,

computational studies of the addition of NH_3 to *E*-1,2-di-*tert*-butyl-1,2-bis(2,4,6-triisopropylphenyl)disilene (**3E**) were conducted in collaboration. Finally, a competition reaction of the addition of both PrNH_2 and $^i\text{PrNH}_2$ to disilene **1** is examined. The results will be used to refine our understanding of the mechanism of the addition of amines to disilene.

3.1.1 Literature Review of the Mechanism of the Addition of Ammonia to Disilenes.

In recent work, Inoue and coworkers investigated the addition of NH_3 to imino(silyl)disilene **9Z** both experimentally and computationally.⁴ Ammonia was found to add nucleophilically as a monomer or a dimer via an “*anti*-addition pathway” to give the *anti*-isomer of the disilylamine (**10A**). Path I involving dimeric ammonia was found to be energetically more favored ($\Delta G = 14.4$ kcal/mol) compared to Path II using monomeric NH_3 ($\Delta G = 20.5$ kcal/mol) (**Scheme 3.2**).⁴



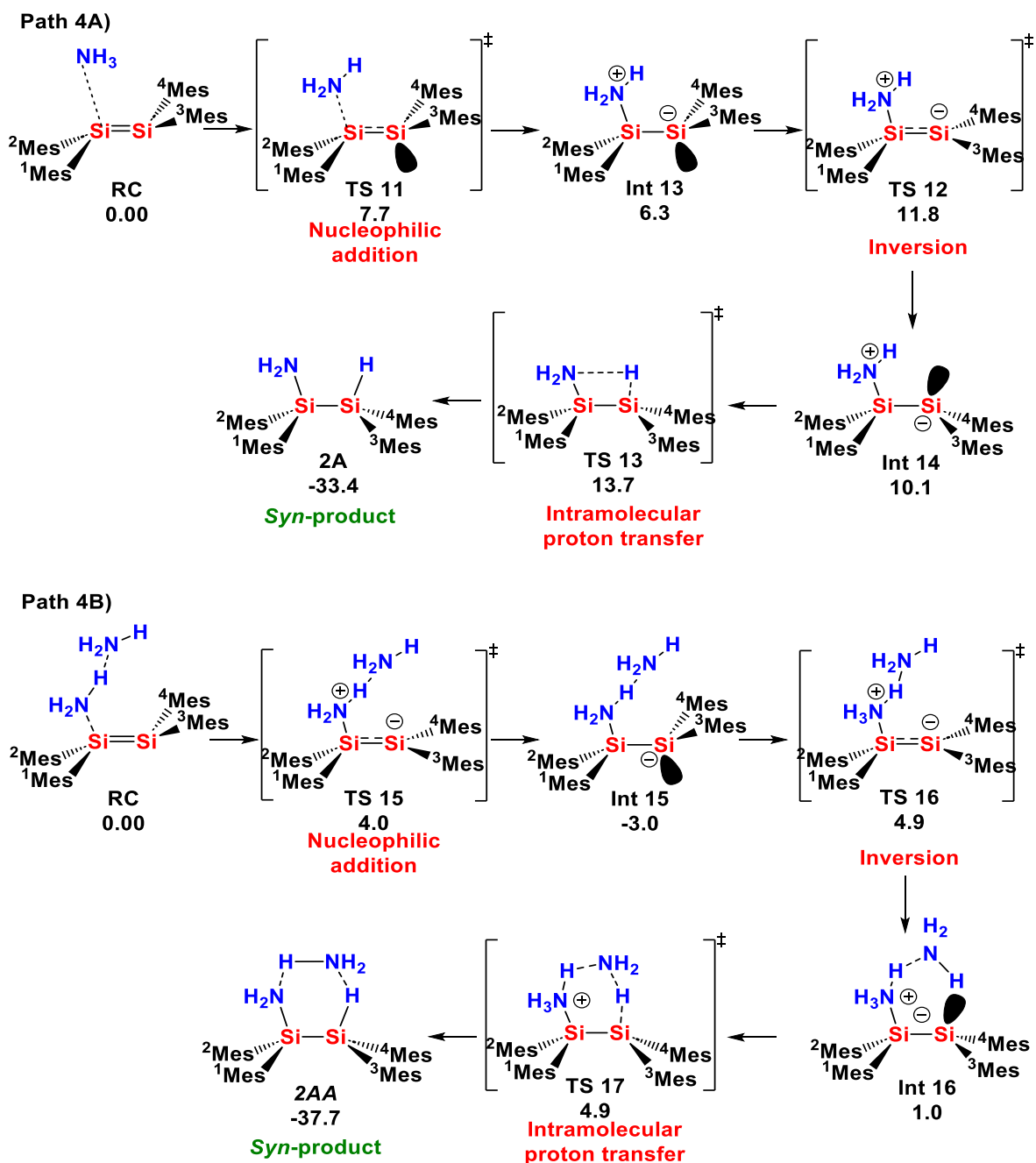
Scheme 3.2: a) Addition of NH_3 to imino(silyl)disilene **9Z**; to give disilylamine **10**, b) intermediate and transition states via Path I) with dimer, Path II) with monomeric ammonia.⁴

In the proposed mechanism (**Scheme 3.2**), the intermediate **Inta 12** only includes the approach of the nucleophile to a silicon center, not taking into consideration which face of the *trans*-bent silicon center the HX attacks, i.e., the apex of pyramidal Si_I or the base of pyramidal Si_{II} , as the

substituents in **Inta 12** are shown planar even though the disilene is highly folded and twisted ($\theta = 37.89, 39.03^\circ$, $\tau = 23.1^\circ$). Most importantly, the transition state going to **Inta 12** was not presented, nor discussed. Upon examination of the data provided,⁴ the stereochemistry of the intermediate observed after the nucleophilic addition was the *anti*-oriented donor adduct.⁵

Unlike the currently accepted mechanism for the addition of water and alcohols to disilenes, which includes two elementary steps, the mechanism proposed by Inoue and coworkers is a single step mechanism.^{2, 4} Baines and Özpınar further investigated the addition of NH₃ to disilenes using tetramesityldisilene (**I**), a prototypical, tetraaryldisilene as the substrate. Experimentally, the addition of NH₃ and amine proceeds to the expected σ -addition products. The mechanism of the addition was investigated computationally where the individual mesityl substituents can be tracked, and hence, the stereochemistry of the addition can be understood.⁵

Four different reaction pathways were investigated, all of which begin with the formation of a nucleophilic reactant complex (RC) between ammonia (or its dimer) and the disilene. The four pathways are 1) formation of a *syn*-oriented donor adduct and intramolecular *syn*-transfer of the proton, 2) formation of *anti*-oriented donor adduct and intermolecular transfer of the proton, 3) formation of an *anti*-oriented donor adduct followed by rotation about the Si-Si bond and then intramolecular *syn*-transfer of the proton. The most energetically favored pathway located is 4) the nucleophilic addition of NH₃ (as a monomer or a dimer) to give the *anti*-oriented donor adduct, **Int 13** followed by inversion via **TS 12** at the silicon bearing the formal negative charge to form **Int 14**. Finally, an intramolecular *syn*-transfer of a proton to give the *syn*-isomer of disilylamine **2A** occurs (**Scheme 3.3**).⁵ Path 4B, involving dimeric ammonia as the nucleophile, is the most energetically favored pathway (**Scheme 3.3B**).⁵



Scheme 3.3: Addition of NH_3 as Path 4A) a monomer or Path 4B) a dimer to **1**. The relative free energies are in (kcal/mol in benzene, at 298 K and 1 atm).⁵

The computational study of the addition of NH_3 to **1** highlighted several points: (1) the stereochemical outcome of the reaction relies on the understanding of the stereochemical implications of all elementary steps of the reaction mechanism, (2) the formation of the *anti*-oriented donor adduct is energetically favored over the *syn*-oriented donor adduct intermediate in

the initial step, (3) the activation barriers decrease with dimeric NH_3 as the nucleophile, (4) the bulk and electronic nature of the substituents of the disilene evidently influences the stereochemical outcome of the reaction.⁵

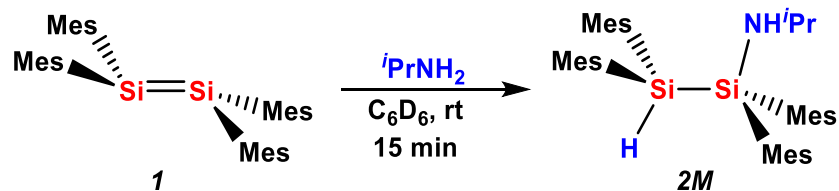
To further support the proposed mechanistic pathway for the addition of NH_3 to disilenes, kinetic experiments on the addition of *isopropyl* amine ($i\text{PrNH}_2$) to **I** using VTNA and KIE experiments were conducted.^{6,7} Moreover, in collaboration with Gül Altınbaş Özpınar and Thomas Müller from Carl von Ossietzky Universität Oldenburg, computational studies of the addition of NH_3 to *E*-1,2-di-*tert*-butyl-1,2-bis(2,4,6-triisopropylphenyl)disilene (**3E**) will be discussed.

3.2 Results and Discussion

The data obtained for the VTNA and KIE analysis were conducted under an inert atmosphere of nitrogen and the reaction progress was monitored by ^1H NMR spectroscopy.

3.2.1 VTNA of the Addition of $i\text{PrNH}_2$ to Tetramesityldisilene **1**

Initial VTNA experiments were carried out using NH_3 and **3E**, as the isolation and purification of **3E** is easier compared to that of **3Z**. However, due to the volatility of NH_3 , it was difficult to obtain reproducible data. For that reason, amines, which are liquid at room temperature, such as propylamine (PrNH_2) and *isopropyl*amine ($i\text{PrNH}_2$), were added to **3E**. However, the reaction between **3E** and PrNH_2 or $i\text{PrNH}_2$ was too slow to be monitored for a reasonable period of time, and thus, the disilene was changed to tetramesityldisilene **I**, a less bulky tetraaryldisilene. The addition of PrNH_2 to disilene **I** was examined; however, the reaction was very fast; conversion of 50 % within 20 seconds of addition was observed. Thus, the bulkier amine, $i\text{PrNH}_2$, was utilized and the reaction with **I** occurred in a reasonable time frame and provided reproducible data (Scheme 3.4).



Scheme 3.4: Addition reaction of $i\text{PrNH}_2$ to **1**.

The initial studies of the reaction between PrNH_2 and **1** indicated that both the disilene and amine influence the rate of the reaction giving a general rate equation of:

$$\text{Rate } (r) = k [\text{Disilene}]^X [\text{Amine}]^Y \quad (1)$$

The VTNA experiments were conducted by monitoring the formation of **6** by ^1H NMR spectroscopy. The initial rates of reaction were used to find the reactant order by plotting the concentration of the product against $\Sigma[B]^\beta \Delta t$, the sum of the concentration of reagent $[B]$ to the power of the reactant order (β) times the normalized change in time (Δt), which can be calculated using **equation 2**.⁶

$$\Sigma [B]^\beta \Delta t = \sum_{i=1}^n \left(\frac{[B]_i + [B]_{i-1}}{2} \right)^\beta (t_i - t_{i-1}) \quad (2)$$

To determine the order in $i\text{PrNH}_2$, the experiments were conducted using concentrations of 0.23 M or 0.45 M of $i\text{PrNH}_2$ and a constant concentration of **1** (0.019 M) (**Figure 3.1**). To determine the order in disilene **1**, the concentrations of **1** examined were 0.019 M or 0.028 M, while the concentration of $i\text{PrNH}_2$ was held constant at 0.45 M (**Figure 3.2**). The data were then plotted varying the order β of **1** or $i\text{PrNH}_2$ against product **2M**.

Finally, a competition reaction of equal number of moles (0.019, 0.094, 0.19 mmol, 0.0015, 0.0077, 0.015 mL) of PrNH_2 and $i\text{PrNH}_2$ to disilene **1** were examined. The reactions were completed in ~ 10 minutes and gave only the product derived from the addition of PrNH_2 to disilene **1**. It can be concluded that the less bulky the amine, the faster the rate compared to the bulkier amine, giving clear evidence of nucleophilic addition.

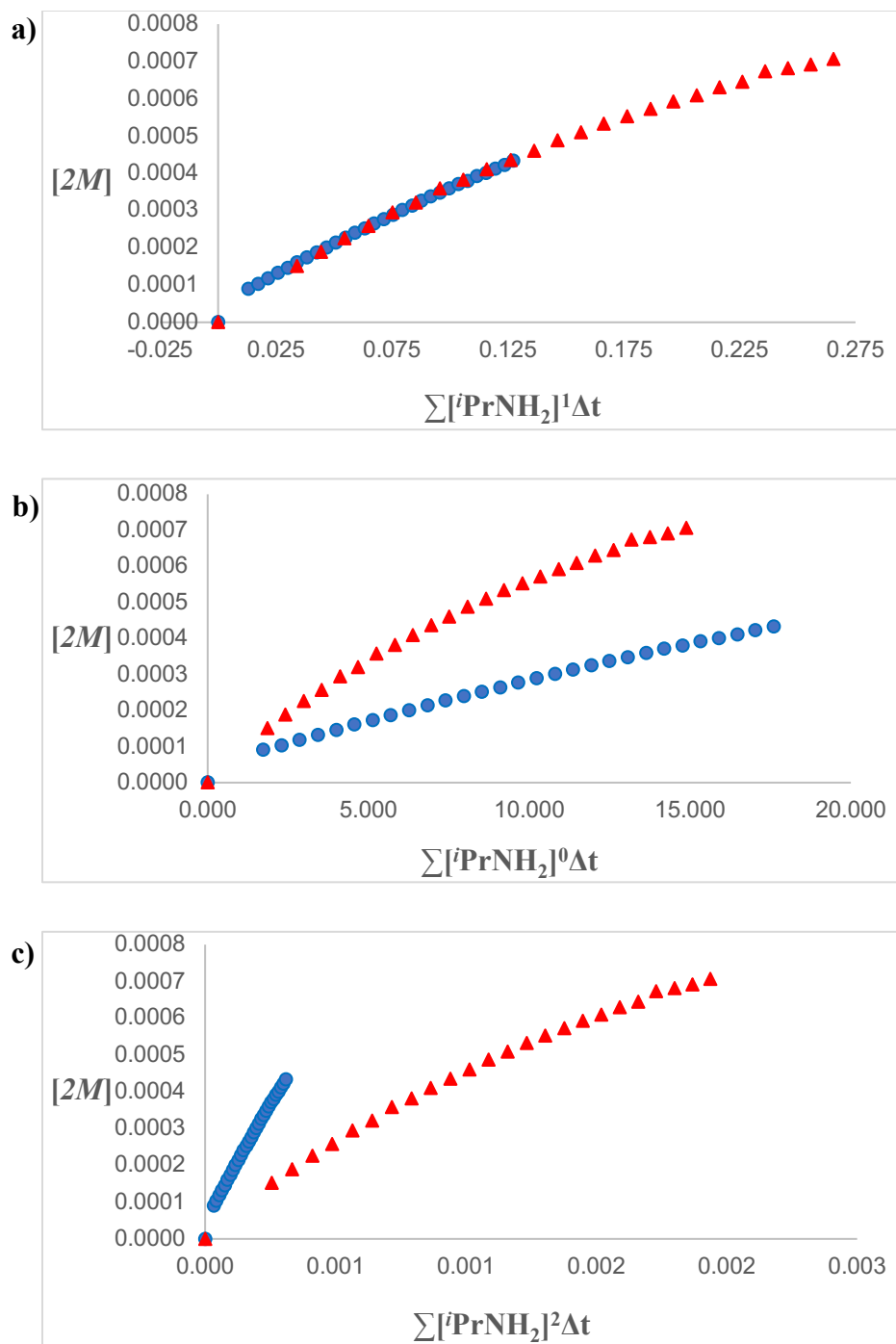


Figure 3.1: Plot of product $[2M]$ versus $\Sigma [iPrNH_2]^\beta \Delta t$ when a) $\beta = 1$, b) $\beta = 2$, c) $\beta = 3$ for two concentrations of $iPrNH_2$. (Concentrations in M; average of two runs).

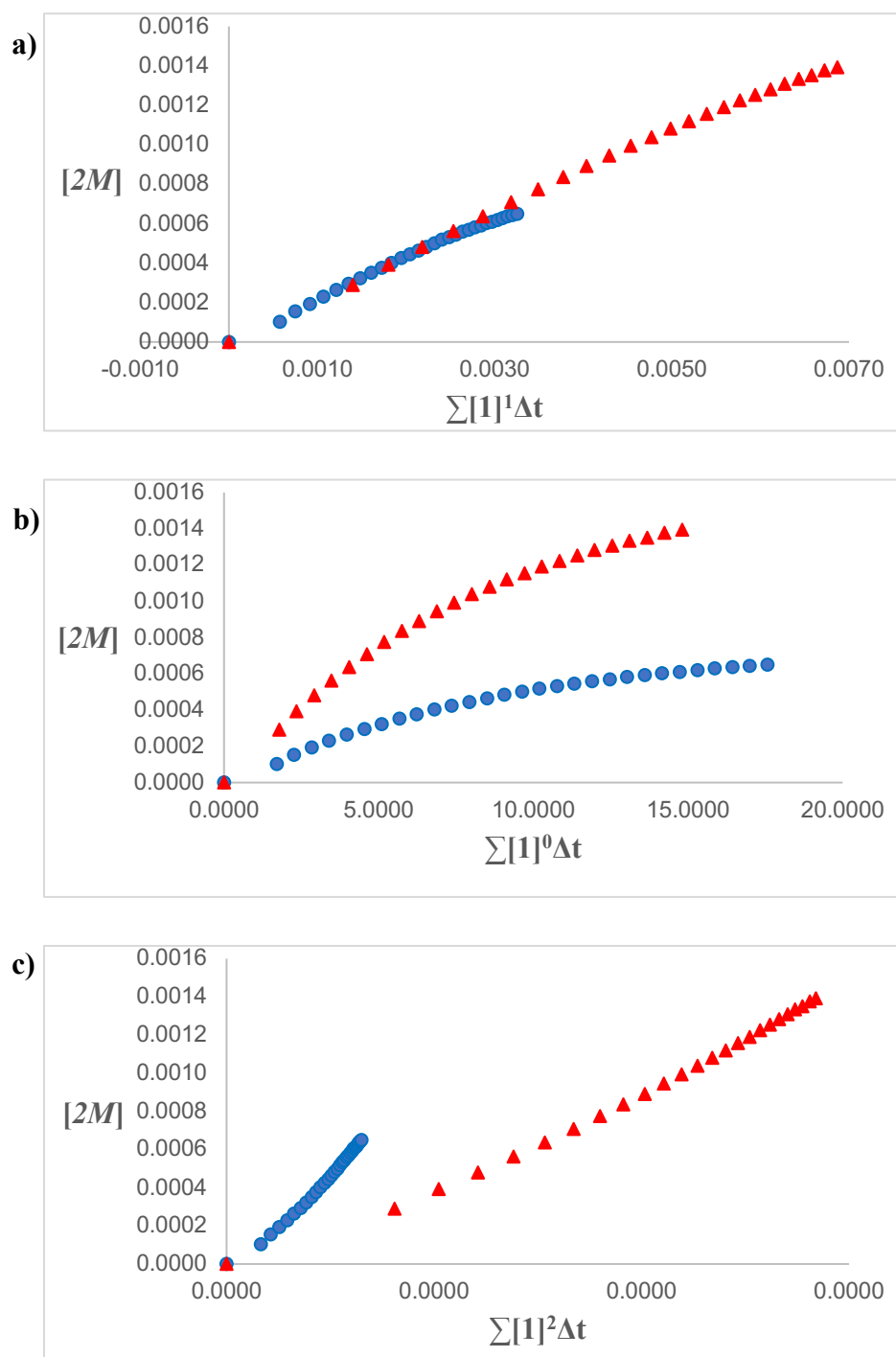


Figure 3.2: Plot of product $[2M]$ versus $\Sigma[\text{Disilene } I]^\beta \Delta t$ when a) $\beta = 1$, b) $\beta = 2$, c) $\beta = 3$ for two concentrations of I . (Concentrations in M; average of two runs).

On the basis of the visual analysis of the plots (**Figures 3.1 and 3.2**), the best overlap of data is observed with $\beta = 1$ for disilene **1** meaning the rate of the reactant order for disilene **1** is first order. The order of the reactant $i\text{PrNH}_2$ is also first order, and thus, the reaction is second order overall.

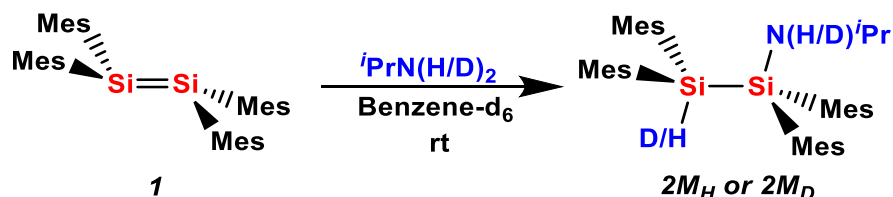
$$\text{Rate} = k [\text{tetramesityldisilene}]^1 [i\text{PrNH}_2]^1 \quad (3)$$

$i\text{PrNH}_2$ is more sterically encumbered compared to NH_3 which, evidently, leads to the reaction as a monomer not a dimer.

3.2.2 KIE Study of the Addition of $i\text{PrN(H/D)}_2$ to Tetramesityldisilene **1**

Kinetic Isotopic Effect (KIE) studies are commonly used to determine if the bond breakage of an isotopically labelled bond occurs during the rate determining step (rds) of a reaction. Thus, the addition of $i\text{PrN(H/D)}_2$ to **1** was carried out to determine if the breakage of the N-H bond occurs during the rds. The observed KIE in methyl radical attack on N-H and N-D bonds in ammonia and methyl amine are $k_{\text{H}}/k_{\text{D}} = 2.6$ for NH_3 and ND_3 and for $k_{\text{H}}/k_{\text{D}} = 4.2$ for CH_3NH_2 and CH_3ND_2 .⁸ The authors concluded these are *primary* KIE. Other examples, such as in the hydroamination of alkenes and alkynes, the KIE was found to be ≈ 2.2 -3.2 at 353-363 K, indicating the breaking of the N-H bond occurs in the rds.⁷

The rate of the addition of $i\text{PrNH}_2$ or $i\text{PrND}_2$ to **1** was determined using ^1H NMR spectroscopy (**Scheme 3.5**). The experiments were conducted in C_6D_6 at 298 K and the formation of the products $2M_{\text{H}}$ or $2M_{\text{D}}$, were monitored, respectively. Two experimental runs were conducted using concentrations of $i\text{PrN(H/D)}_2 = 0.18$ and 0.45 M, holding the disilene concentration constant at 0.019 M. The signal attributed to the aromatic CH at 6.65 ppm of disilene **1** was used to monitor the reaction progress and perform the calculations.



Scheme 3.5: KIE experiment of the addition of $i\text{PrNH}_2$ or $i\text{PrND}_2$ to **1**.

The initial rates were recorded and the k_H/k_D were calculated using **equation 4** as it expresses the KIE in terms of the ratios of the change in concentration of protonated amine to deuterated amine. An average KIE of 3.04 was determined (**Table 3.1**).

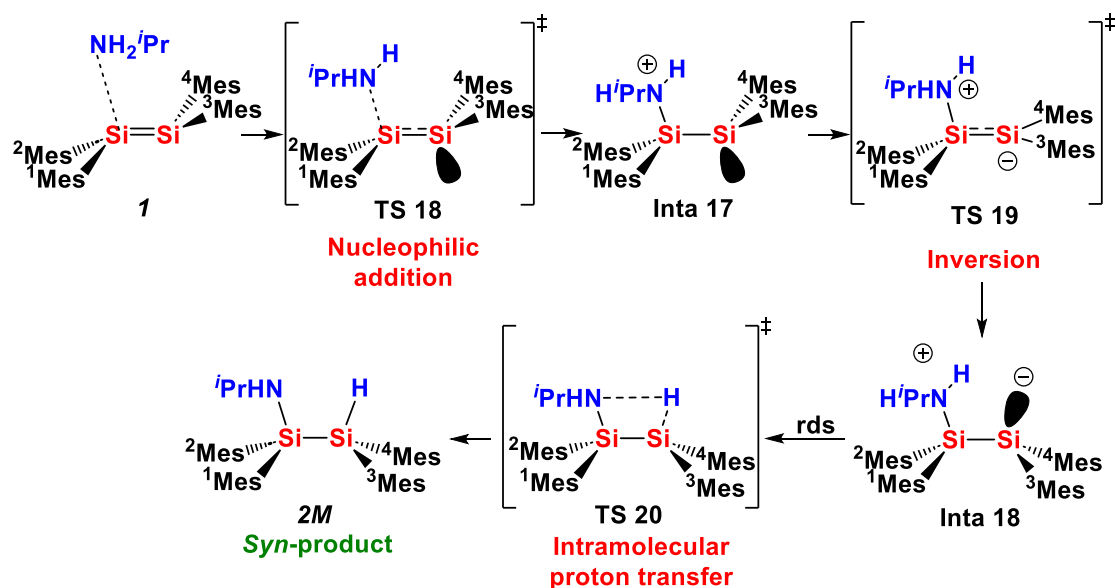
$$KIE = \frac{k_H}{k_D} = \frac{\Delta[H]}{\Delta[D]} \approx \frac{Int_{H(t_0)} - Int_H(t)}{Int_{D(t_0)} - Int_D(t)} \quad (4)$$

Table 3.1: Experimental data for the KIE of the addition of $i\text{PrNH}_2$ and/or $i\text{PrND}_2$ to **1**.

Experiment	$i\text{PrN(H/D)}_2$	Rate in M/min	KIE
1	$i\text{PrND}_2$	0.00022	3.00
	$i\text{PrNH}_2$	0.00066	
2	$i\text{PrND}_2$	0.00023	3.09
	$i\text{PrNH}_2$	0.00072	

The magnitude of KIE for the addition of $i\text{PrN(H/D)}_2$ ($k_H/k_D = 3.04$ at 298 K) is within the range of a *primary* KIE based on literature precedents indicating that the N-H bond breaks as part of the rds of the reaction.

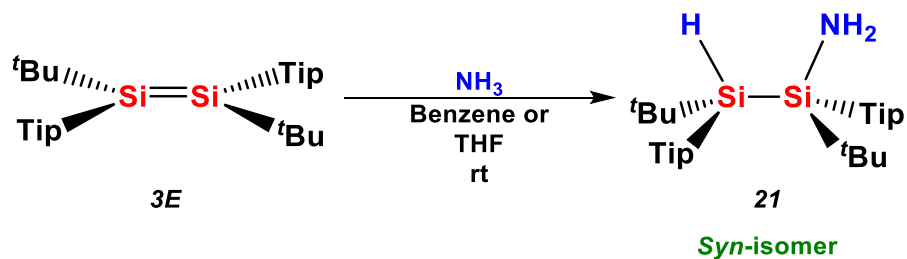
On the basis of the results of the kinetic studies and the previous calculations of the mechanism,⁵ the mechanism of the addition of $i\text{PrNH}_2$ to **1** is proposed as follows: 1) nucleophilic addition of $i\text{PrNH}_2$ as a monomer giving intermediate **Inta 17**, an *anti*-oriented adduct of the amine and the disilene, 2) inversion at the silicon bearing the negative charge (**TS 19**) forming **Inta 18**, then 3) *syn*-transfer of the proton in the rds via **TS 20** giving the *syn*-isomer (**Scheme 3.6**).



Scheme 3.6: Proposed mechanism of the addition $i\text{PrNH}_2$ to **1**.

3.2.3 Computational Studies of the Addition of Ammonia to *E*-1,2-di-*tert*-butyl-1,2-bis(2,4,6-triisopropylphenyl)disilene **3E**

The addition of NH_3 to 1,2-di-*tert*-butyl-1,2-bis(2,4,6-triisopropylphenyl)disilene **3E** was conducted and product **21** was isolated and then identified by single crystal X-ray diffraction as the *syn*-isomer (**Scheme 3.7**). Other amines such as PrNH_2 and $i\text{PrNH}_2$ were examined; however, the addition did not take place.

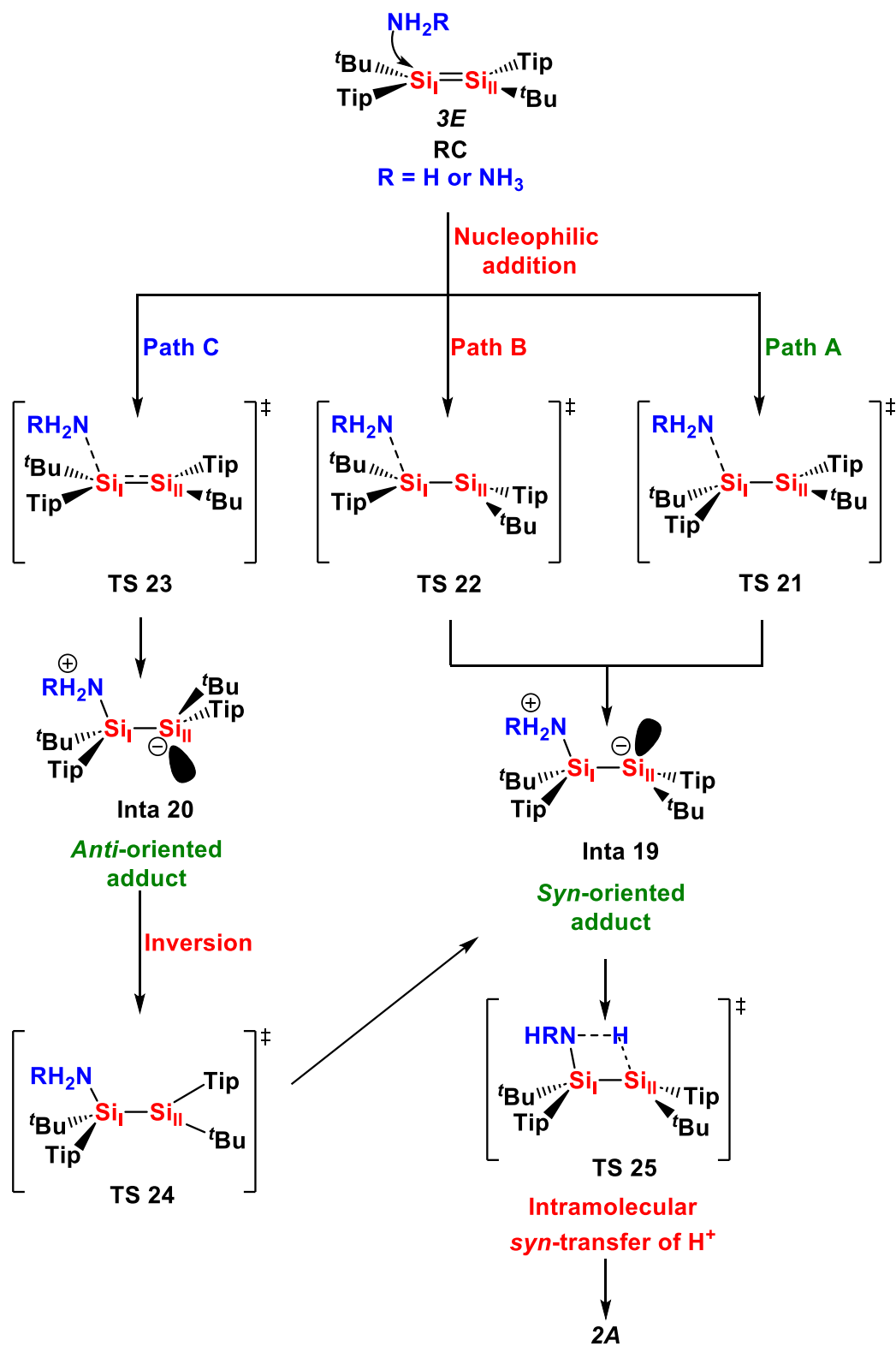


Scheme 3.7: The addition of NH_3 to **3E** giving the *syn*-isomer **21**.

Understanding the fundamental chemistry for the mechanism of the σ -addition of NH_3 to disilenes will allow the development of future applications of activating of ammonia using disilenes. Thus,

computational studies using M06-2X/6 311+G(d,p) model chemistry were conducted in collaboration with Gül Altınbaş Özpınar and Thomas Müller to understand the mechanism of the addition of NH₃ to **3E** and the formation of the *syn*-isomer. A key difference between disilene **I** and **3E** is the degree of *trans*-bending about the Si-Si double bond. Disilene **I** exhibits a greater degree of *trans*-bending about the Si-Si double bond (θ in deg, Si_I = 12, Si_{II} = 14 °) and a twist angle (τ = 3 °). However, **3E** is planar about the double bond.⁹

Only reaction complexes where the ammonia is nucleophilically associated with the disilene were found on the potential energy surface consistent with the experimental data of Sakurai and coworkers and previous computational studies.² The high stereospecificity of the reaction as determined experimentally indicates no silicon intermediate with a planar silicon bearing a positive charge is formed as a mixture of diastereomers would be expected. Three initial transition states were located (**Scheme 3.8**). Path A: the addition of NH₃ to Si_I with a change to tetrahedral geometry (**TS 21**). Path B involves addition of NH₃ to Si_I and a simultaneous pyramidization at Si_{II} (**TS 22**). Both Path A and B lead to the *syn*-oriented donor adduct **Inta 19** which then undergoes intramolecular *syn*-transfer of H⁺ to give the *syn*-isomer **7**. Path C involves the addition of NH₃ to Si_I (**TS 23**). The two silicon atoms remain planar in the **TS 23** which then gives the *anti*-oriented adduct **Inta 20**. Inversion at Si_{II} (**TS 24**) forms the *syn*-oriented donor adduct **Inta 19**. Finally, an intramolecular *syn*-transfer of the proton leads to the *syn*-product **2A** (**Scheme 3.8**). The energetics for Paths A-C for the NH₃ monomer and dimer were calculated in kcal/mol in benzene at 298 K (**Figure 3.3**).



Scheme 3.8: Proposed paths of the addition of NH₃ monomer and/or dimer to disilene **3E**.

The simultaneous addition of the NH₃ monomer and the formation of an *anti*-oriented donor adduct is energetically favored compared to the *syn*-oriented donor adduct, which is consistent with what was observed in the addition of NH₃ to **1**. The *anti*-oriented donor adduct must then undergo inversion to give the *syn*-oriented donor adduct followed by *syn*-transfer of the proton to give the *syn*-isomer **2A**. The inversion is the rate determining step based on the calculated energies. Paths A and B are energetically accessible; however, the formation of the *anti*-oriented donor adduct (**Inta 20**) in Path C is favored over the formation of the *syn*-oriented donor adduct (**Inta 19**) and inversion is necessary for the formation of the *syn*-isomer (**Figure 3.3**).

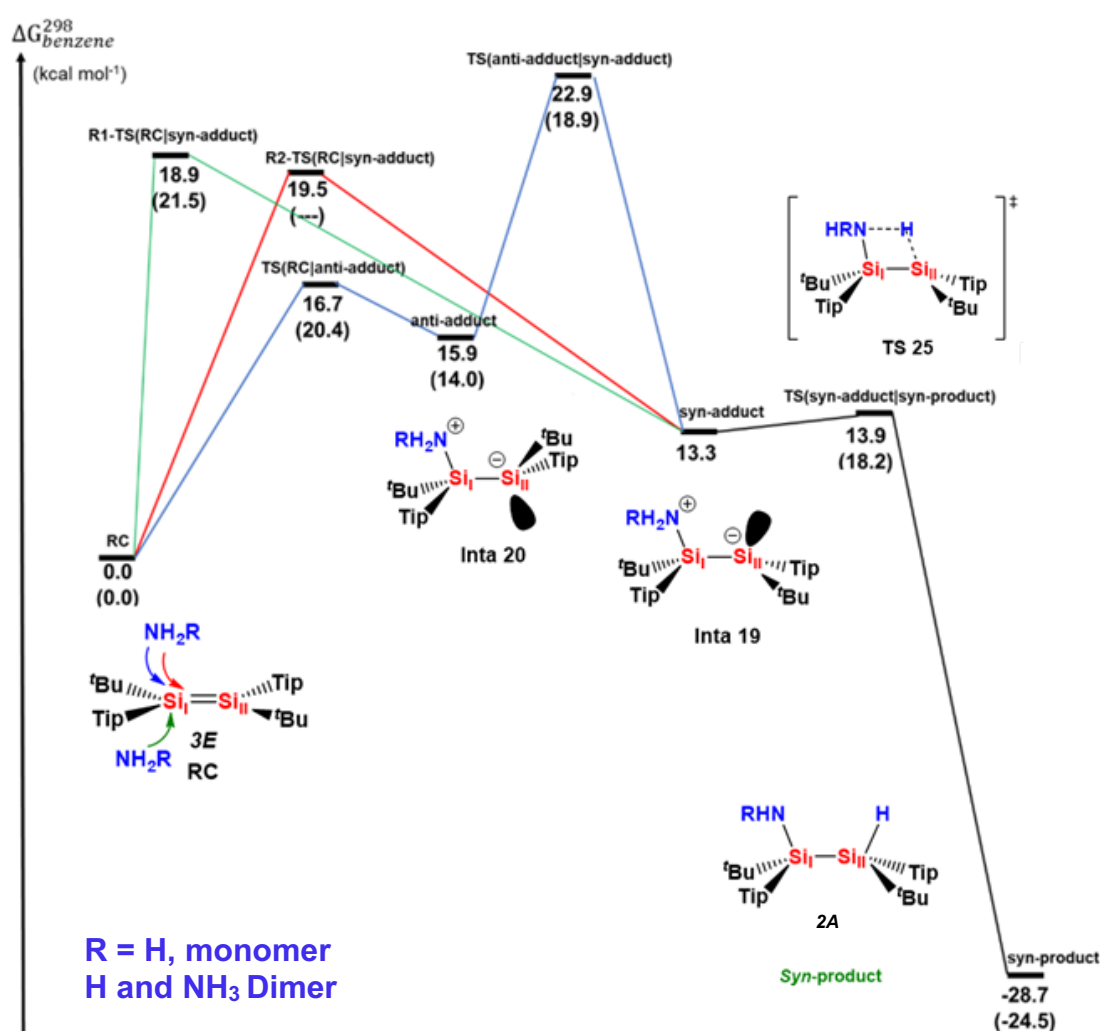


Figure 3.3: Relative free energies (in kcal/mol, at 298 K and 1 atm) with NH₃ monomer or dimer (NH₂-NH₂) given in parenthesis. Computational level used is M06-2X/6-311+G(d,p). Path A (green), Path B (red), Path C (blue).

The rotation of the Si-Si bond from the *anti*-oriented donor adduct to the *syn*-oriented donor adduct was also investigated by scanning the dihedral angle (*t*-Bu)-Si1-Si2-(*t*-Bu) of **Inta 20** with a 60 ° fold. The energy profile of the rotation is given in **Figure 3.4**. The rotational barrier of **Inta 20** was found to be very high leading to the breakage of the Si-Si bond reducing the possibility of the formation of the *syn*-isomer via rotation (**Figure 3.4**).

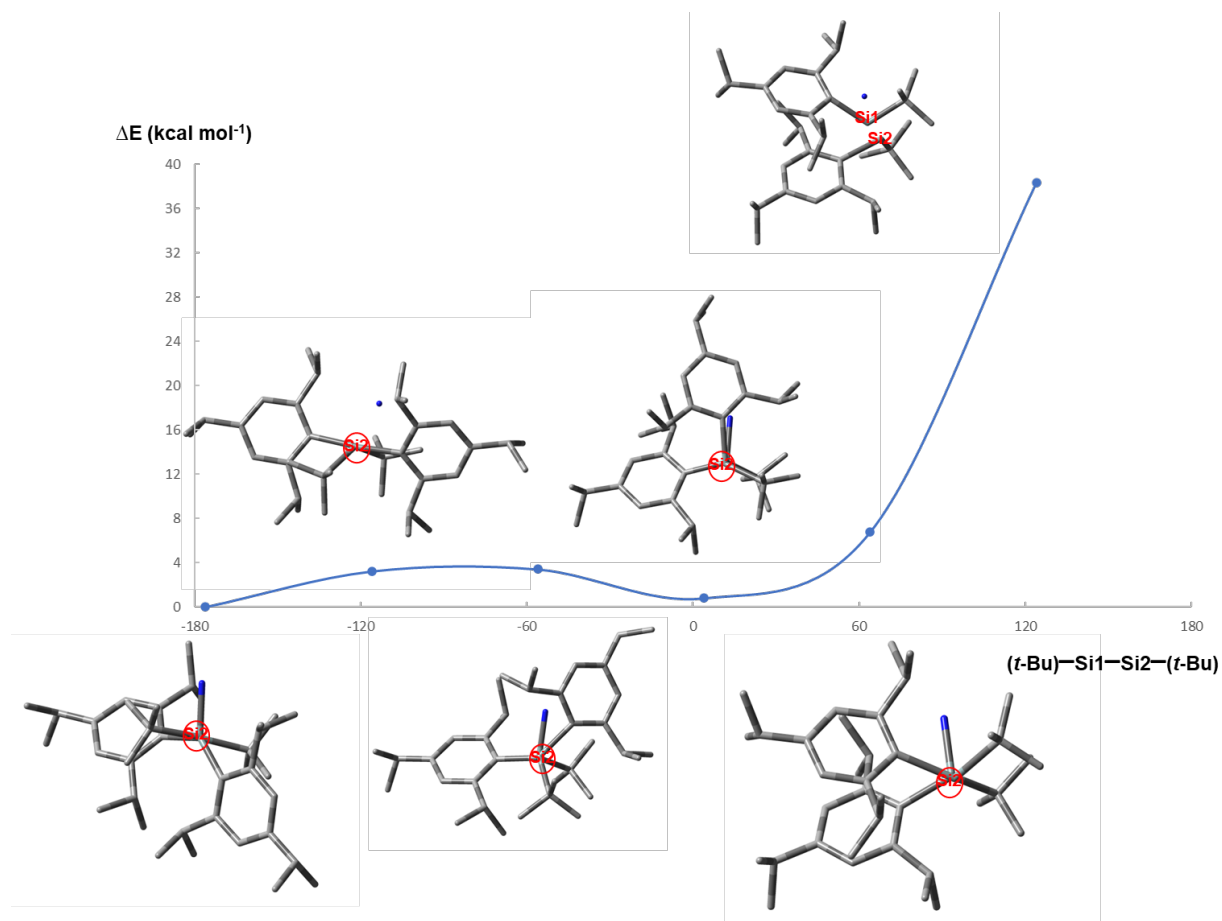


Figure 3.4: The energy profile for the rotation about Si1-Si2 bond in **Inta 20** computed with the M06-2X/6-311+G(d,p) level. Hydrogens are omitted for clarity.

On the basis of the experimental work and the computational mechanistic studies, the formation of the *syn*-isomer for the addition of ammonia to **3E** was predicted and, indeed, observed. It is proposed that **3Z** follows the same reaction pathway giving the *syn*-isomer.

3.2.4 Discussion of the Mechanism and Stereochemistry in the Addition of Ammonia and Amines to Disilenes

On the basis of the experimental and computational studies, a general mechanism for the addition of ammonia to disilene **3E** is proposed with three steps; 1) The formation of an *anti*-donor adduct as for disilene **1**. Although formation of the *syn*-oriented donor adduct in the reaction of **3E** is energetically possible, it is less favored. 2) Inversion or rotation at the silicon bearing the lone pair in the *anti*-donor adduct is directly influenced by the substituents. The larger the cone angle for the substituents, the larger the rotational barrier expected. Inversion is favored in both disilene **1** and **3E** with cone angles θ of ~ 119 and 127° for the Si-Mes and Si-Tip groups, respectively. ^d (Figure 3.5).

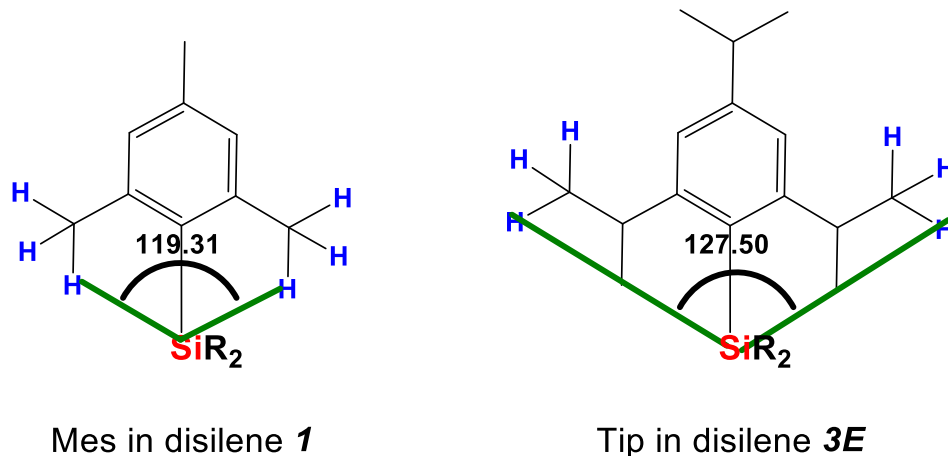


Figure 3.5: Average cone angle in for (Mes = 2,4,6-methylbenzene) substituent in disilene **1** and (Tip = 2,4,6-*isopropyl*benzene) **3E** in degrees. ^d

However, in disilene **9Z**, rotation was energetically more favorable even though the substituents are bulky. The highly twisted geometry of the disilene evidently favors rotation over inversion.

^d Measured using Mercury software, the angle is an average between the *p*-*isopropyl* CH₃ protons and the silicon center.

The inversion barrier is 12.7 kcal/mol^e in the *anti*-donor adduct between ammonia and **9Z** and the rotational barrier will be calculated. The substituents, NI^tBu and Si(SiMe₃)₃ in disilene **9Z** are electronically different compared to the substituents of disilene **1** and **3E** which contain only hydrocarbon substituents. It is hypothesized that the electronic nature of the substituents influences the degree of *trans*-bending and twisting leading to rotation of 60 ° rather than rotation of 180 ° or inversion. 3) The *syn*-transfer of the proton was observed in all reactions. The intermolecular transfer of proton is energetically not favorable in non-polar solvents⁵. Clearly, the electronic nature of the substituents can have an influence on the stereochemical outcome.⁵

3.3 Experimental Details

All reactions were conducted under an inert atmosphere of dried argon using Schlenk line techniques, or under an atmosphere of nitrogen in an MBraun glovebox. The glassware was dried prior to use by heating at 120 °C in an oven for approximately 20 hrs.

Dried solvents were obtained from an Innovative Technologies 400-5 Solvent Purification System. Solvents were stored over activated 4 Å molecular sieves before use. Tetramesityldisilene **1** was synthesized as previously described.¹⁰ Isopropylamine and propylamine were obtained from Sigma Aldrich.

¹H NMR spectra were recorded in C₆D₆ on a INOVA 600 MHz NMR spectrometer. ²H NMR (92 MHz) spectra was recorded on 400 MHz spectrometer.

^e Computed with the B3LYP-D3/def2svp computational level.

3.3.1 Synthesis of ${}^i\text{PrND}_2$

The synthesis of PrND_2 was used to make the ${}^i\text{PrND}_2$ with slight change in reaction time.¹¹ Under argon, *isopropylamine* (5.00 mL, 61.0 mmol) was dissolved in D_2O (25.0 mL) and three droplets of concentrated HCl were added. The reaction was refluxed for 2 days. Conversion to ${}^i\text{PrND}_2$ was monitored over time by analysis of aliquots of the solution by ${}^1\text{H}$ NMR spectroscopy until the integration value of the $-\text{NH}_2$ stopped decreasing. The resulting solution was extracted using *d*-benzene (~ 3 mL) and dried over CaH_2 , then distilled. Analysis of the product was done by using ${}^1\text{H}$ NMR spectroscopy indicated that the sample was 87.0 % deuterated. The percent deuteration was determined by calculating the relative ratio of remaining $-\text{NH}_2$ to CH in ${}^i\text{PrND}_2$.

3.3.2 VTNA Experiments

3.3.2.1 Order in Amine

Disilene **1** (0.0188 mmol in 0.50 mL C_6D_6), trimethoxybenzene (0.030 mmol in 0.20 mL C_6D_6 used as standard) and ${}^i\text{PrNH}_2$ (1.120 mmol or 2.160 mmol in 0.30 mL in C_6D_6) were added to an NMR tube. C_6D_6 was added such that the total volume of the solution was 1.0 mL. The reaction was monitored by ${}^1\text{H}$ NMR spectroscopy. The integration of the signal in ${}^1\text{H}$ NMR spectra assigned to SiH of **2M** compound was used to monitor the reaction and perform the calculations for the formation of product **2M**. The signal for the $-\text{NH}_2$ was used to calculate the decay over time in the reactant.

3.3.2.2 Order in Disilene

Disilene **1** (0.0188 mmol or 0.0939 mmol in 0.50 mL C_6D_6), trimethoxybenzene (0.0300 mmol in 0.20 mL C_6D_6 , used as standard), and ${}^i\text{PrNH}_2$ (2.160 mmol in 0.30 mL C_6D_6) were added to an NMR tube. C_6D_6 was added such that the total volume of solution was 1.00 mL. The reaction was monitored by ${}^1\text{H}$ NMR spectroscopy. The integrations of the signal in the ${}^1\text{H}$ NMR spectra assigned to the SiH in **2M** were used to monitor the reaction and perform the calculations for plot,

and for the reactant. The aromatic protons assigned to Ar-CH for disilene **1** were used to calculate the decay over time.

3.3.3 KIE Experiment

Disilene **1** (0.0188 mmol in 0.50 mL C₆D₆), trimethoxybenzene (0.0300 mmol in 0.20 mL C₆D₆) and ⁱPrNH₂ or ⁱPrND₂ (2.160 mmol in 0.30 mL C₆D₆) were added to an NMR tube. C₆D₆ was added such that the total volume of the solution was 1.00 mL. The reaction was monitored by ¹H NMR spectroscopy. The ²H NMR spectra were referenced externally to a sample of C₆D₆ (7.16 ppm) for Mes₂DSi=SiNDPrMes₂ (**29**). The ¹H NMR spectrum data for the analogue's molecule Mes₂HSi=SiNHPrMes₂ (**28**)¹¹ was reported previously. The chemical shifts in **29** are in close proximity to **28**. The ²H NMR spectrum data and ¹H-²⁹Si HMBS spectrum data are reported herein.

²H NMR (92 MHz, C₆D₆): 5.65 (s, SiD), 0.54 (br s, SiND).

The KIE was calculated using the ratio of the slope (slope run 1/slope run 2) of the linear component of the [P] vs $\Sigma[{}^i\text{PrN}(\text{D}/\text{H})_2]^1\Delta t$ to find the value of k_H and k_D to be within with 95 % confidence level. The integration of the signal assigned to the CH of the *d-isopropyamine* peak in the ¹H NMR spectra of **2M_D** was used to monitor the formation of the product **2M_D**, and the aromatic peak assigned to Ar-CH at 6.65 ppm for the disilene was used to monitor the decay in the reactants.

3.3.4 Computational Methodology

Calculations were done using the Gaussian 16.¹² program package. The geometries of all stationary points and transition states on the potential energy surfaces of the proposed pathways were optimized at M06-2X/6-311+G(d,p) computational level. Transition states were located by executing standard transition state optimizations. Frequency computations were performed to characterize the nature of transition states (one imaginary frequency) and the local minima (no imaginary frequency) at the same computational level. Intrinsic reaction coordinate (IRC) calculations for the transition states optimized using the standard method were also carried out at

the same level to connect the transition states to the reactants and products.¹³ Solvent effects were investigated by performing single point energy computations at the same computational level using the Integral Equation Formalism-Polarizable Continuum Model (IEF-PCM)¹⁴ and benzene as the solvent. To compute zero-point corrected electronic energy and Gibbs energy values in the solvent phase, thermodynamic corrections at 298 K obtained from the frequency calculations were added to the electronic energy obtained from single point IEF-PCM computations.

The transition state R1-TS (RC|*syn*-adduct) was located by executing the coordinate-driving potential scan computation on the N-Si bond of the *syn*-oriented donor adduct and was optimized under the constraint of the N-Si bond distance. Similarly, the inversion transition states TS (*anti*-adduct|*syn*-adduct) was also located under the constraint of the N-Si bond distance.

3.4 References

1. T. L. Morkin, T. R. Owens, W. J. Leigh. Kinetic Studies of the Reactions of Si = C and Si = Si Bonds. In: *The Chemistry of Functional Groups*; Z. Rappoport and Y. Apeloig. Eds.; John Wiley & Sons, Ltd: Japan, 2009; Vol. 2, pp 1-78.
2. H. Sakurai. Mechanism and Structures in Alcohol Addition Reactions of Disilenes and Silenes. In *The Chemistry of Organic Silicon Compounds*; Z. Rappoport and Y. Apeloig. Eds.; John Wiley & Sons, Ltd: Japan, 1998; Vol. 2, pp 827-855.
3. S. Boomgaarden, W. Saak, M. Weidenbruch, *Z. Anorg. Allg. Chem.*, 2002, **627**, 349-352.
4. D. Wendel, T. Szilvási, D. Henschel, P. J. Altmann, C. Jandl, S. Inoue, B. Rieger, *Angew. Chem. Int. Ed.* 2018, **57**, 14575-14579.
5. S. L. McOnie, G. A. Özpınar, J. L. Bourque, T. Müller, K. M. Baines, *Dalton Trans.*, 2021, **50**, 17734-17750.

6. C. D. T. Nielsen, J. Burès, *Chem. Sci.*, 2019, **10**, 348-353.
7. M. G. Gallego, M. A. Sierra, *Chem. Rev.*, 2011, **111**, 4857-4963.
8. a) J. C. J. Thynne, *Trans. Faraday Soc.*, 1964, **60**, 2207-2213, b) J. A. Kerr, R. C. Sekhar, A. F. Trotman-Dickenson, *J. Chem. Soc.*, 1963, **599**, 3217-3225.
9. M. Kira, *Proc. Jpn. Acad., Ser.*, 2012, **88**, 167-191.
10. M. J. Fink, M. J. Michalczyk, K. J. Haller, R. West, J. Michl, *Organometallics*, 1984, **3**, 793-800.
11. J. Zhang, W. Zhang, M. Xu, Y. Zhang, X. Fu, H. Fang, *J. Am. Chem. Soc.* 2018, **140**, 6656-6660
12. M. J. Frisch, G. W. Trucks, H. B. Schlegel, G. E. Scuseria, M. A. Robb, J. R. Cheeseman, G. Scalmani, V. Barone, G. A. Petersson, H. Nakatsuji, X. Li, M. Caricato, A. V. Marenich, J. Bloino, B. G. Janesko, R. Gomperts, B. Mennucci, H. P. Hratchian, J. V. Ortiz, A. F. Izmaylov, J. L. Sonnenberg, D. Williams-Young, F. Ding, F. Lipparini, F. Egidi, J. Goings, B. Peng, A. Petrone, T. Henderson, D. Ranasinghe, V. G. Zakrzewski, J. Gao, N. Rega, G. Zheng, W. Liang, M. Hada, M. Ehara, K. Toyota, R. Fukuda, J. Hasegawa, M. Ishida, T. Nakajima, Y. Honda, O. Kitao, H. Nakai, T. Vreven, K. Throssell, J. A. Montgomery, Jr., J. E. Peralta, F. Ogliaro, M. J. Bearpark, J. J. Heyd, E. N. Brothers, K. N. Kudin, V. N. Staroverov, T. A. Keith, R. Kobayashi, J. Normand, K. Raghavachari, A. P. Rendell, J. C. Burant, S. S. Iyengar, J. Tomasi, M. Cossi, J. M. Millam, M. Klene, C. Adamo, R. Cammi, J. W. Ochterski, R. L. Martin, K. Morokuma, O. Farkas, J. B. Foresman, and D. J. Fox, Gaussian, Inc., Wallingford CT, 2016.
13. a) K. Fukui, *Acc. Chem. Res.*, 1981, **14**, 363-368; b) H. P. Hratchian and H. B. Schlegel, in *Theory and Applications of Computational Chemistry: The First 40 Years*, Ed. C. E. Dykstra, G. Frenking, K. S. Kim, G. Scuseria (Elsevier, Amsterdam, 2005) 195-249.
14. G. Scalmani, M. J. Frisch, *J. Chem. Phys.*, 2010, **132**, 114-110.

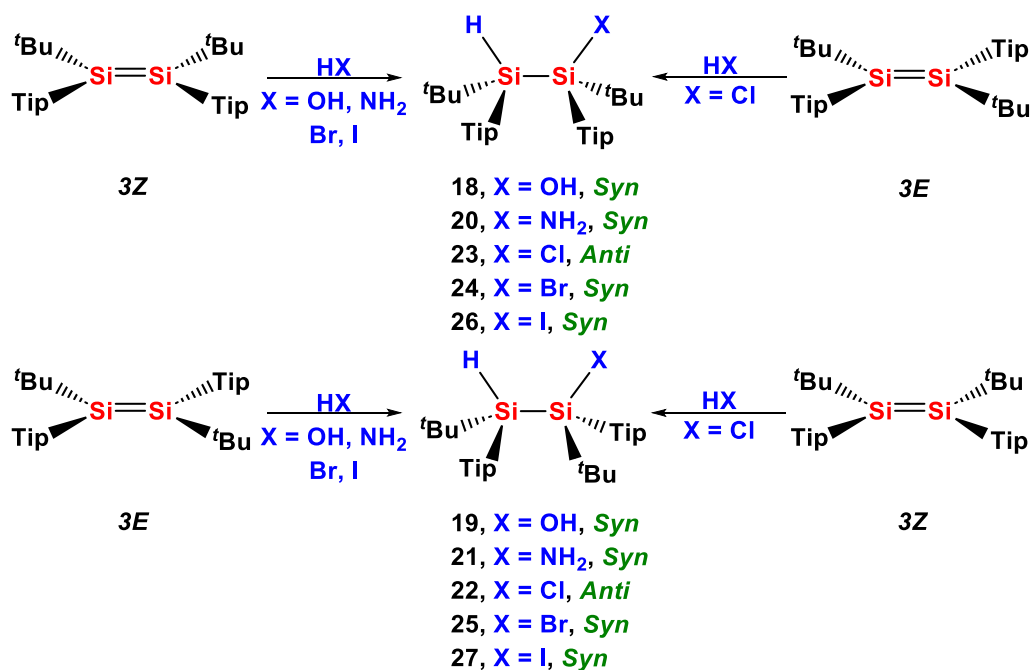
Chapter 4

4 Summary, Conclusion and Future Work

4.1 Summary

Herein, the stereochemistry of the addition of water, ammonia and HX (X = Cl, Br, I) to **3Z** or **3E** were examined. The influence of the reaction conditions, such as solvent, reagent concentration and temperature, on the stereochemistry of the reaction were also investigated. In addition, the stereochemistry of the hydrolysis of disilylamines and disilyl halides was investigated. Finally, mechanistic studies using kinetic experiments, specifically Variable Time Normalization Analysis (VTNA) and Kinetic Isotopic Effect (KIE) studies on the reaction of tetramesityldisilene with isopropylamine ($i\text{PrNH}_2$) were carried out to further understand the mechanism of the addition of amines to disilenes.

The addition of HX (X = OH, NH₂, Br, I) to disilene **3Z** or **3E** in benzene is 100 % stereospecific resulting in the exclusive formation of the *syn*-isomer. Interestingly, the addition of hydrochloric acid to **3E** and **3Z** gives the *anti*-isomer, 100 % stereospecifically (**Scheme 4.1**). Changing the solvent (benzene, THF), temperature, or concentration of the reagents had no effect on the stereochemistry of the addition reactions to disilene **3Z** or **3E**. The reactions were 100 % stereospecific in either benzene or THF. Increasing the temperature from rt to 40 °C only reduced the reaction time and led to the formation of more impurities. Increasing the concentration of water or ammonia from 0.012 to 1.15 M reduced the reaction time and did not affect the stereochemical outcome of the reaction.



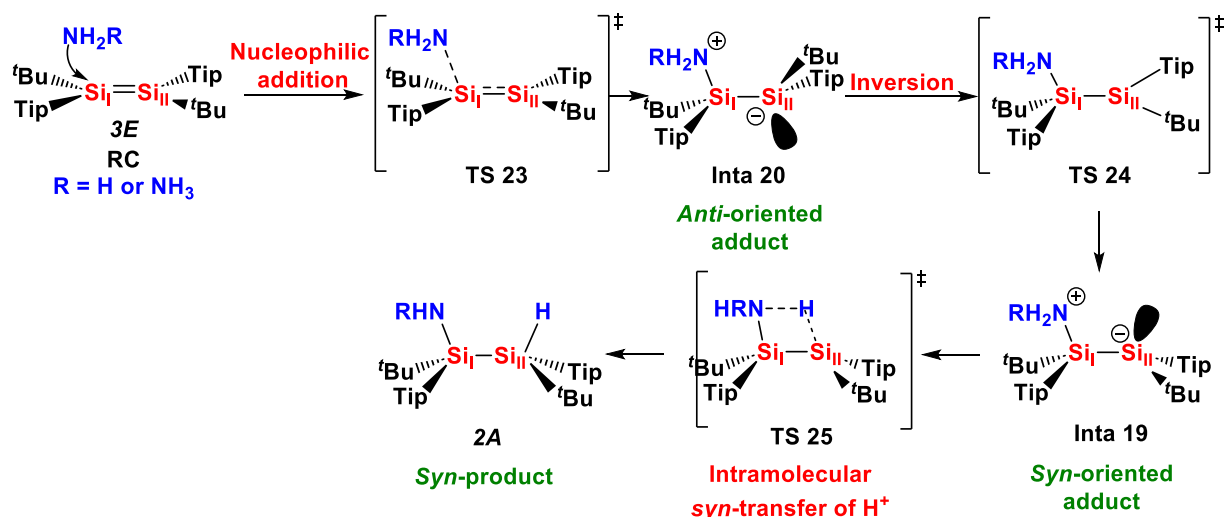
Scheme 4.1: Addition of HX (X = OH, NH₂, Cl, Br, I) to **3Z** or **3E**

The hydrolyses of silylamine **20**, **21** and silyl halides **22-27** were 100 % stereospecific resulting in inversion at the functionalized silicon center (Si-X). The hydrolysis of silylamine **20** and **21** requires an acid catalyst to react at a reasonable rate.

VTNA studies of the addition of ⁱPrNH₂ to disilene **1** revealed the order of the reaction to be 2 and the order of reactant to be 1 for both ⁱPrNH₂ and disilene **1**. The KIE experiments revealed a ratio of $k_H/k_D = 3.04 \pm 0.06$ at 298 K indicating a *primary* KIE, meaning the proton transfer is part of the rds. Computational studies indicate that the mechanism is nucleophilic addition of ammonia to give the *anti*-oriented donor adduct, inversion about the silicon with the lone pair, and then intramolecular *syn*-transfer of the proton. The rds was found to be the inversion in the addition of ammonia to disilene **3E** and **3Z**.

On the basis of the experimental studies and the computational work, the following mechanism is proposed for the addition of ammonia to disilene **3E** (**Scheme 4.2**). Nucleophilic addition of ammonia to silicon-silicon double bond results in the *anti*-donor adduct, then inversion about the silicon with the lone pair and then intramolecular *syn*-transfer of proton. Inversion is the rds and

is energetically more favored than rotation around the Si-Si bond as the rotational barrier is very high, breaking the Si-Si bond.



Scheme 4.2: The energetically favored pathway for the addition of ammonia or dimer to disilene **3E**.

4.2 Conclusion

The importance of understanding the mechanism allows to control the activation of small molecules such as ammonia and other small molecules by disilenes for future applications. Controlling the stereochemistry is an important factor for pharmaceutical compounds, highlighting the importance of this work in understanding and refining the fundamental reactivity of disilenes in σ -addition reactions.

Addition reactions of disilene **3E** or **3Z** are 100 % stereospecific, and thus, there is no planar silicon along the reaction pathway, and any silicon with a lone pair must have a significant barrier to inversion. These conclusions must be accounted for in any proposed mechanism for σ -addition to disilenes. For the addition of amines to disilenes, the three main steps in the mechanism are: formation of the donor adduct, inversion or rotation, and intramolecular *syn*-transfer of the proton.

The results of studies¹ to date lead to the following refinements of our understanding of the mechanism: 1) the order of amine can vary depending on the bulk of the substituents on the amine. Although the addition of the ammonia dimer to disilene **1** or **3E** is energetically accessible, and, in the case of disilene **1**, preferred, the experimental study of the addition of *i*PrNH₂ to disilene **1** is first order in amine. 2) the rds of the reaction pathway for the addition of amines to disilene varies depending on the bulk of the substituents on the disilene. For example, for disilene **1**, with Mes substituents, the rds is the intramolecular *syn*-transfer of the proton as demonstrated with NH₃, (NH₃)₂ and *i*PrNH₂ as the reagent. However, for the addition of NH₃ to disilene **3E**, with the Tip and *t*Bu substituents, the rds is inversion at the silicon bearing the lone pair in the donor adduct.

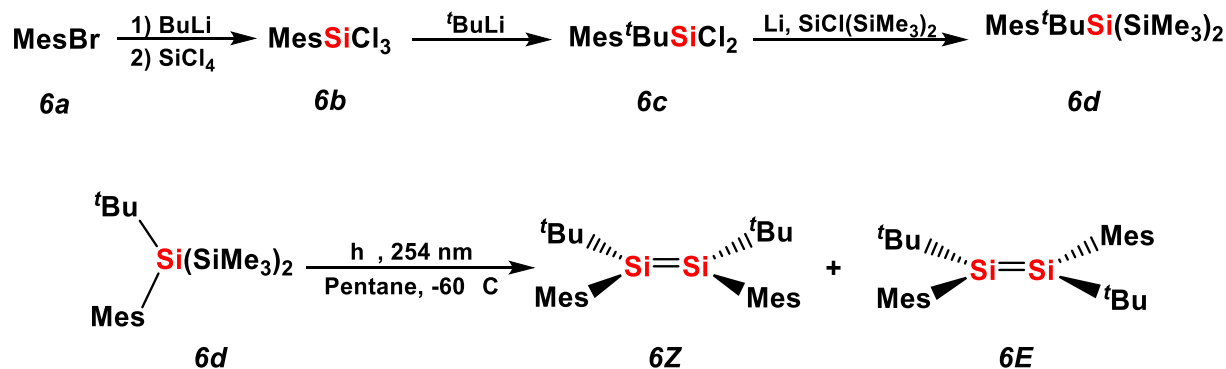
Moreover, preference for formation of the *anti*-donor adduct does not appear to depend on substituents on the disilene. For example, the addition of ammonia to disilene **1**, **3E** and **9Z**² give the *anti*-donor adduct despite the variation in the nature of the substituents on the disilene. Finally, whether a disilene will give the *anti*-product or the *syn*-product depends primarily on the twist angle of the disilene which, in turn, depends on the bulk/electronic effects of the substituents.

4.3 Future Work

The addition of HCl to disilenes **3E** or **3Z** gives the *anti*-isomer compared to the addition of HBr and HI, which give the *syn*-isomer. To understand the unique stereochemical outcome of the HCl addition, computational studies, in collaboration with Gül Altınbaş Özpınar and Thomas Müller from the Carl von Ossietzky Universität Oldenburg, the mechanism of the halide addition reaction should be carried out.

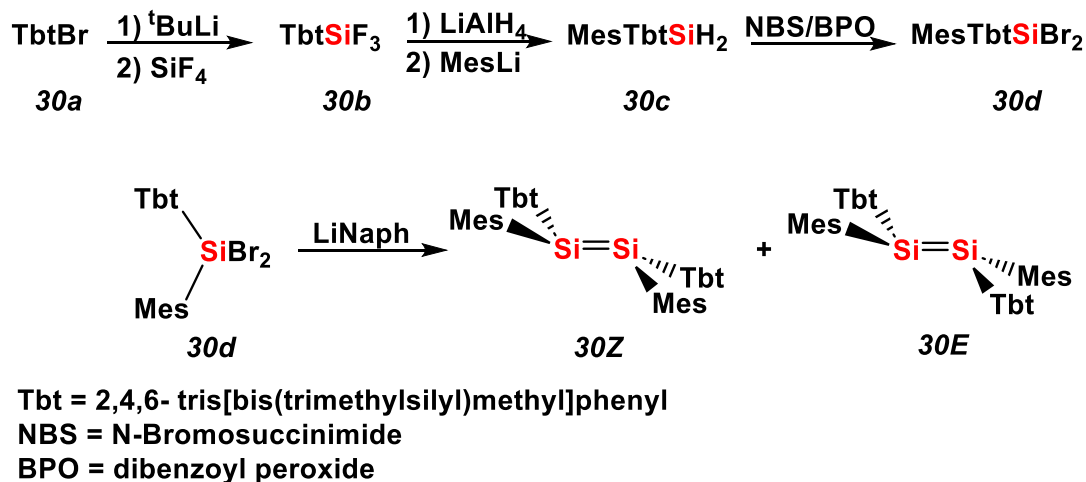
The addition of water, HCl and alcohols to disilene **6E**³ give a diastereomeric mixture of products. In contrast to the stereospecific addition reactions of **3E** and **3Z** observed in this work, it is difficult to understand these conflicting results. Thus, it was attempted to understand the formation of the diastereomeric mixtures by repeating the addition of HX to disilene **6E**. However, the literature procedure for the synthesis of the precursor of disilene **6E**, Mes^{*t*}BuSi(SiMe₃)₂,⁴ was not successful despite multiple attempts. The procedure was modified to be the same as the synthesis of the

precursor to disilene **3E**, $\text{Tip}^t\text{BuSi}(\text{SiMe}_3)_2$;⁵ however, only low yield (~ 5 %) was obtained of $\text{Mes}^t\text{BuSi}(\text{SiMe}_3)_2$ (**Scheme 4.3**).



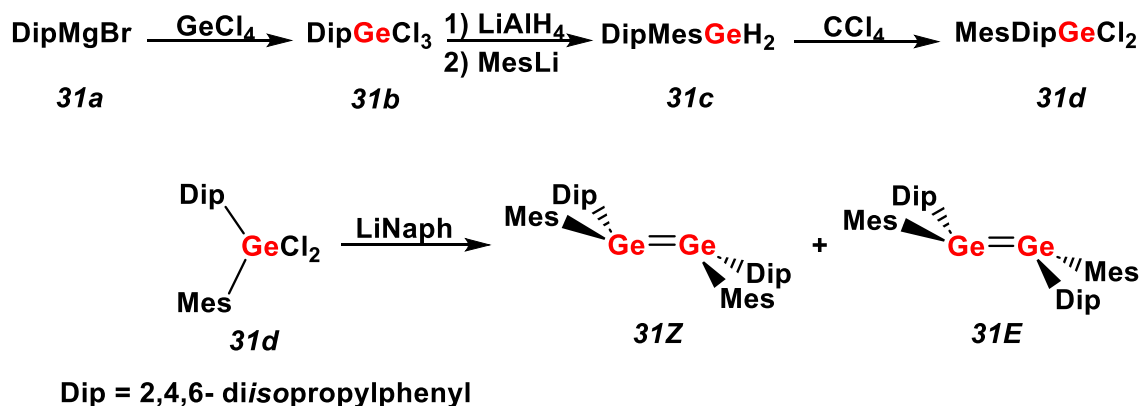
Scheme 4.3: Synthesis of disilene **6E** and **6Z**

Photolysis of $\text{Mes}^t\text{BuSi}(\text{SiMe}_3)_2$ using the procedure reported by West and coworkers gave a 1:1 ratio of **6Z**:**6E**.⁴ It was not possible to cleanly separate the isomers. Further work is required to develop a clean synthesis of **6E** and **6Z** which are required to reinvestigate the stereochemistry of the addition of H_2O and HCl and other reagents to **6E** and **6Z**. Possibly, the diastereomeric mixture of products resulted from the reaction of a mixture of disilene **6E** and **6Z**, and this may explain the anomalous results obtained by West and coworkers. Disilene 1,2-bis(2,4,6-tris[bis(trimethylsilyl)methyl]phenyl)-1,2-bis(2,4,6-trimethylpropylphenyl)disilene (**30Z** or **30E**) have twist angles of 9.3° and 14.6° , respectively, and can be explored with the addition of HX (**Scheme 4.4**).⁶ Although, the twist angle is not as high of disilene **9Z** ($\tau = 23.1^\circ$), it is a potential disilene with a twist that can be explored to determine if the stereochemistry of the product depends primarily on the twist angle of the disilene. The results can be compared to those of disilenes **1**, **3Z/E** and **6Z/E**.



Scheme 4.4: Synthesis of disilene **30E** and **30Z**.⁶

Finally, exploring the stereochemistry of σ -addition in digermenes is of interest as there is very little known about the stereochemistry of digermene σ -additions. One of the few examples explored is the addition of NH_3 and PrNH_2 to tetramesityldigermene.¹ However, as a symmetrical digermene, there is no stereochemistry associated with the reaction. An asymmetrical digermene that can be utilized in future stereochemical studies as the substrate are the *E* and *Z* isomers of 1,2-bis(2,4-diisopropylphenyl)-1,2-bis(2,4,6-trimethylpropylphenyl)digermenes (**31Z** and **31E**) (Scheme 4.5).⁷



Scheme 4.5: Synthesis of digermene **31E** and **31Z**.⁷

The understanding of the reaction mechanism experimentally and computationally for the σ -addition to disilene will hopefully inspire future work into the area of disilene chemistry. And allow a better understanding to control the reactivity of disilenes.

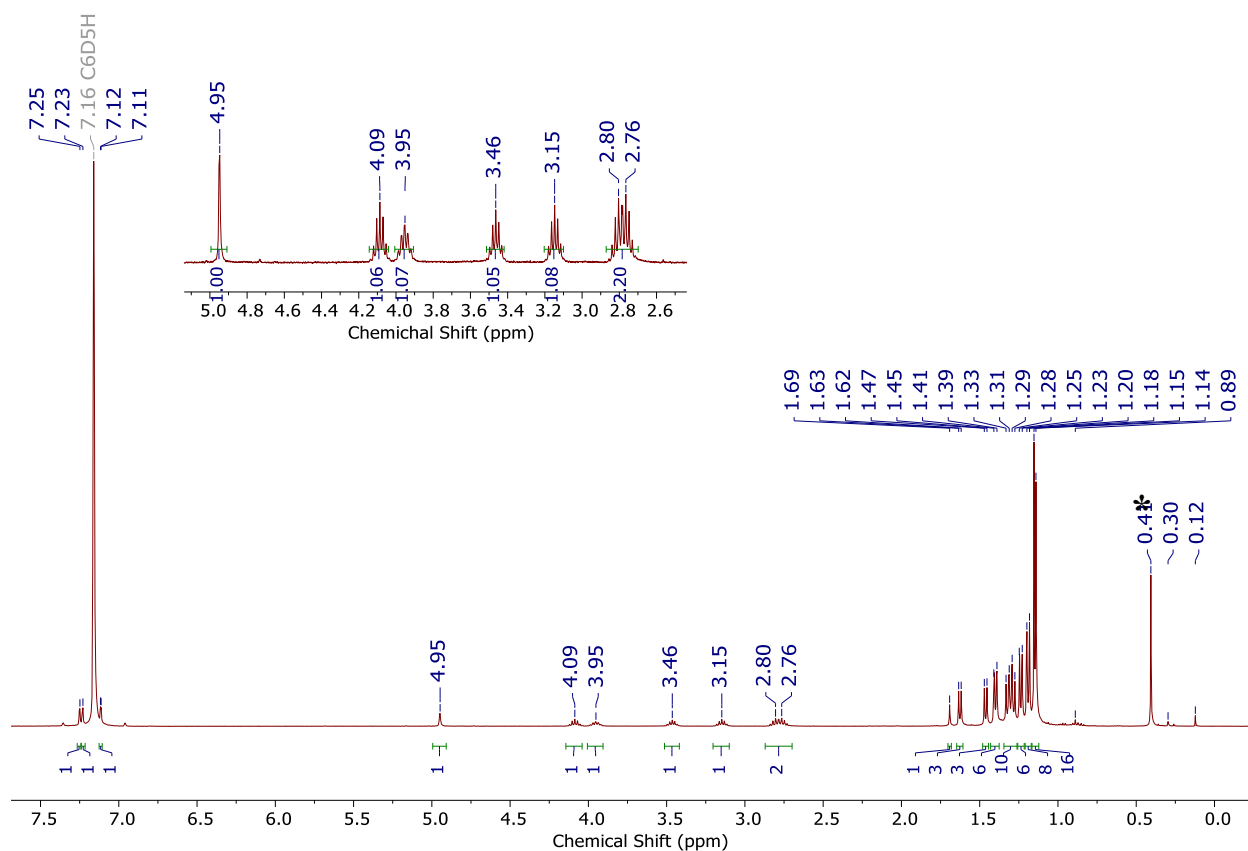
4.4 References

1. S. L. McOnie, G. A. Özpınar, J. L. Bourque, T. Müller, K. M. Baines, *Dalton Trans.*, 2021, **50**, 17734-17750.
2. D. Wendel, T. Szilvási, D. Henschel, P. J. Altmann, C. Jandl, S. Inoue, B. Rieger, *Angew. Chem. Int. Ed.*, 2018, **57**, 14575-14579.
3. M. J. Fink, M. J. Michalczyk, K. J. Haller, R. West, J. Michl, *Organometallics*, 1984, **3**, 793-800.
4. D. J. De Young, M. J. Fink, R. West, *Main Group Met. Chem.*, 1987, **10**, 19-43.
5. R. S. Archibald, Y. V. Winkel, A. J. Millevolte, J. M. Desper, R. West, *Organometallics*, 1992, **11**, 3276-3281.
6. H. Suzuki, N. Tokitoh, R. Okzaki, *Organometallics*, 1995, **14**, 1016-1022.
7. J. Park, S. A. Batcheller, S. Masamune, *J. Organomet. Chem.*, 1989, **367**, 39-45.

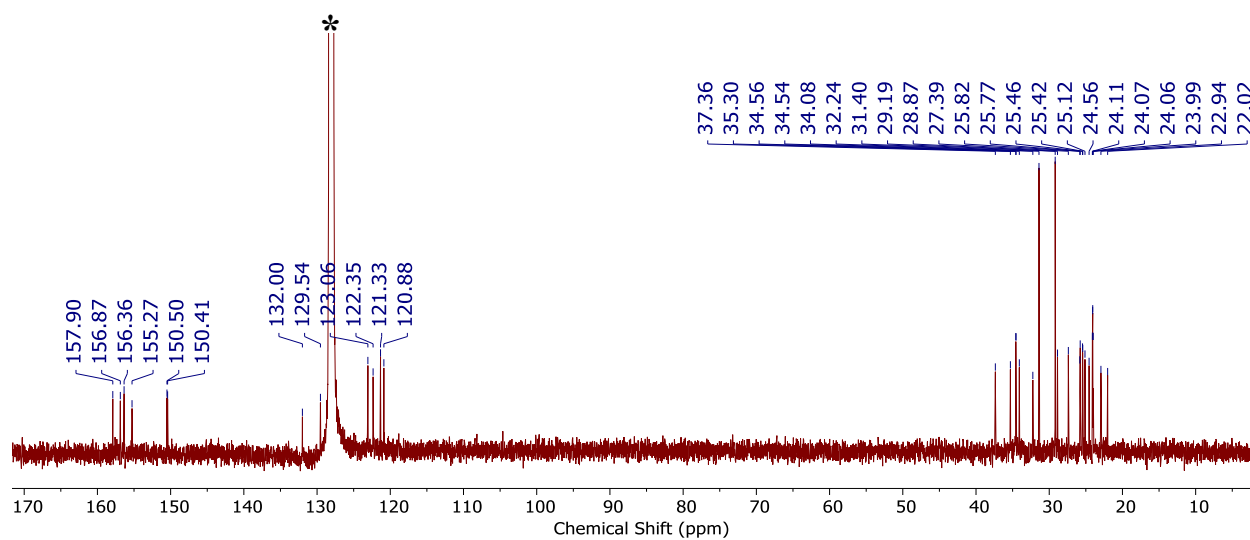
5 Appendices

5.1 Appendix A: Supplementary Material for Chapter 2

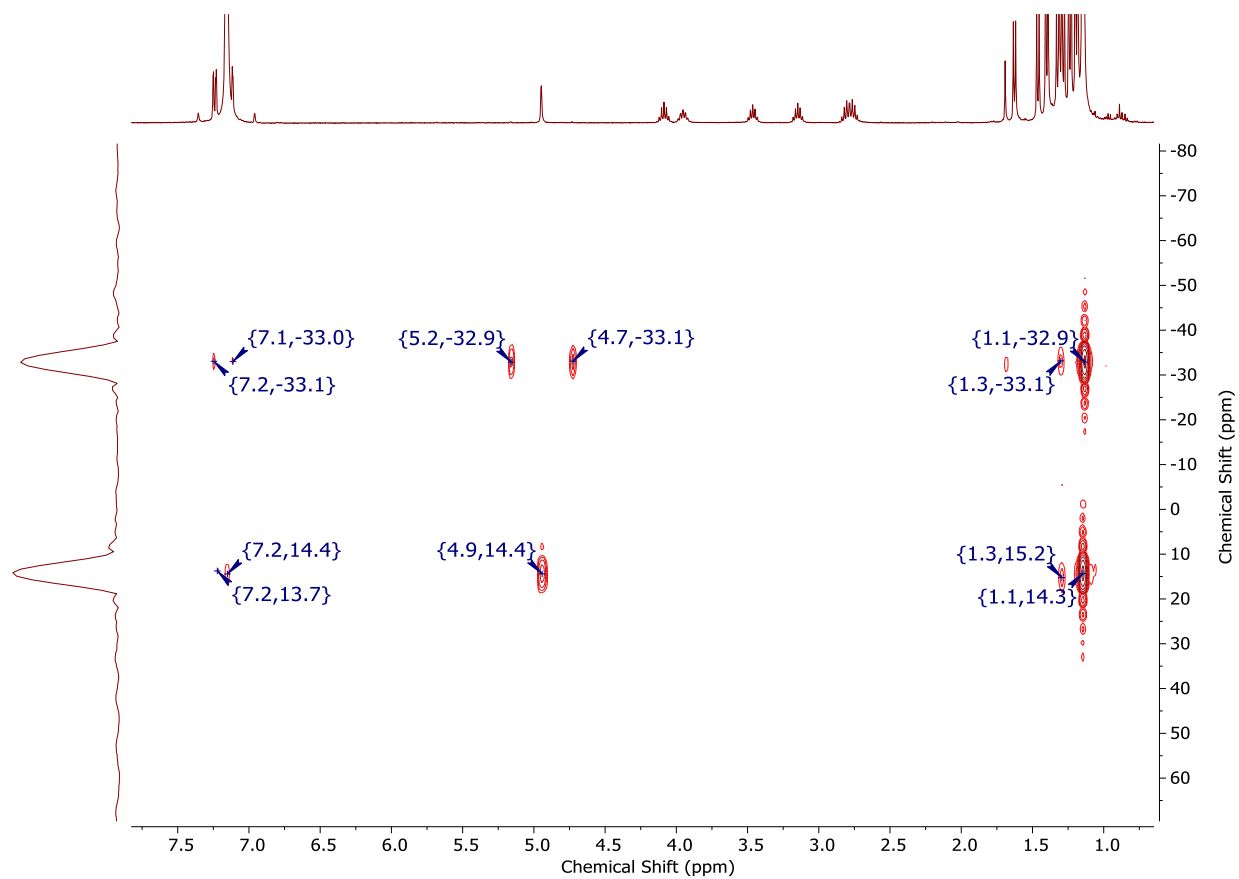
5.1.1 NMR Spectra Data for Compounds **18-27**



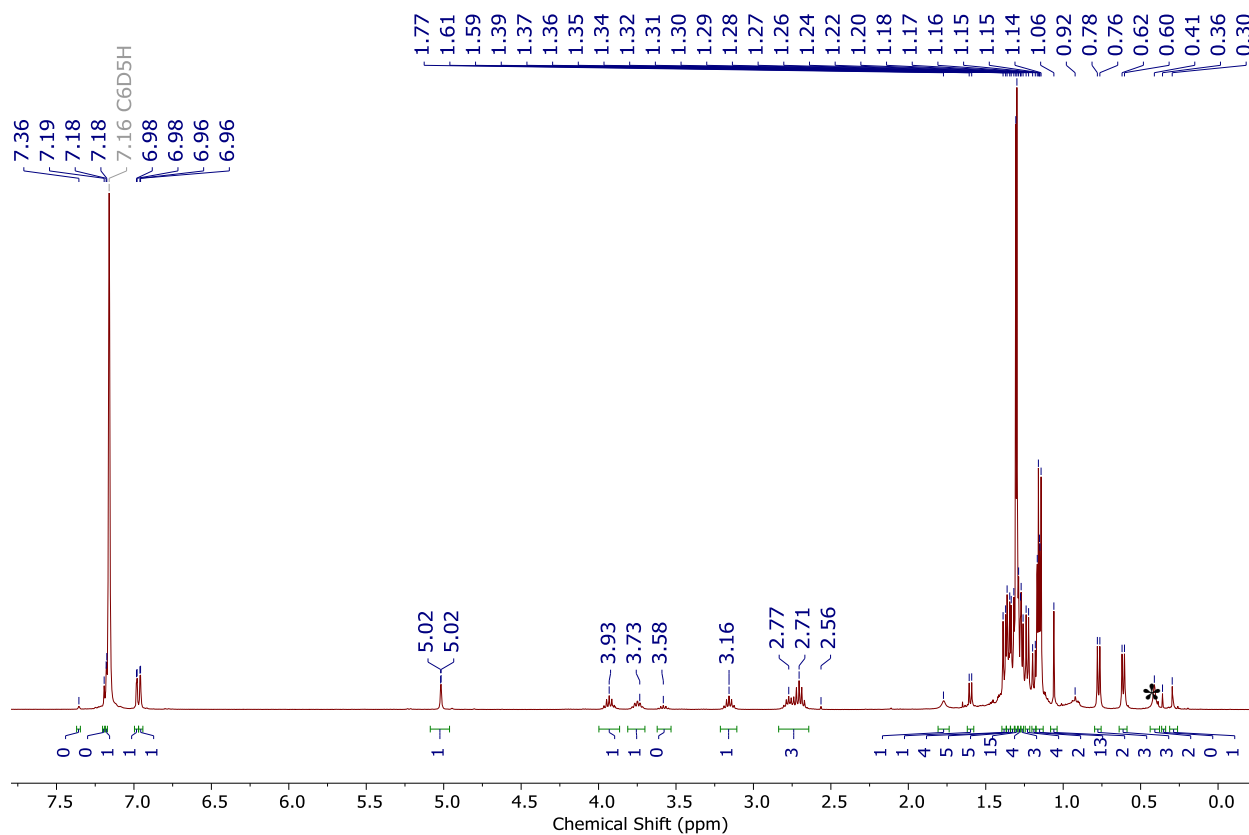
AA Figure 1 ^1H NMR spectrum (400 MHz, $\text{C}_6\text{D}_5\text{H}$) of $\text{X} = \text{OH}$, **18** from **3Z**. The signal denoted by * is trace water. Upfield signals in the spectrum are attributed to trace impurities from the synthesis of **18**.



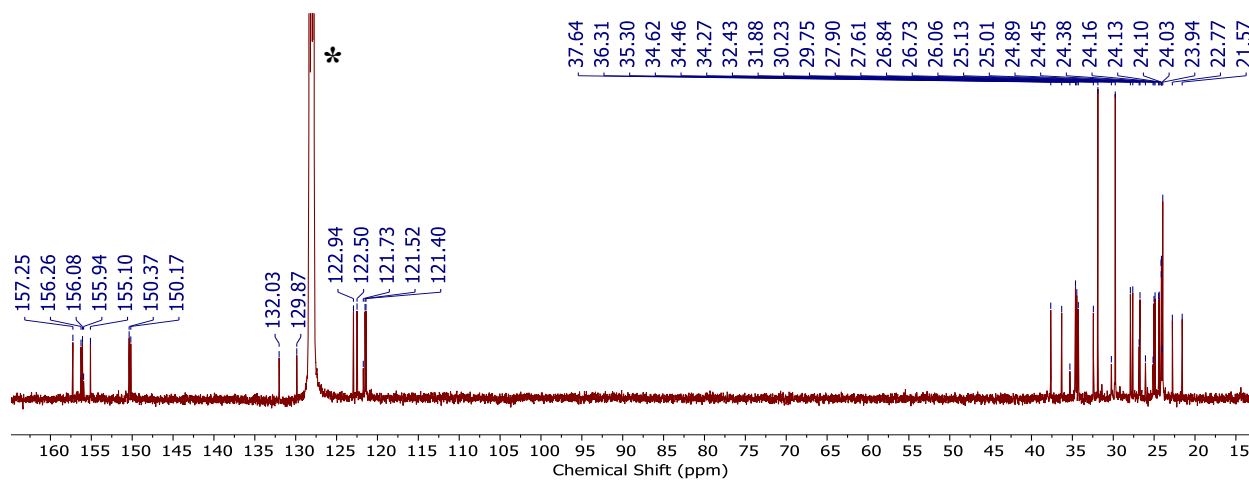
AA Figure 2 $^{13}\text{C}\{^1\text{H}\}$ NMR spectrum (100 MHz, C_6D_6) of $\text{X} = \text{OH}$, **18**. The signal denoted with * is the solvent C_6D_6 .



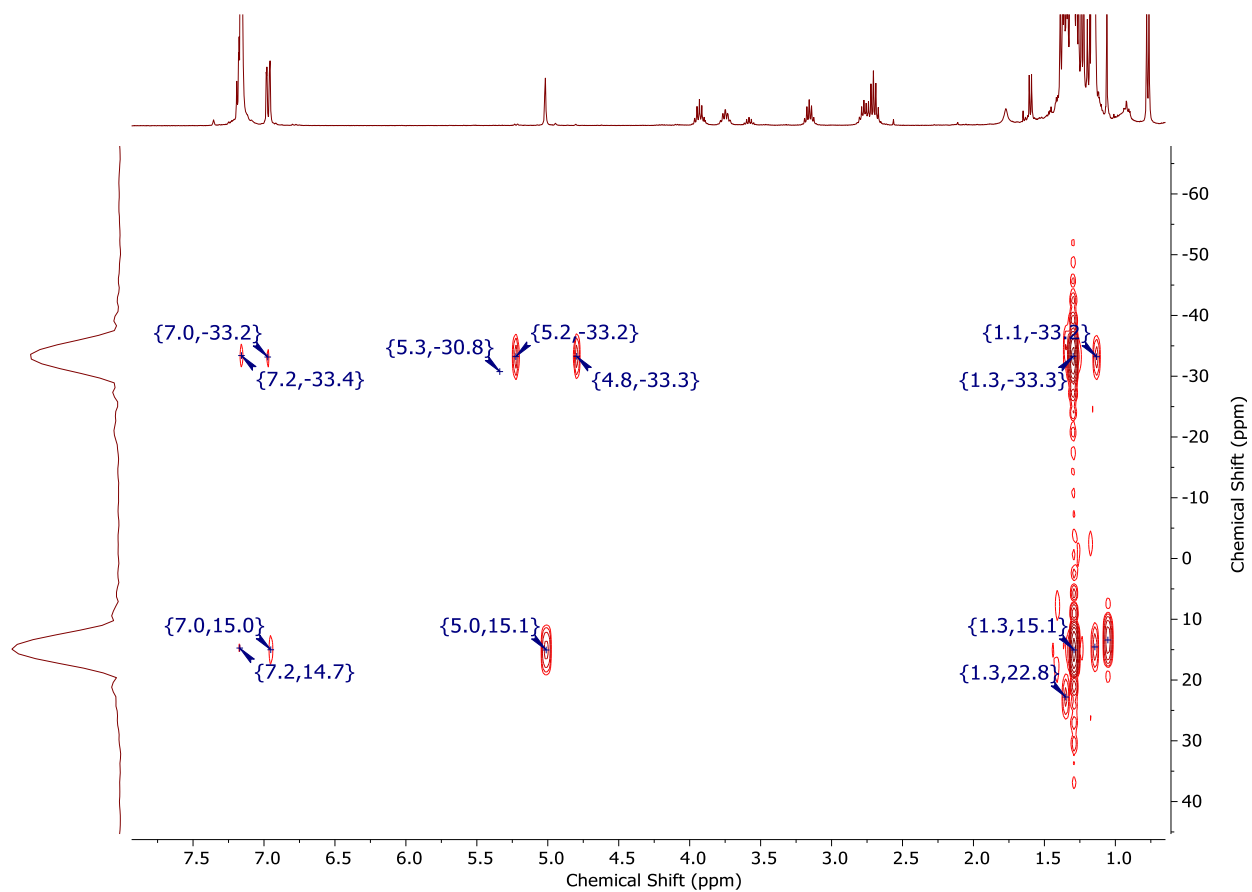
AA Figure 3 $^1\text{H}\text{-}^{29}\text{Si}$ gHMBC spectrum (C_6D_6) of $\text{X} = \text{OH}$, **18**.



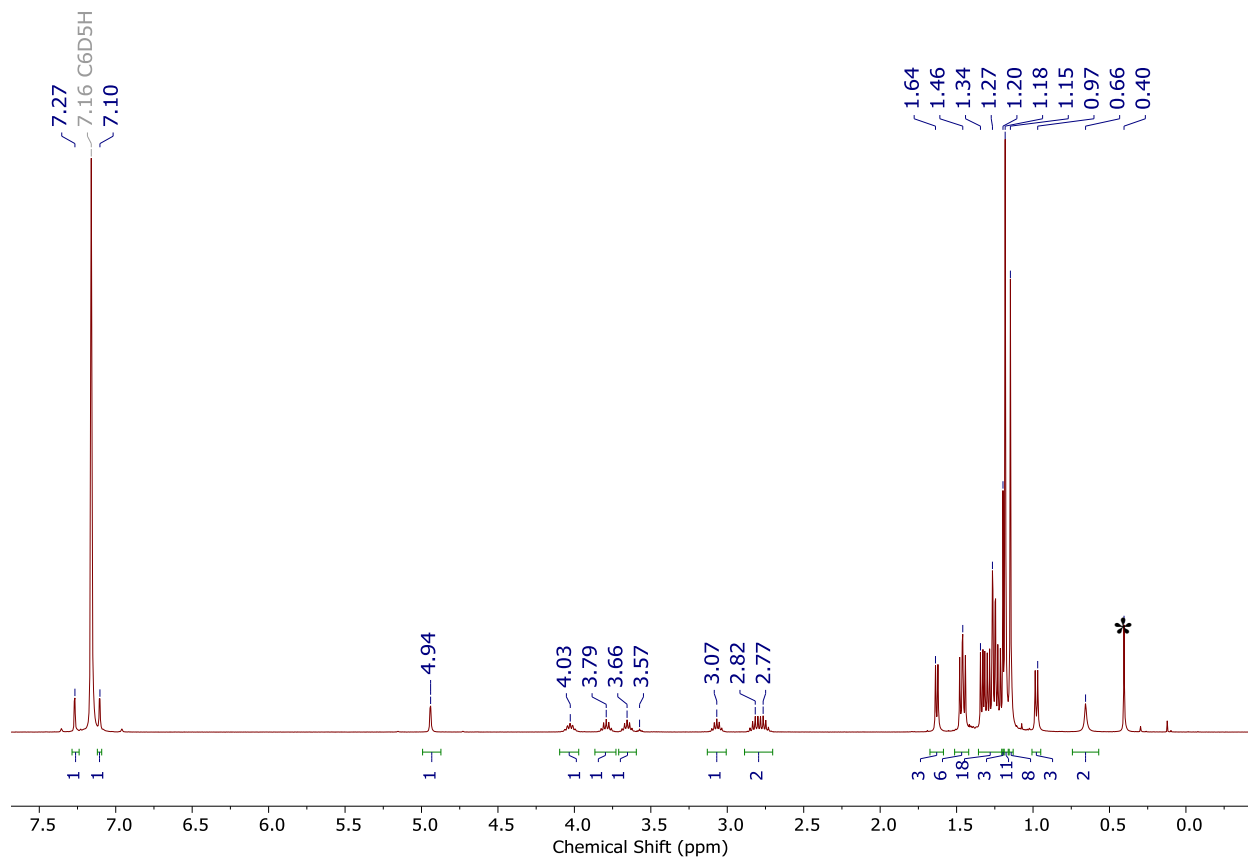
AA Figure 4 ¹H NMR spectrum (400 MHz, C₆D₅H) of **X = OH**, **19** from **3E**. The signal denoted by * is trace water. Upfield signals in the spectrum are attributed to trace impurities from the synthesis of **19**.



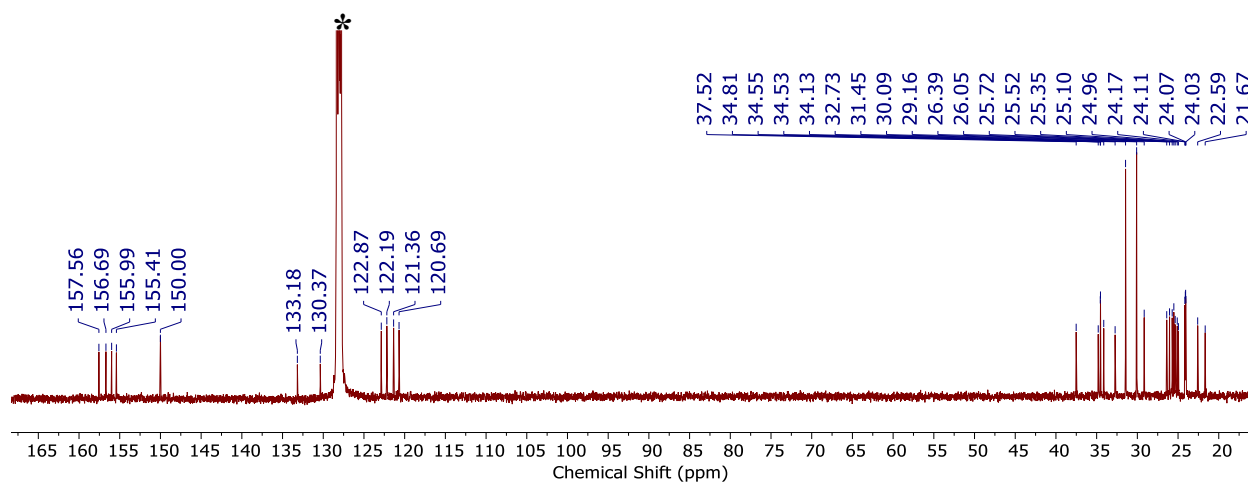
AA Figure 5 $^{13}\text{C}\{^1\text{H}\}$ NMR spectrum (100 MHz, C_6D_6) of $\text{X} = \text{OH}$, **19** from **3E**. The signal denoted with * is the solvent C_6D_6 .



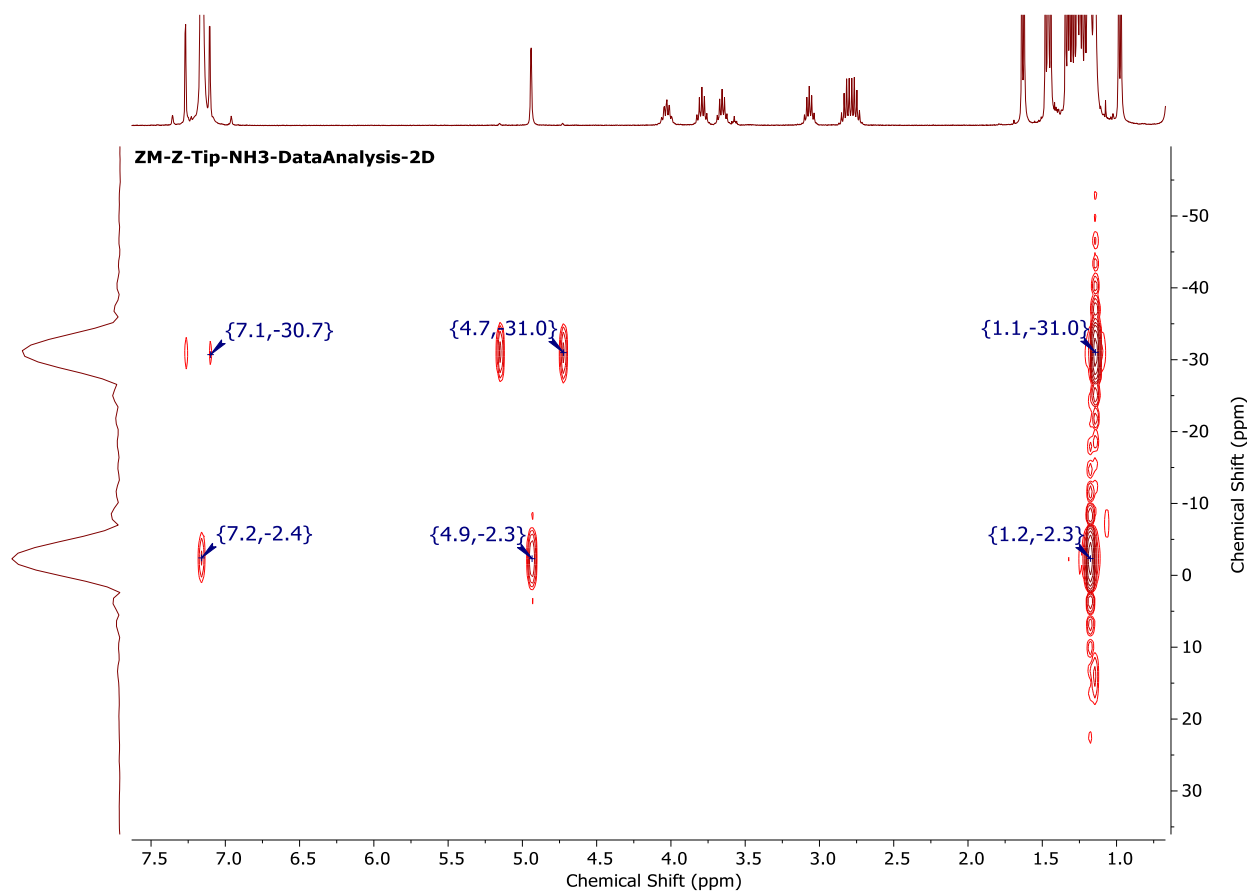
AA Figure 6 $^1\text{H}-^{29}\text{Si}$ gHMBC spectrum (C_6D_6) of $\text{X} = \text{OH}$, **19** from **3E**.



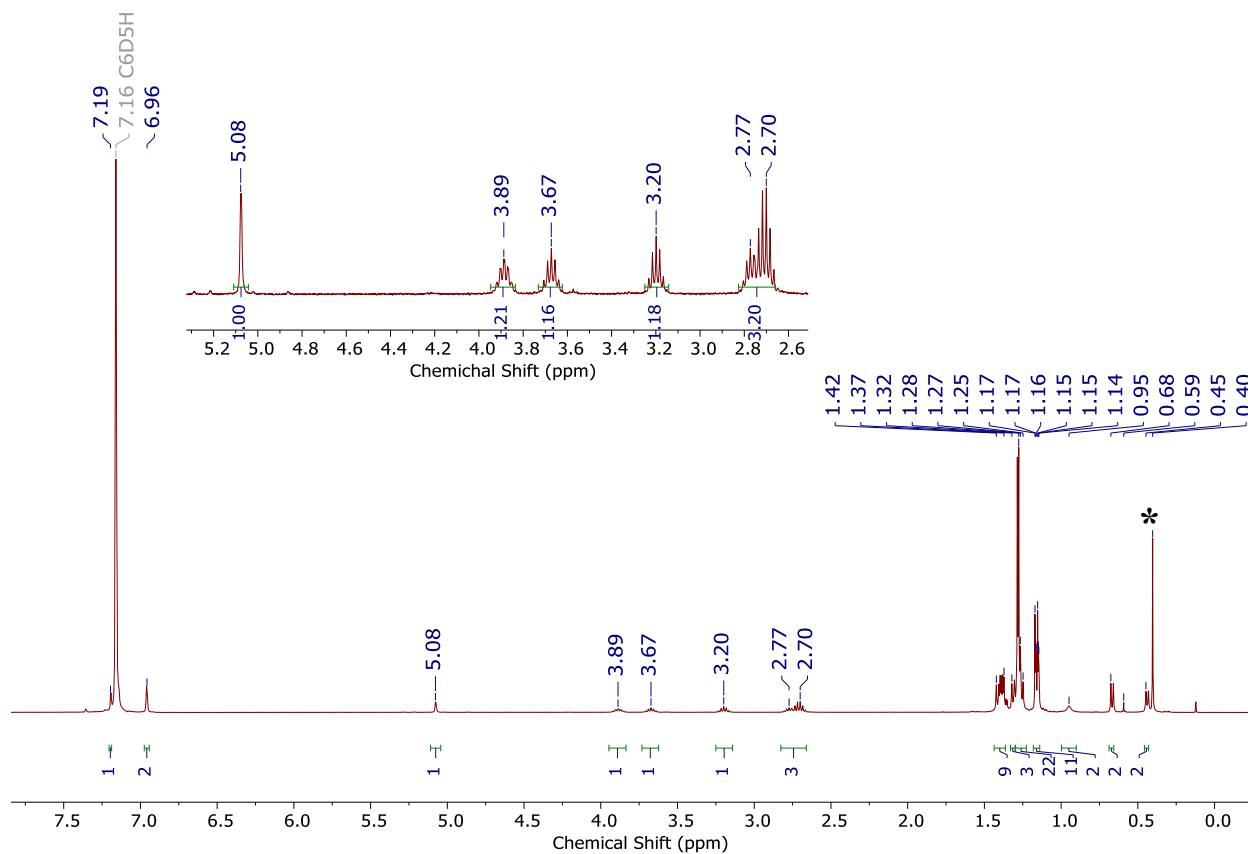
AA Figure 7 ^1H NMR spectrum (400 MHz, $\text{C}_6\text{D}_5\text{H}$) of $\text{X} = \text{NH}_2$, **20** from **3Z**. The signal denoted by * is trace water. Upfield signals in the spectrum are attributed to trace impurities from the synthesis of **20**.



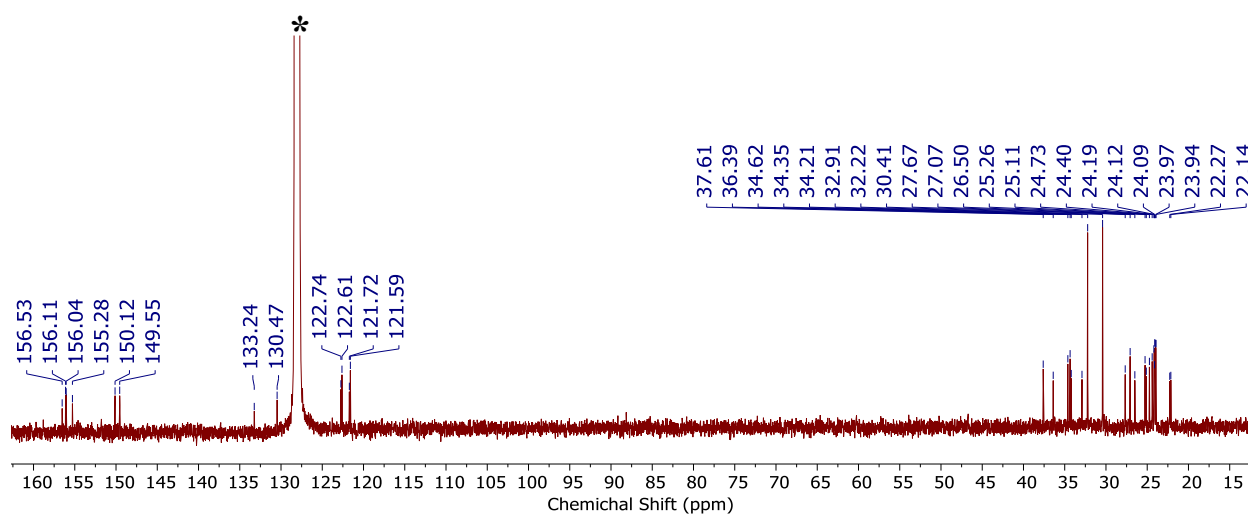
AA Figure 8 $^{13}\text{C}\{^1\text{H}\}$ NMR spectrum (100 MHz, C_6D_6) of $\text{X} = \text{NH}_2$, **20** from **3Z**. The signal denoted with * is the solvent C_6D_6 .



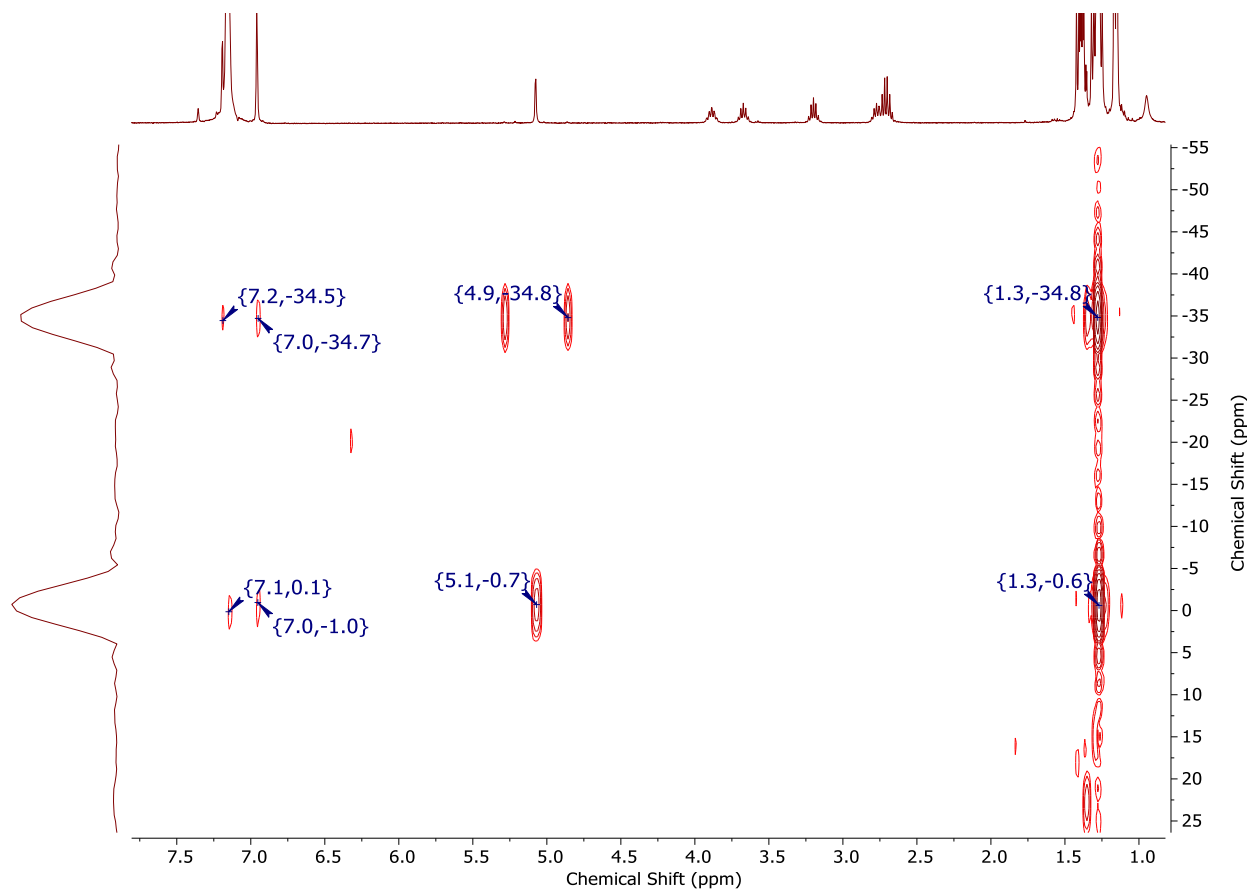
AA Figure 9 ^1H - ^{29}Si gHMBC spectrum (C_6D_6) of $\text{X} = \text{NH}_2$, **20** from **3Z**.



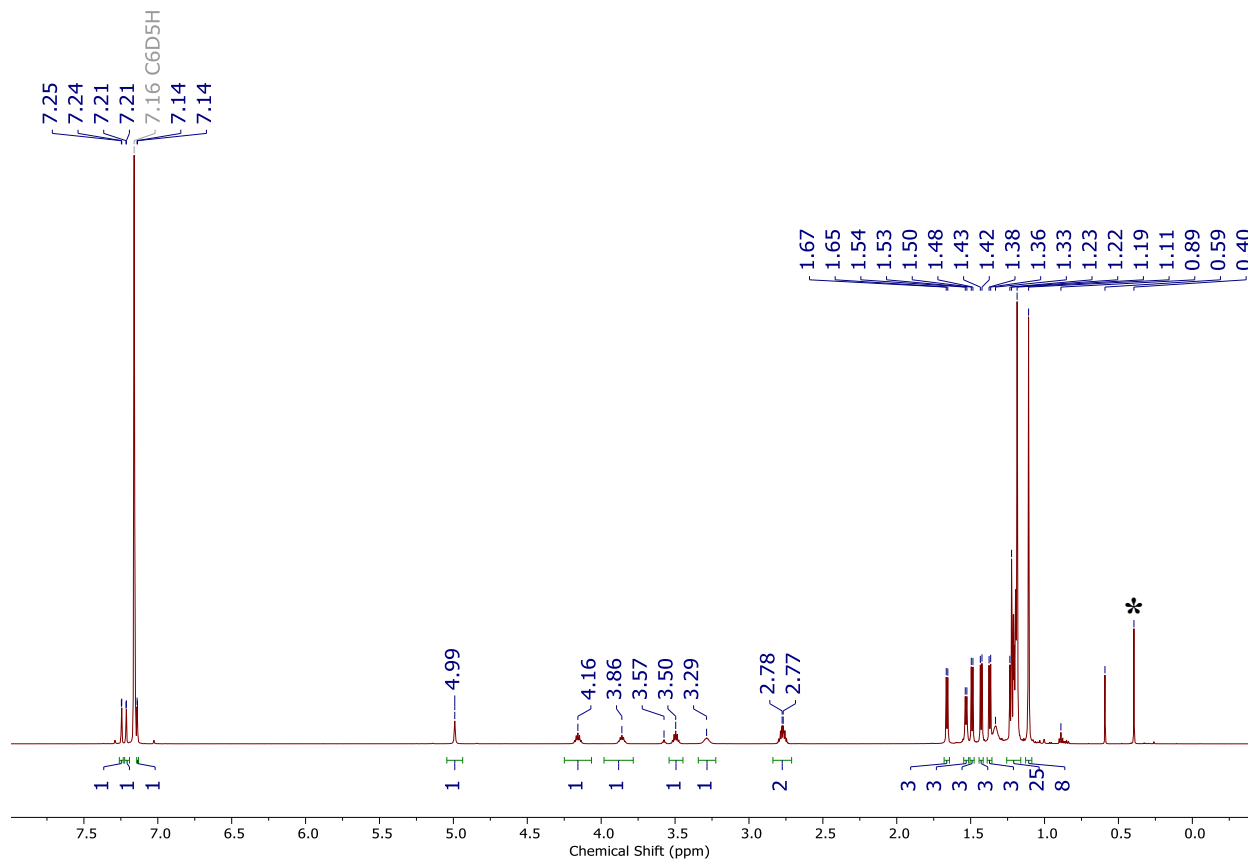
AA Figure 10 ^1H NMR spectrum (400 MHz, $\text{C}_6\text{D}_5\text{H}$) of $\text{X} = \text{NH}_2$, **21** from **3E**. The signal denoted by * is trace water. Upfield signals in the spectrum are attributed to trace impurities from the synthesis of **21**.



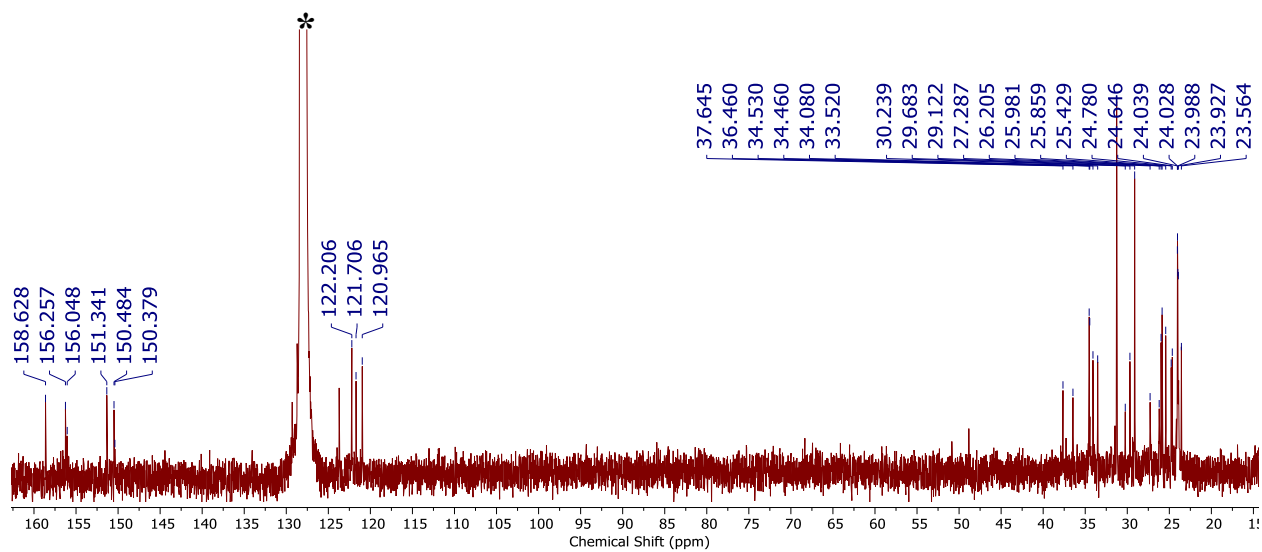
AA Figure 11 $^{13}\text{C}\{^1\text{H}\}$ NMR spectrum (100 MHz, C_6D_6) of $\text{X} = \text{NH}_2$, **21** from **3E**. The signal denoted with * is the solvent C_6D_6 .



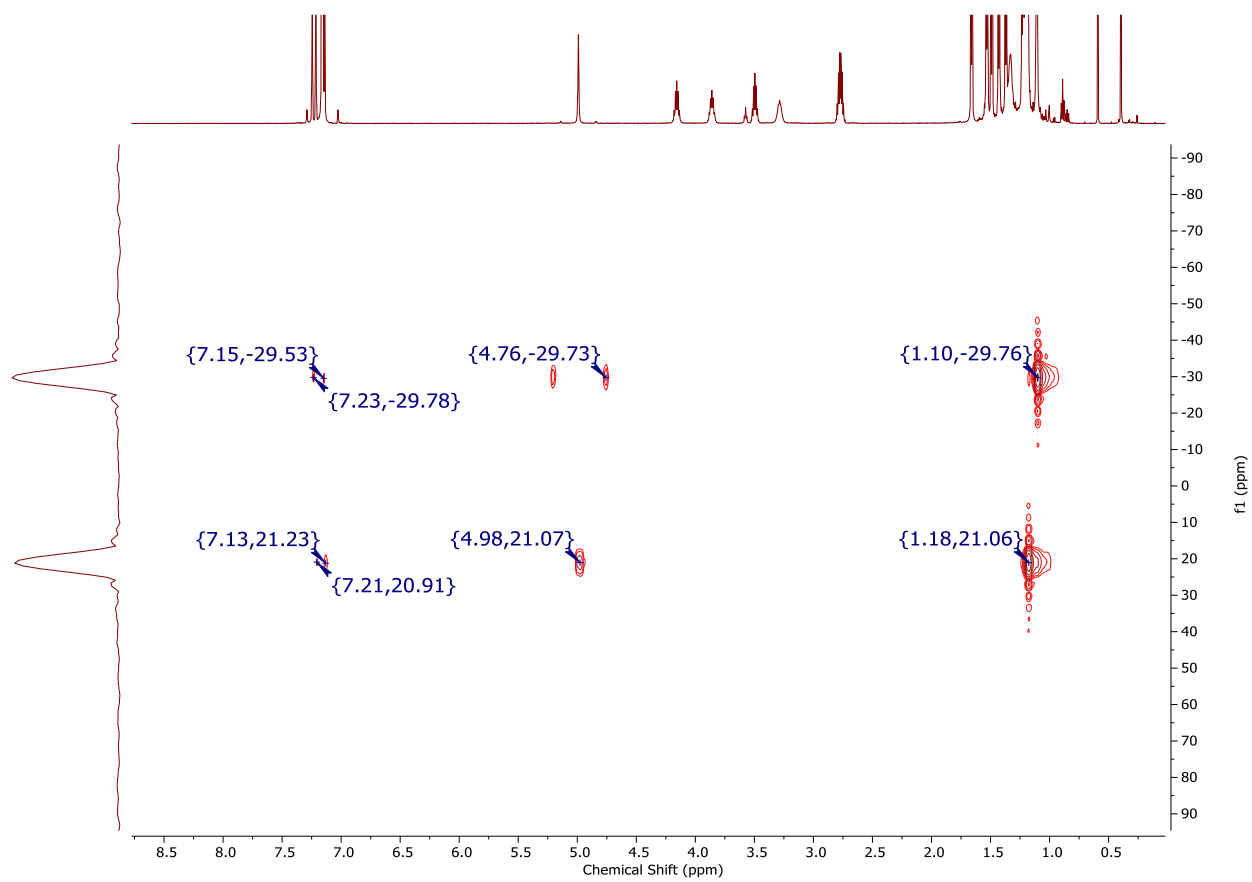
AA Figure 12 ^1H - ^{29}Si gHMBC spectrum (C_6D_6) of $\text{X} = \text{NH}_2$, **21** from **3E**.



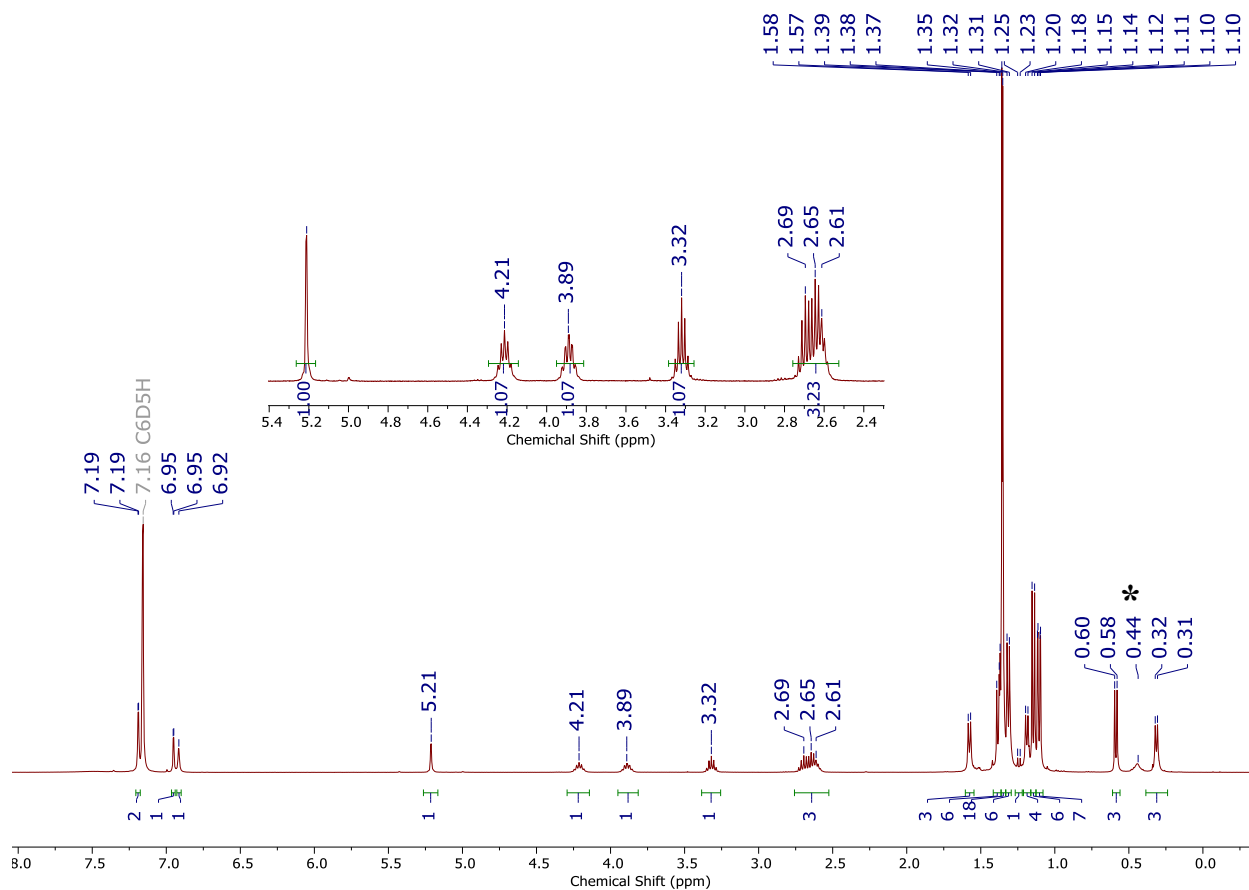
AA Figure 13 ^1H NMR spectrum (400 MHz, $\text{C}_6\text{D}_5\text{H}$) of $\text{X} = \text{Cl}$, **22** from **3Z**. The signal denoted by * is trace water.



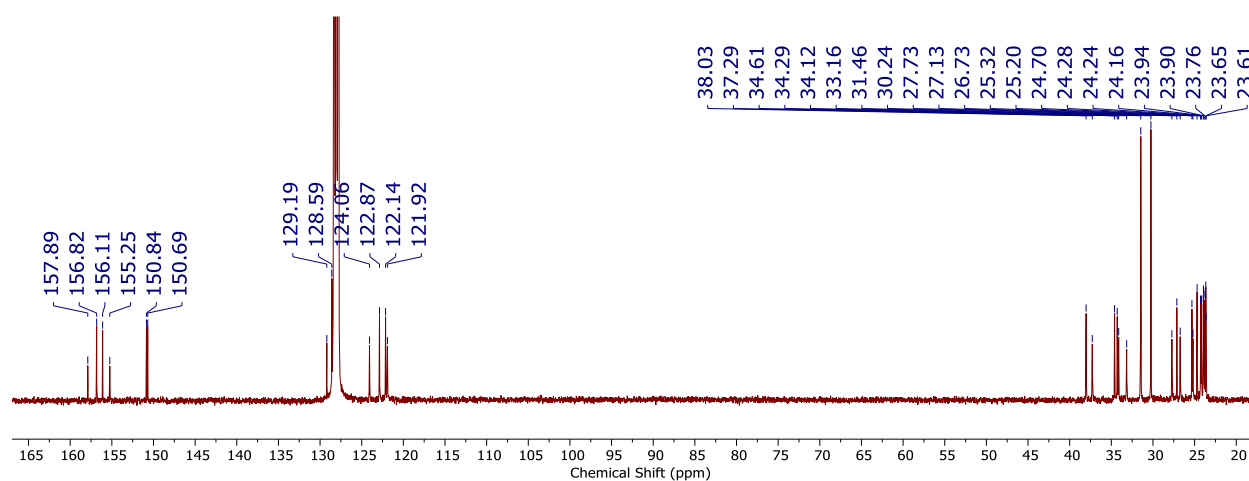
AA Figure 14 $^{13}\text{C}\{^1\text{H}\}$ NMR spectrum (100 MHz, C_6D_6) of $\text{X} = \text{Cl}$, **22** from **3Z**. The signal denoted with * is the solvent C_6D_6 .



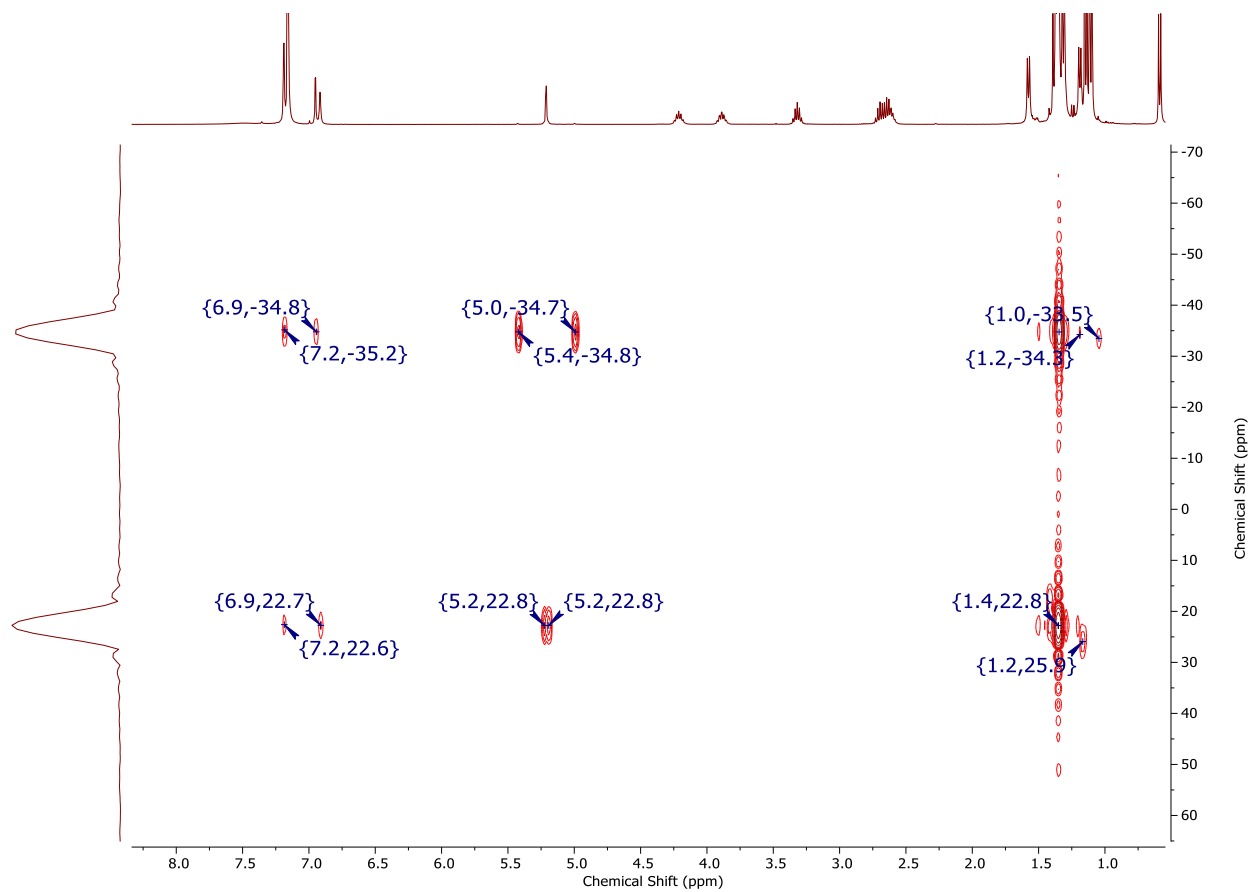
AA Figure 15 ^1H - ^{29}Si gHMBC spectrum (C_6D_6) of $\text{X} = \text{Cl}$, **22** from **3Z**.



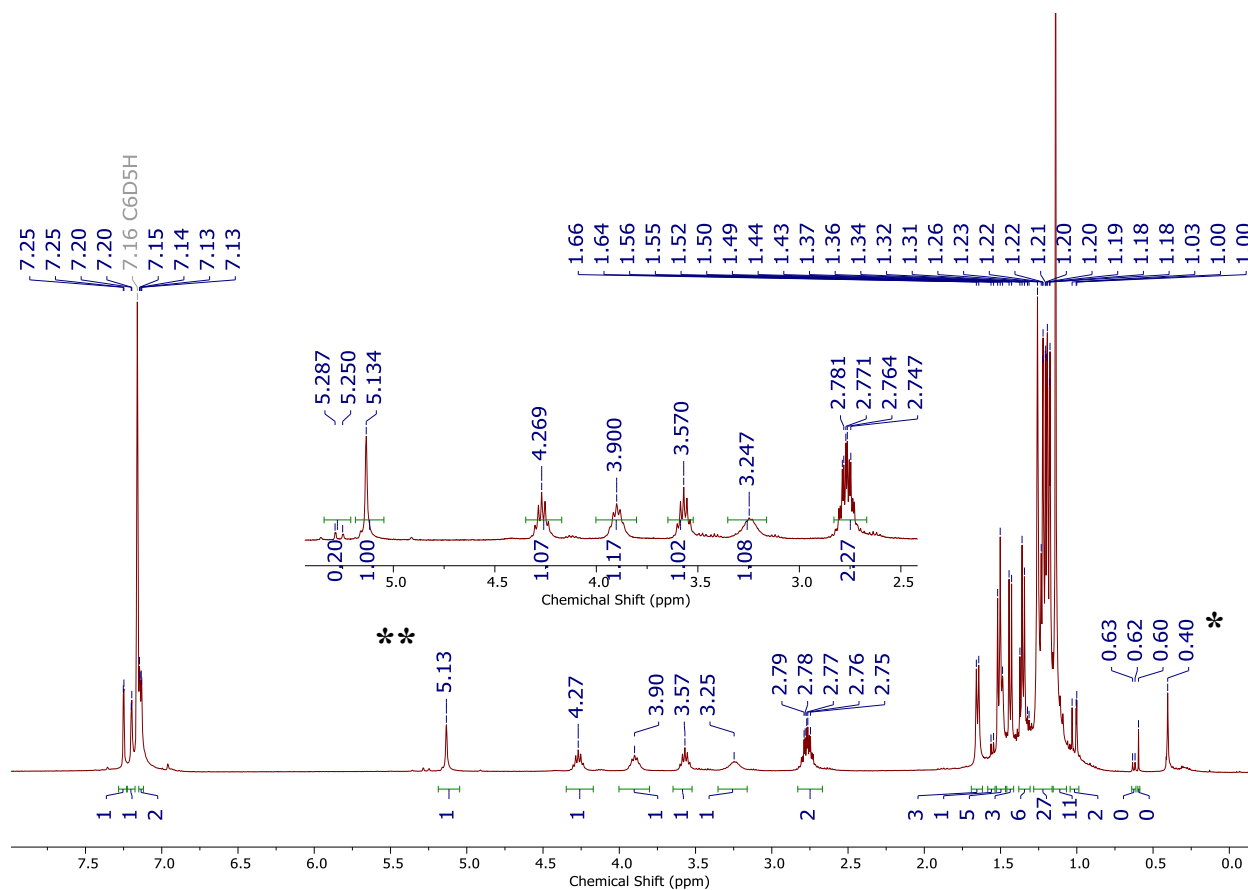
AA Figure 16 ^1H NMR spectrum (400 MHz, $\text{C}_6\text{D}_5\text{H}$) of $\text{X} = \text{Cl}$, **23** from **3E**. The signal denoted by * is trace water. Upfield signals in the spectrum are attributed to trace impurities from the synthesis of **23**.



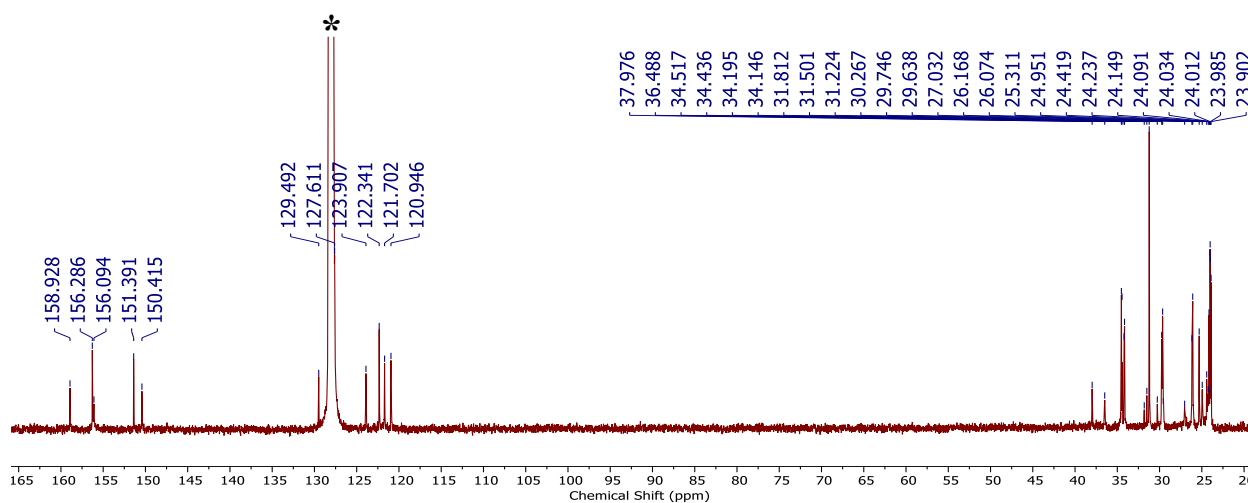
AA Figure 17 $^{13}\text{C}\{^1\text{H}\}$ NMR spectrum (100 MHz, C_6D_6) of $\text{X} = \text{Cl}$, **23** from **3E**. The signal denoted with * is the solvent C_6D_6 .



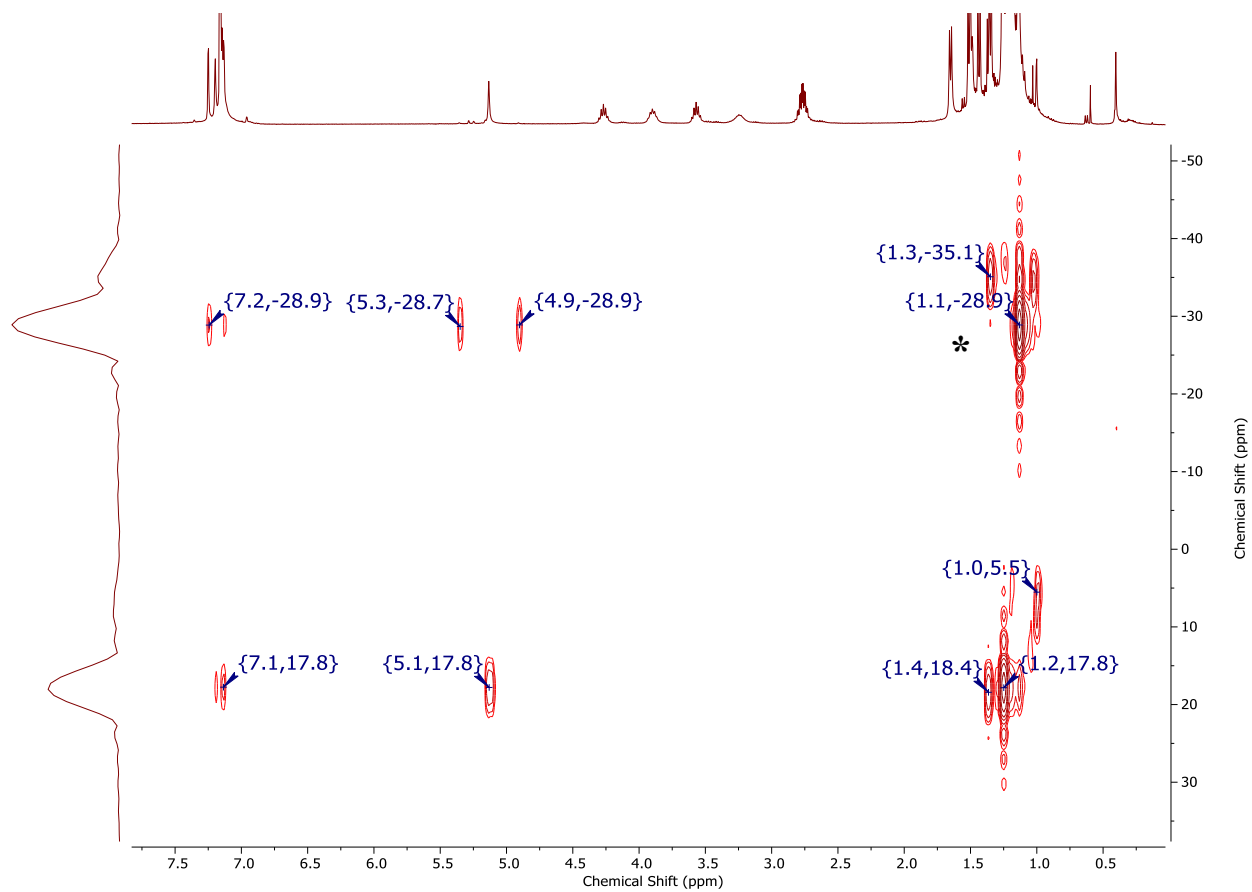
AA Figure 18 ^1H - ^{29}Si gHMBC spectrum (C_6D_6) of $\text{X} = \text{Cl}$, **23** from **3E**.



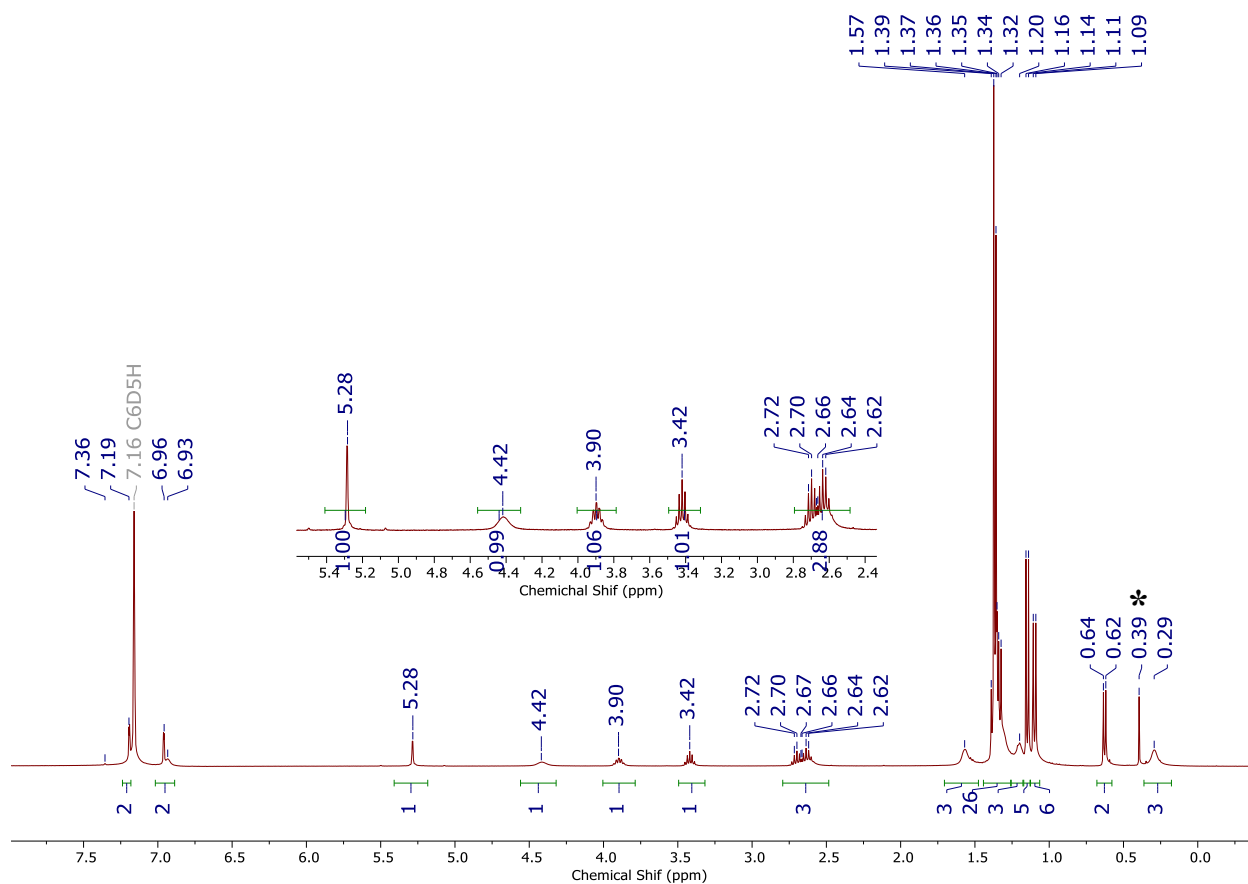
AA Figure 19 ^1H NMR spectrum (400 MHz, $\text{C}_6\text{D}_5\text{H}$) of $\text{X} = \text{Br}$, **24** from **3Z**. The signal denoted by * is trace water. The signal denoted ** is traces of **25** from **3E**.



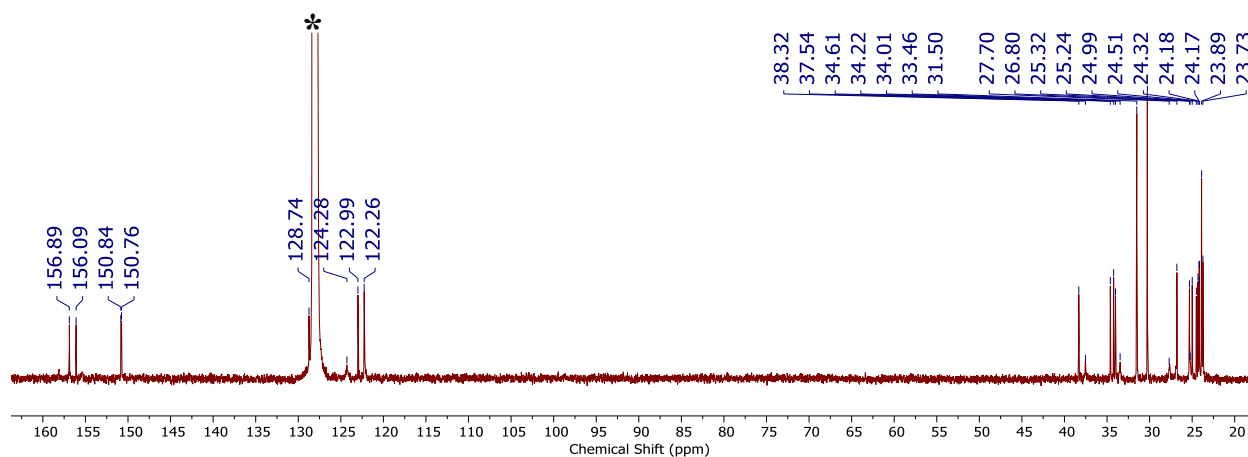
AA Figure 20 $^{13}\text{C}\{^1\text{H}\}$ NMR spectrum (100 MHz, C_6D_6) of $\text{X} = \text{Br}$, **24** from **3Z**. The signal denoted with * is the solvent C_6D_6 .



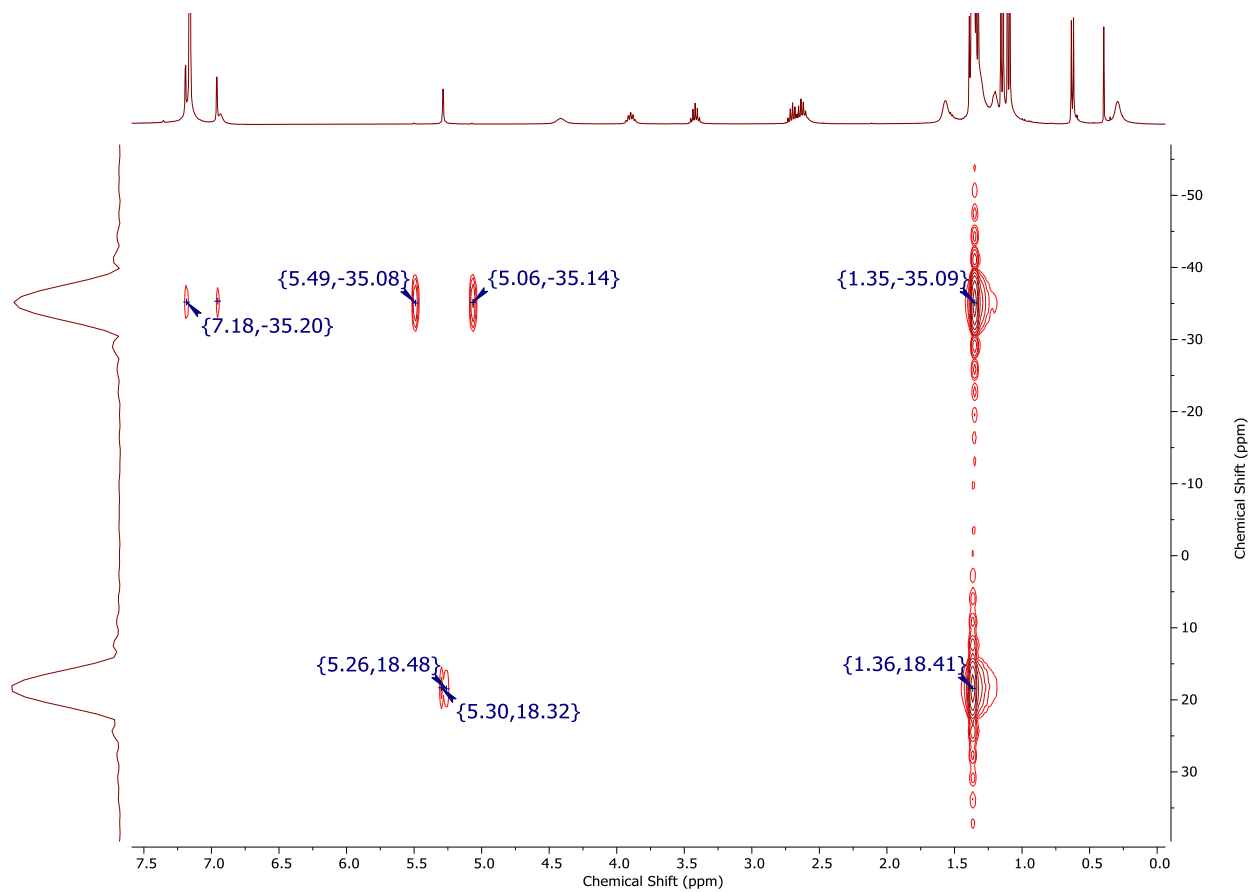
AA Figure 21 ^1H - ^{29}Si gHMBC spectrum (C_6D_6) of $\text{X} = \text{Br}$, **24** from **3Z**. The signal denoted * is traces of **25** from **3E**.



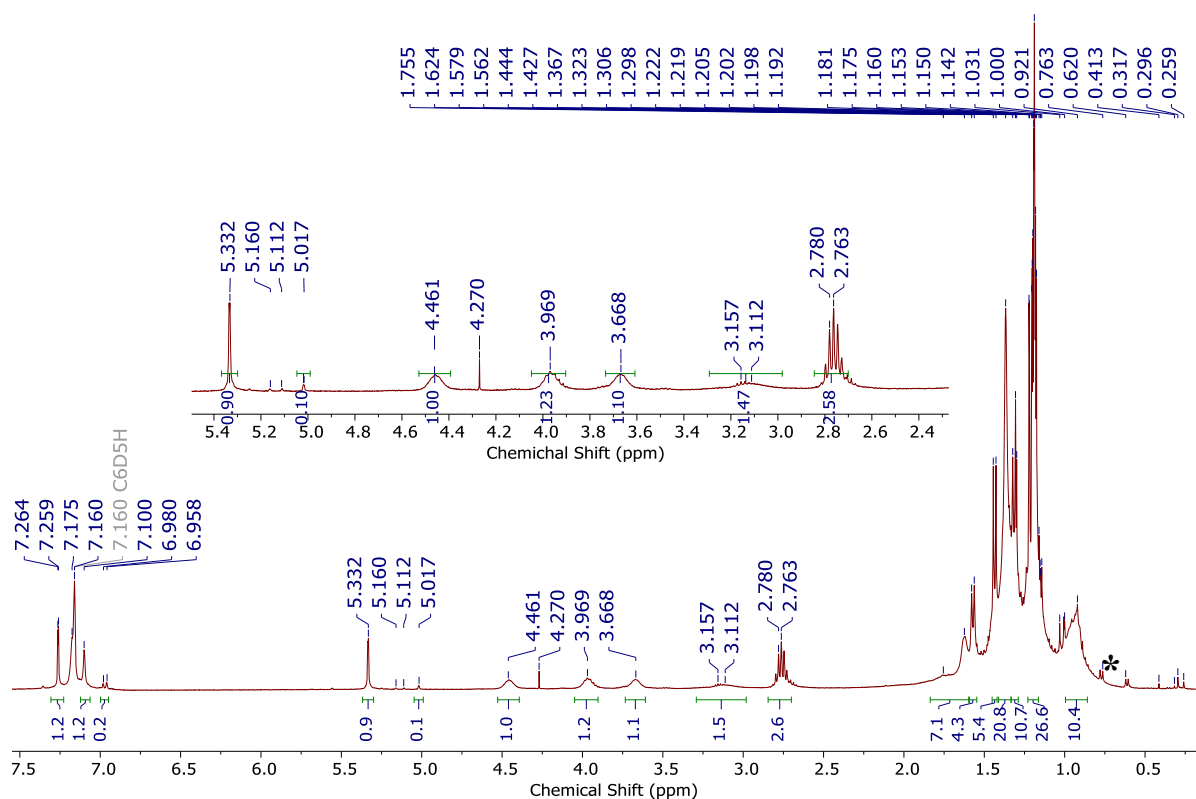
AA Figure 22 ^1H NMR spectrum (400 MHz, $\text{C}_6\text{D}_5\text{H}$) of $\text{X} = \text{Br}$, **25** from **3E**. The signal denoted by * is trace water.



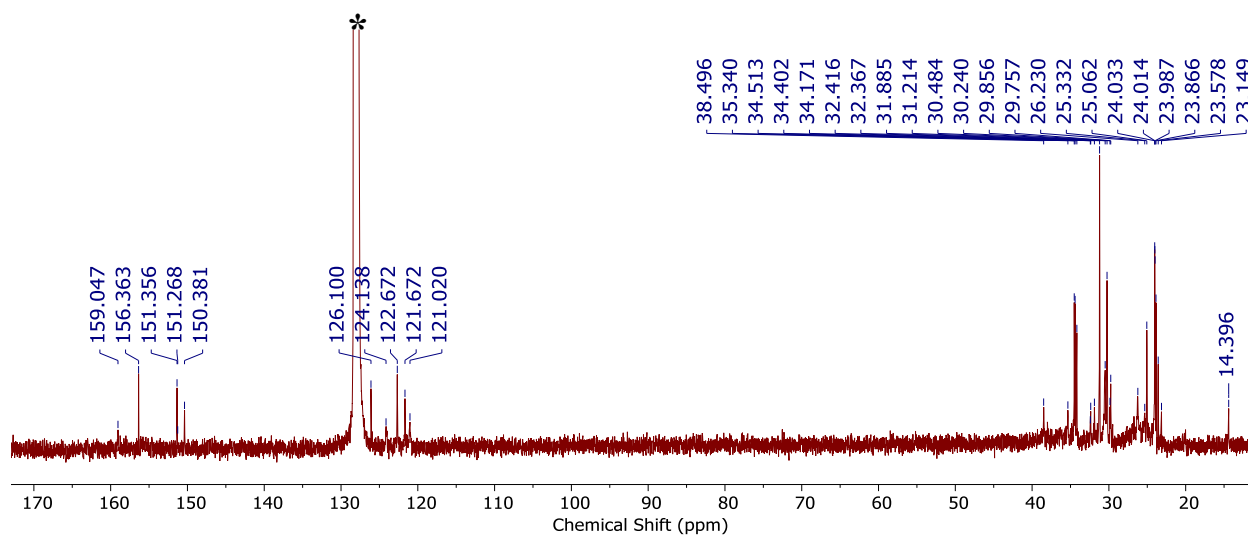
AA Figure 23 $^{13}\text{C}\{^1\text{H}\}$ NMR spectrum (100 MHz, C_6D_6) of $\text{X} = \text{Br}$, **25** from **3E**. The signal denoted with * is the solvent C_6D_6 .



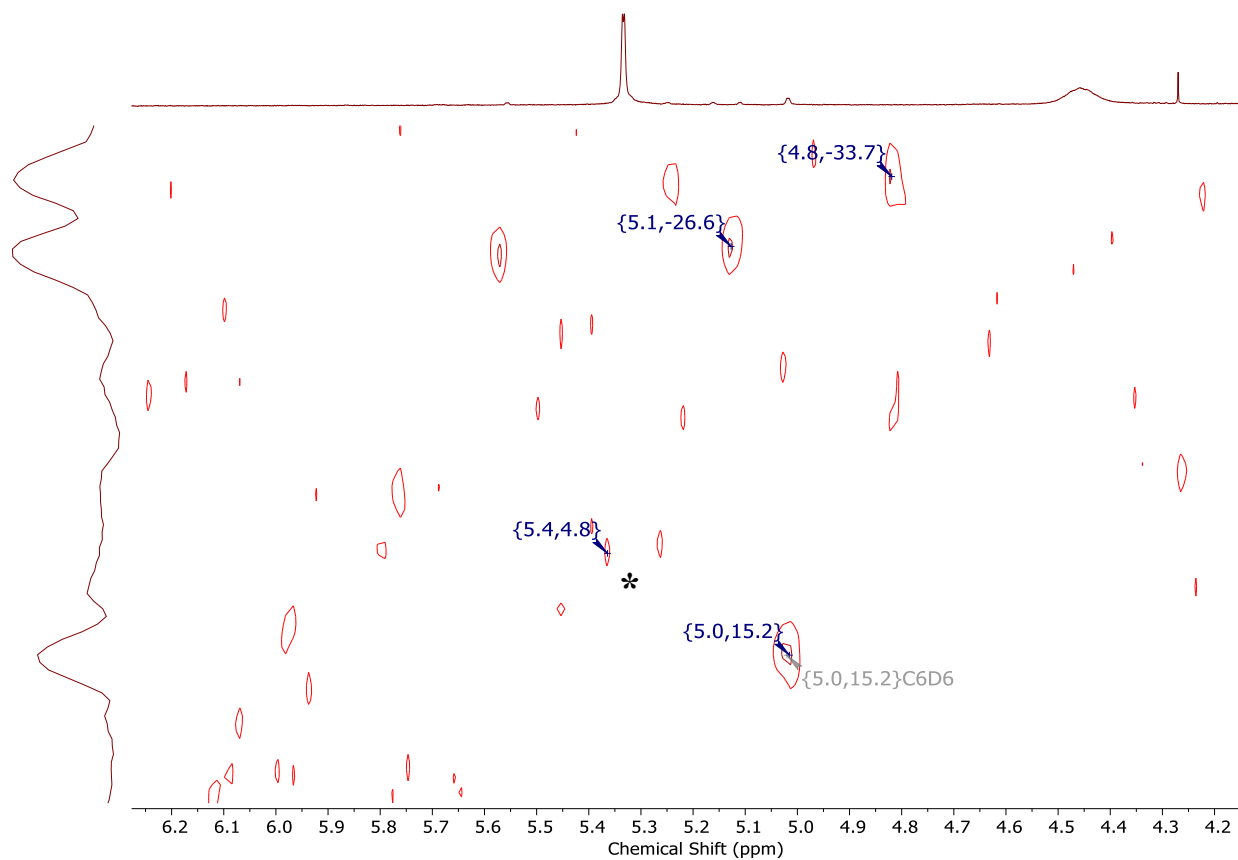
AA Figure 24 ^1H - ^{29}Si gHMBC spectrum (C_6D_6) of $\text{X} = \text{Br}$, **25** from **3E**.



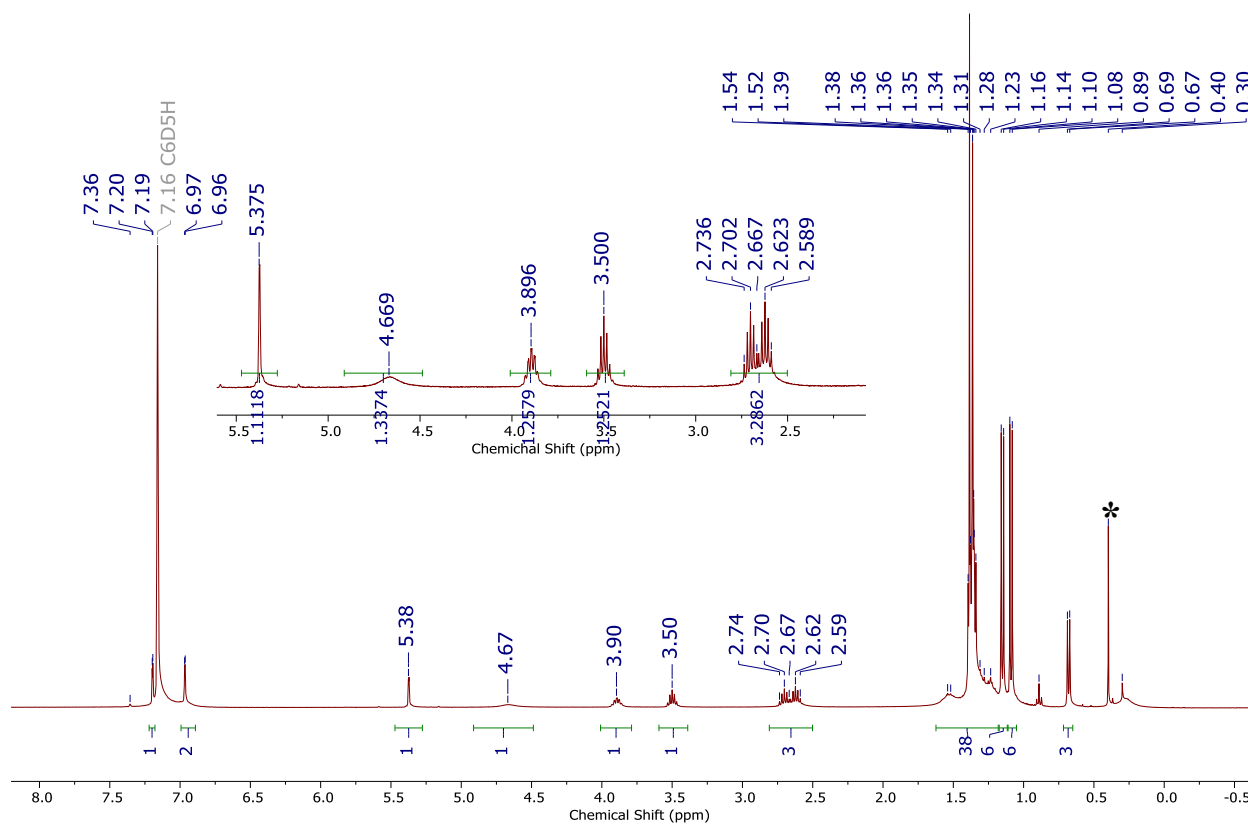
AA Figure 25 ^1H NMR spectrum (400 MHz, $\text{C}_6\text{D}_5\text{H}$) of $\text{X} = \text{I}$, **26** from **3E**. The signal denoted by * is trace water. Upfield signals in the spectrum are attributed to trace impurities from the synthesis of **26**.



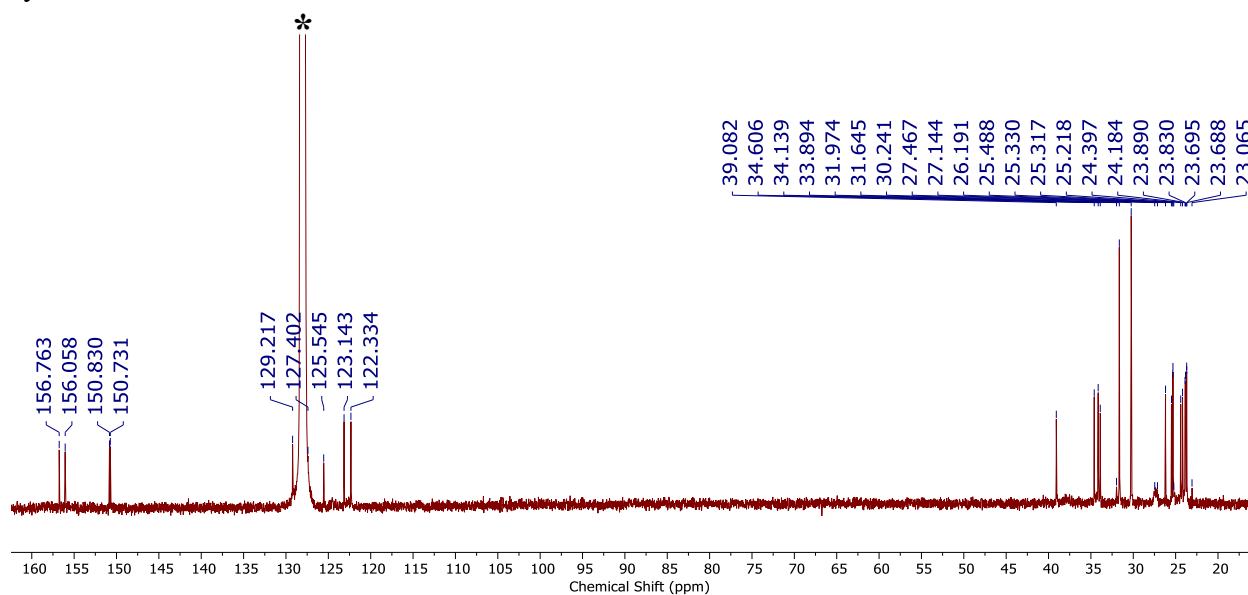
AA Figure 26 $^{13}\text{C}\{^1\text{H}\}$ NMR spectrum (100 MHz, C_6D_6) of $\text{X} = \text{I}$, **26** from **3E**. The signal denoted with * is the solvent C_6D_6 .



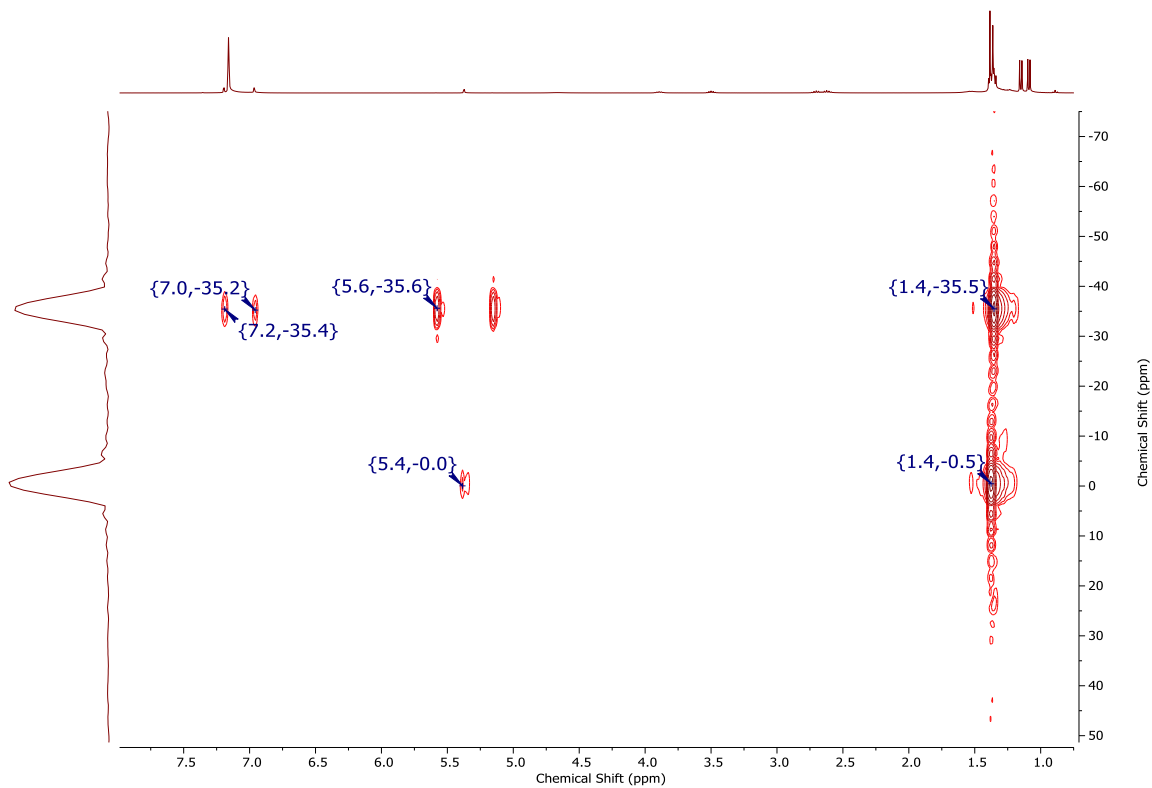
AA Figure 27 ^1H - ^{29}Si gHMBC spectrum (C_6D_6) of **X = I, 26** from **3E**. The signal denoted * is attributed to the SiI attentively.



AA Figure 28 ^1H NMR spectrum (400 MHz, $\text{C}_6\text{D}_5\text{H}$) of $\text{X} = \text{I}$, **27** from **3E**. The signal denoted by * is trace water. Upfield signals in the spectrum are attributed to trace impurities from the synthesis of **27**.

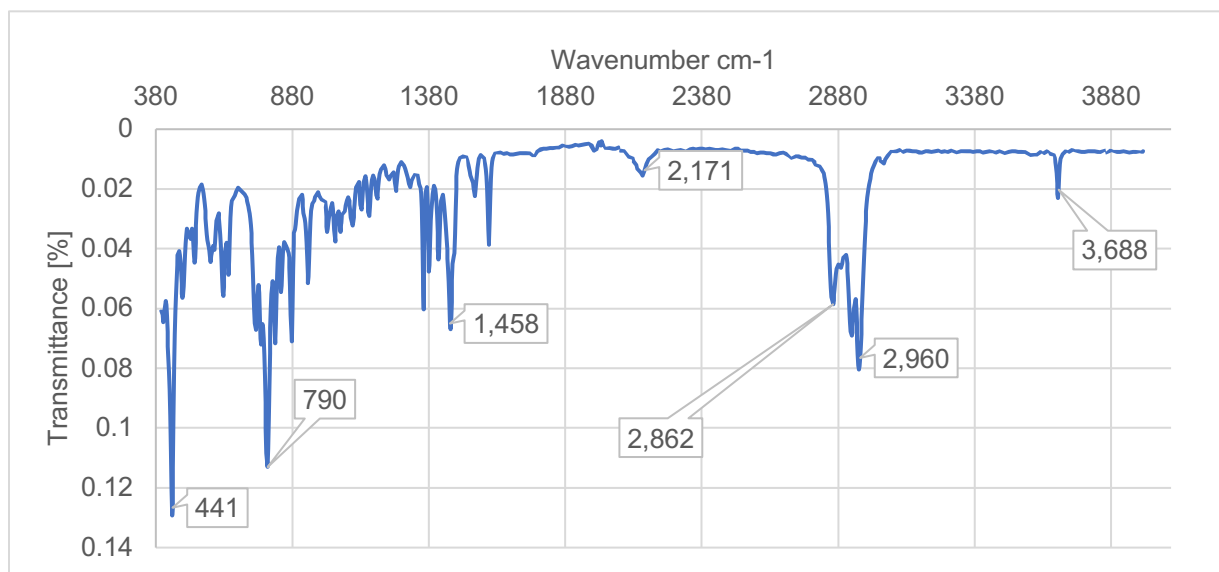


AA Figure 29 $^{13}\text{C}\{^1\text{H}\}$ NMR spectrum (100 MHz, C_6D_6) of $\text{X} = \text{I}$, **27** from **3E**. The signal denoted with * is the solvent C_6D_6 .

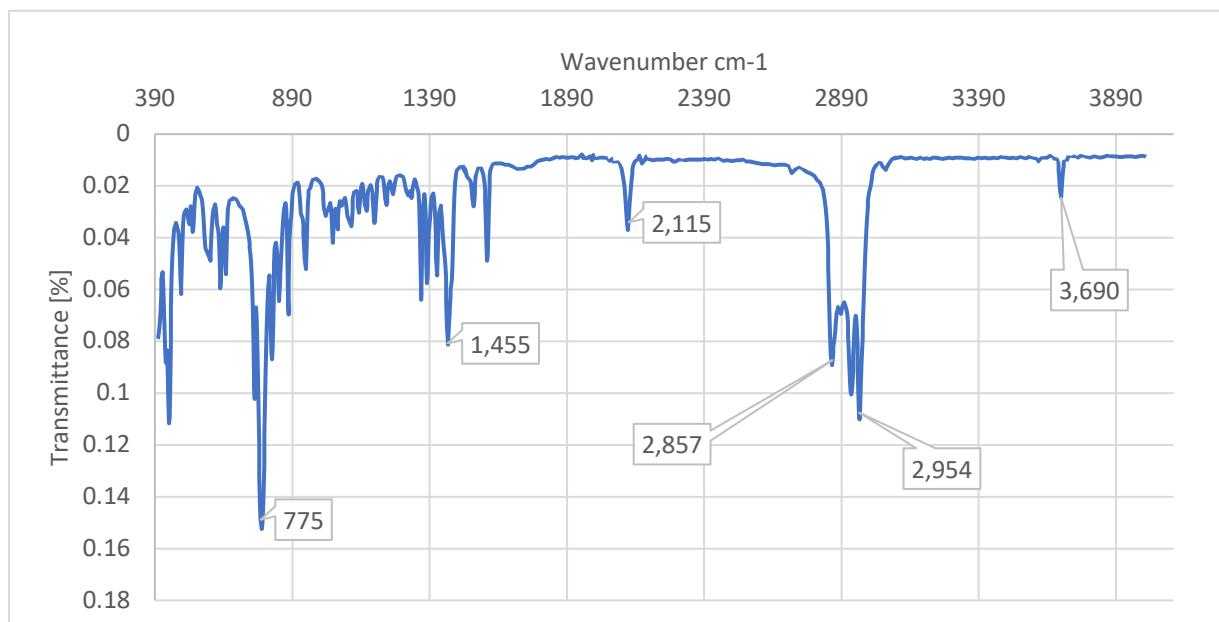


AA Figure 30 ^1H - ^{29}Si gHMBC spectrum (C_6D_6) of $\text{X} = \text{I}$, 27 from $3E$.

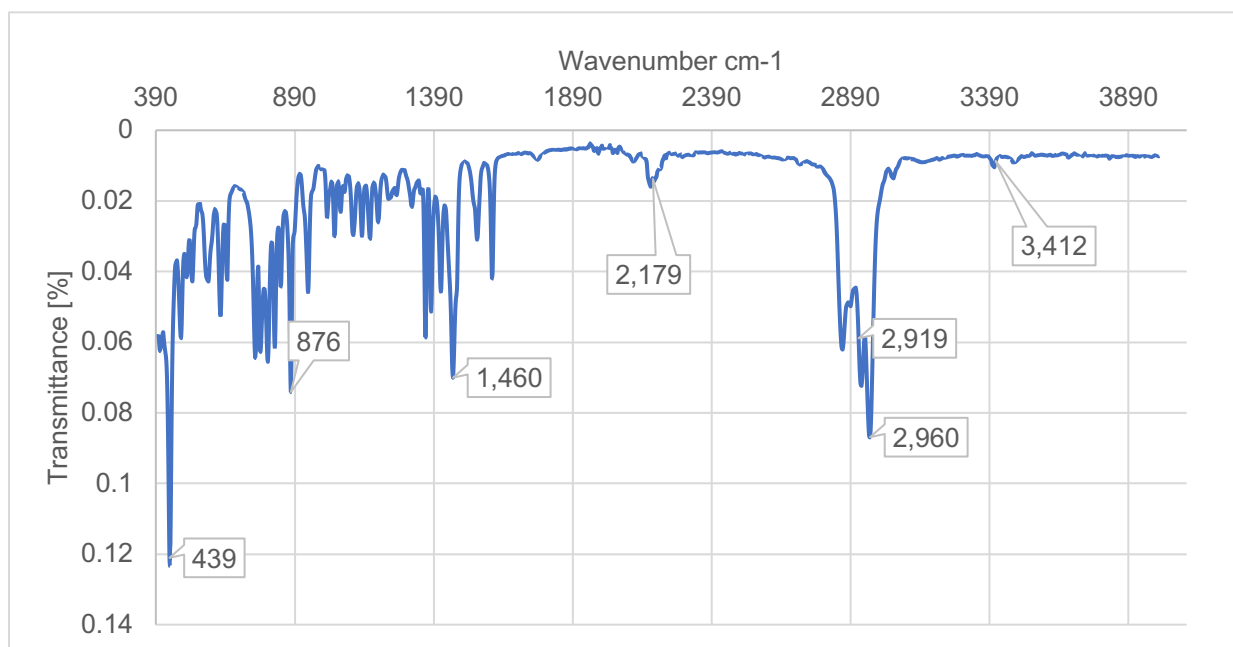
5.2 Appendix A: ATR-IR Data for Chapter 2



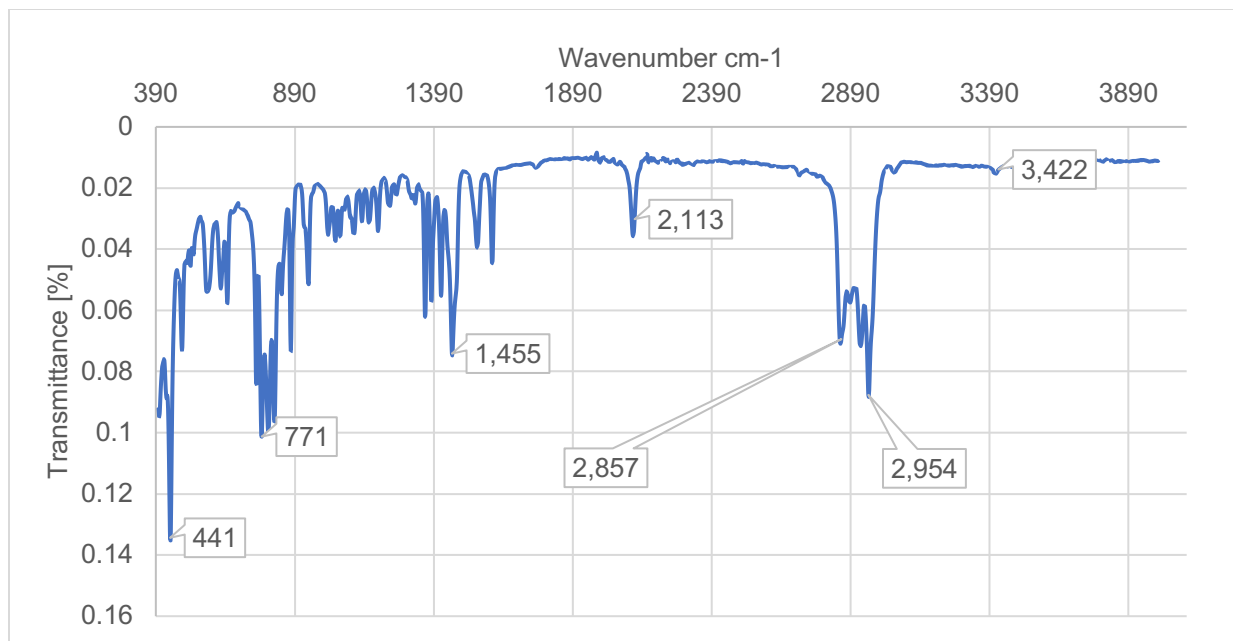
AA Figure 31 ATR-IR $\text{X} = \text{OH}$, 18 from $3Z$.



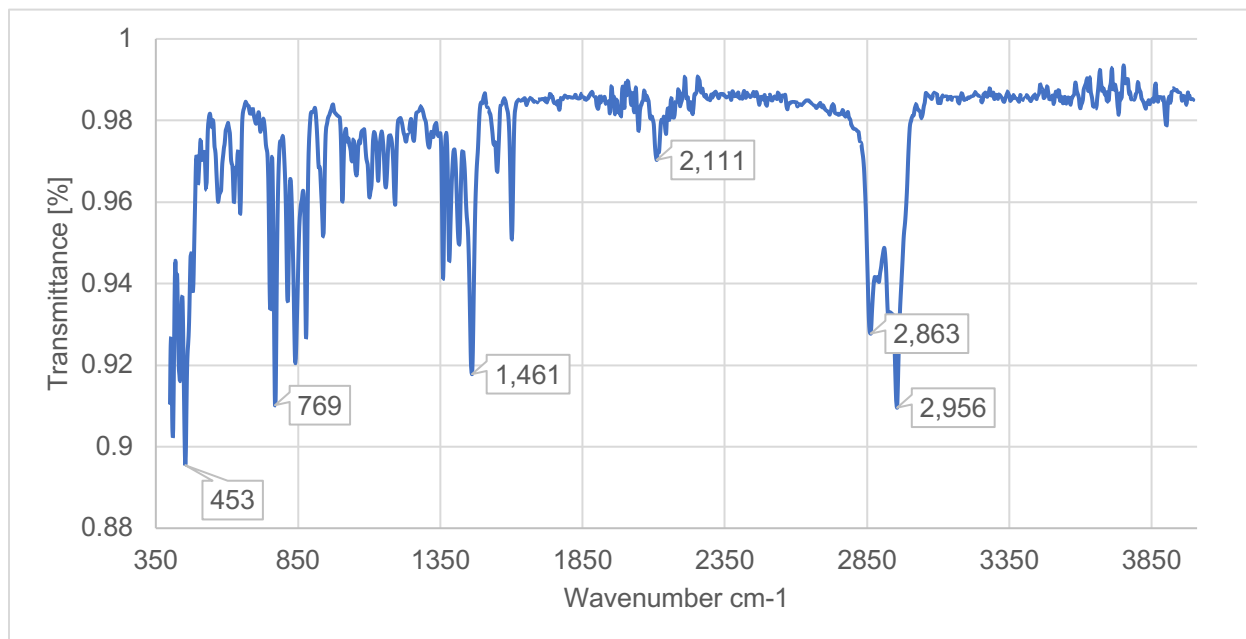
AA Figure 32 ATR-IR X = OH, **19** from **3E**.



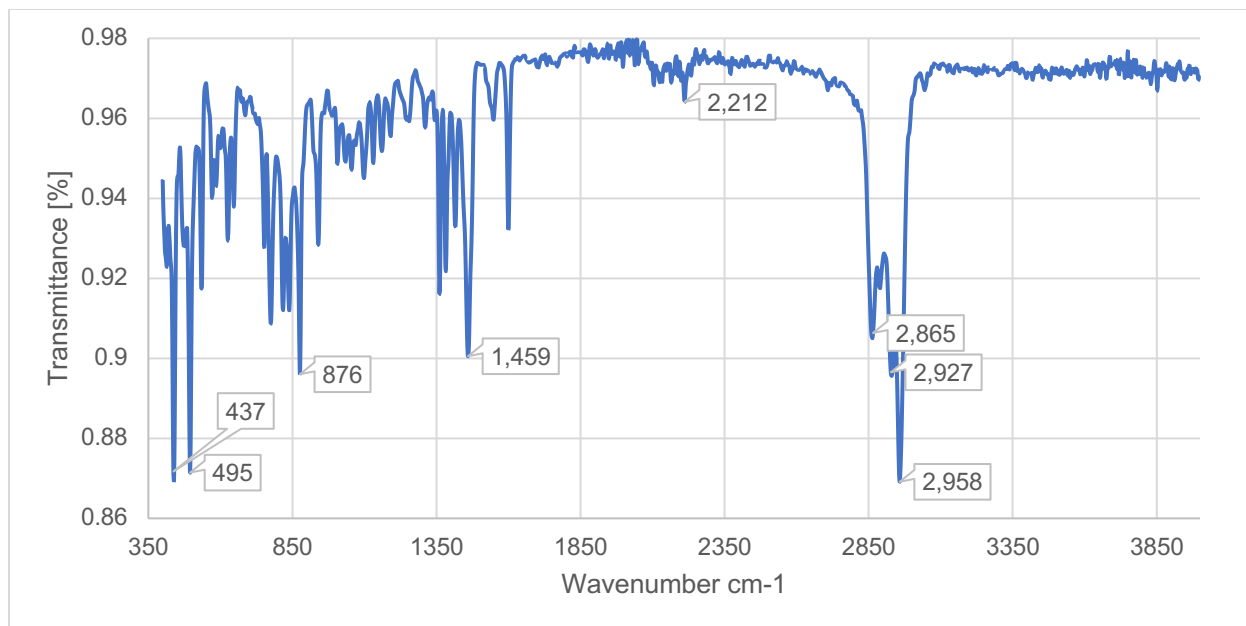
AA Figure 33 ATR-IR X = NH₂, **20** from **3Z**.



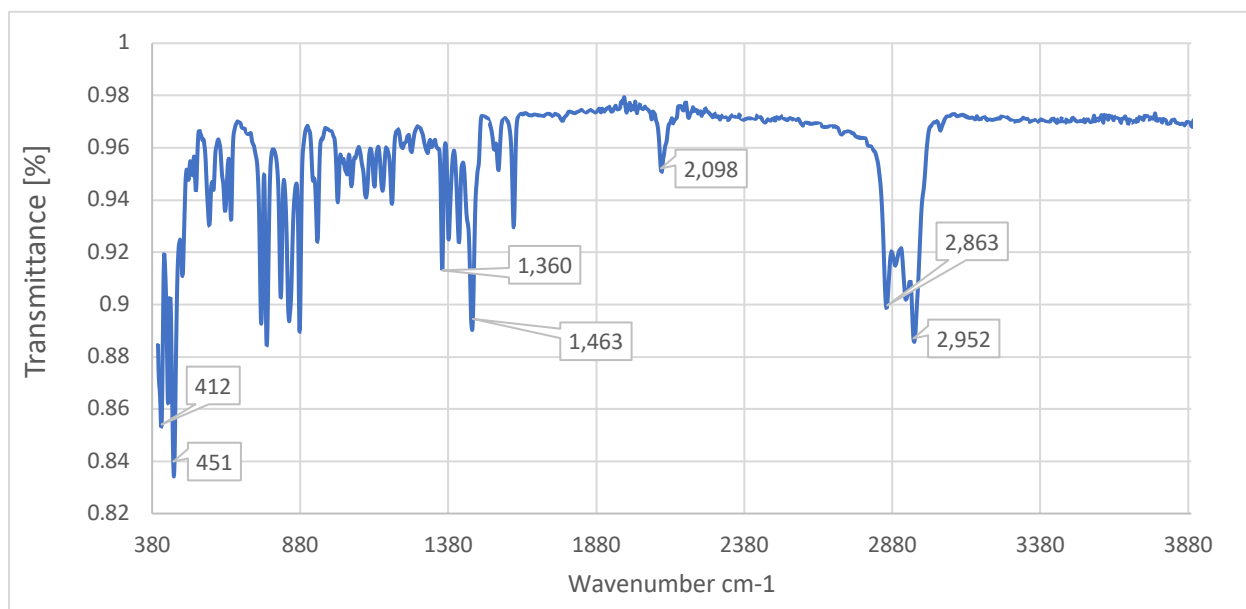
AA Figure 34 ATR-IR X = NH₂, 21 from 3E.



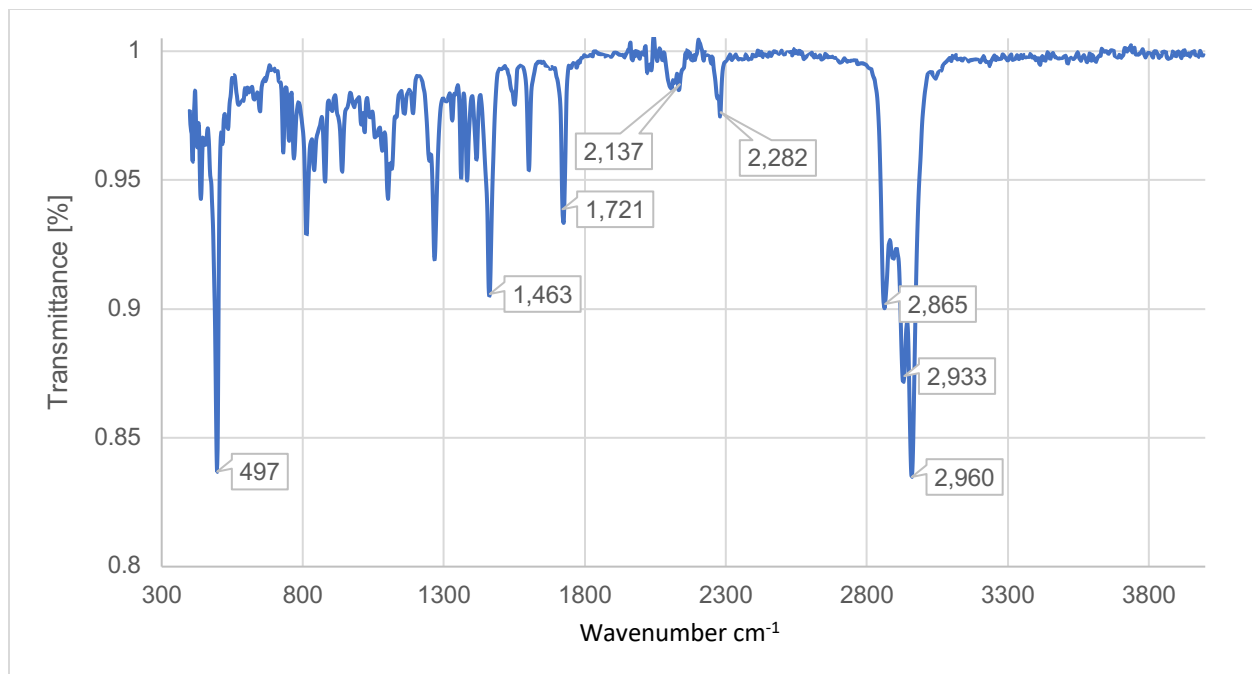
AA Figure 35 ATR-IR X = Cl, 22 from 3Z.



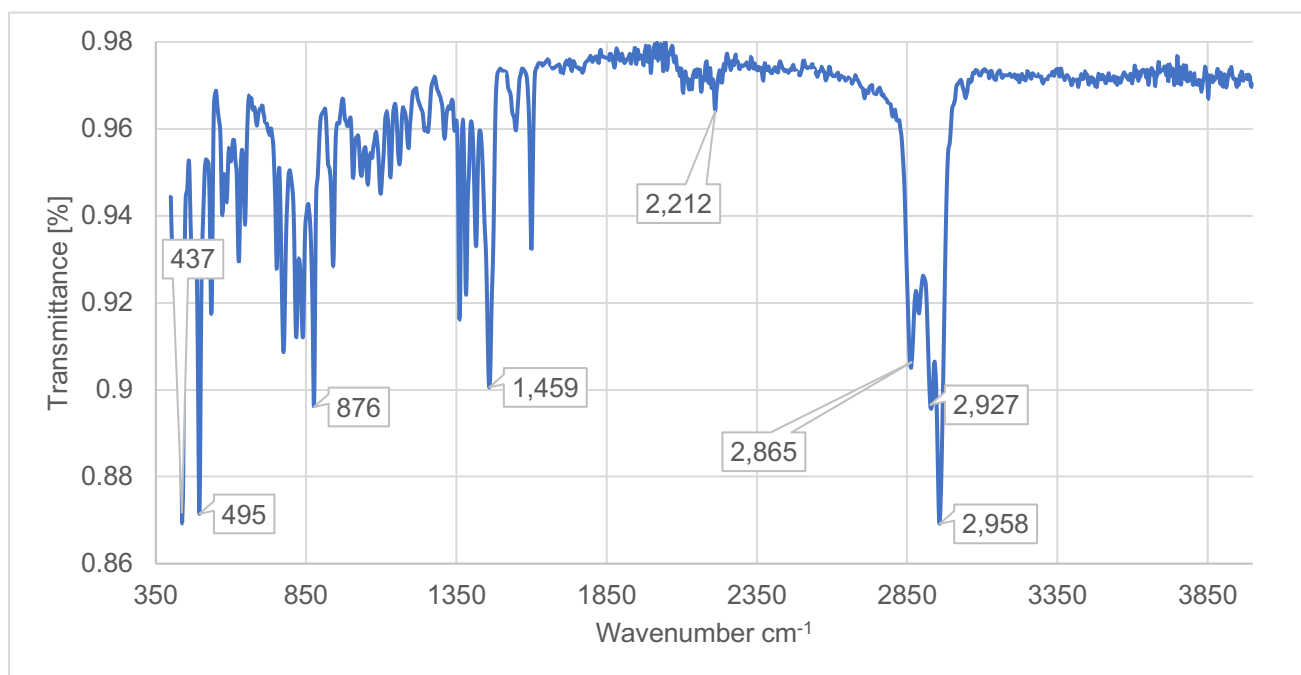
AA Figure 36 ATR-IR X = Cl, 23 from 3E.



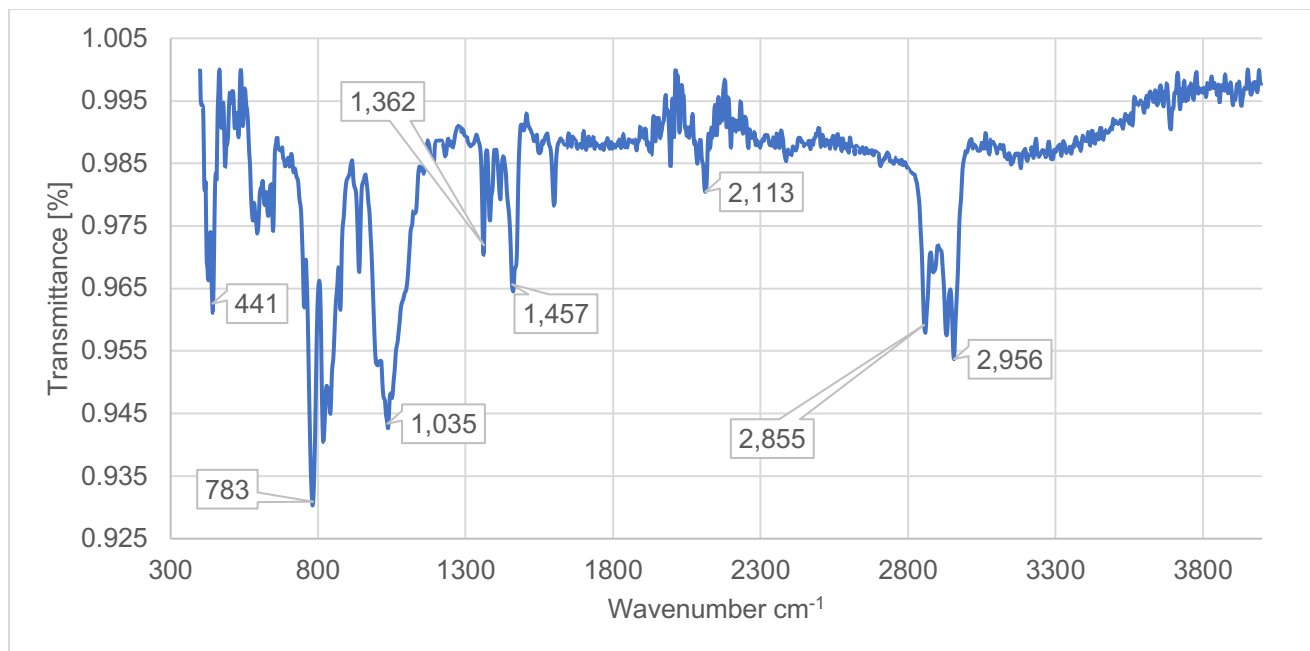
AA Figure 37 ATR-IR X = Br, 24 from 3Z.



AA Figure 38 ATR-IR X = Br, 25 from 3E.



AA Figure 39 ATR-IR X = I, 27 from 3E.



AA Figure 40 ATR-IR X = I, 26 from 3Z.

5.3 Appendix A: Single Crystal X-ray Diffraction Data for Chapter 2

AA Table 1 Summary of crystal data for 18.

Formula	$C_{38}H_{66}OSi_2$
Formula Weight (g/mol)	595.08
Crystal Dimensions (mm)	$0.365 \times 0.309 \times 0.197$
Crystal Color and Habit	colourless prism
Crystal System	triclinic
Space Group	P -1
Temperature, K	110
a , Å	8.796(4)
b , Å	9.885(5)
c , Å	12.404(6)
α , °	97.373(9)
β , °	103.595(11)
γ , °	112.146(16)

V, Å ³	942.4(8)
Number of reflections to determine final unit cell	9891
Min and Max 2θ for cell determination, °	4.58, 67.8
Z	1
F(000)	330
ρ (g/cm)	1.049
λ, Å, (MoKα)	0.71073
μ, (cm ⁻¹)	0.120
Diffractometer Type	Bruker Kappa Axis Apex2
Scan Type(s)	phi and omega scans
Max 2θ for data collection, °	72.726
Measured fraction of data	0.998
Number of reflections measured	67098
Unique reflections measured	9156
R _{merge}	0.0370
Number of reflections included in refinement	9156
Cut off Threshold Expression	I > 2sigma(I)
Structure refined using	full matrix least-squares using F ²
Weighting Scheme	w=1/[sigma ² (Fo ²)+(0.0693P) ² +0.1766P] where P=(Fo ² +2Fc ²)/3
Number of parameters in least-squares	323
R ₁	0.0461
wR ₂	0.1270
R ₁ (all data)	0.0653
wR ₂ (all data)	0.1397
GOF	1.047
Maximum shift/error	0.001
Min & Max peak heights on final ΔF Map (e ⁻ /Å)	-0.359, 0.400

Where:

$$R_1 = \sum (|F_o| - |F_c|) / \sum F_o$$

$$wR_2 = [\sum (w(F_o^2 - F_c^2)^2) / \sum (w F_o^4)]^{1/2}$$

$$GOF = [\sum (w(F_o^2 - F_c^2)^2) / (\text{No. of reflns.} - \text{No. of params.})]^{1/2}$$

AA Table 2 Summary of crystal data for **2I**.

Formula	$C_{38}H_{67}NSi_2$
Formula Weight (<i>g/mol</i>)	594.10
Crystal Dimensions (<i>mm</i>)	$0.354 \times 0.261 \times 0.133$
Crystal Color and Habit	colourless prism
Crystal System	monoclinic
Space Group	C 2/c
Temperature, K	110
<i>a</i> , Å	14.658(4)
<i>b</i> , Å	12.797(3)
<i>c</i> , Å	20.982(6)
α , °	90
β , °	107.879(10)
γ , °	90
<i>V</i> , Å ³	3745.7(17)
Number of reflections to determine final unit cell	9907
Min and Max 2 θ for cell determination, °	4.38, 72.66
<i>Z</i>	4
F(000)	1320
ρ (<i>g/cm</i>)	1.053
λ , Å, (MoK α)	0.71073
μ , (<i>cm</i> ⁻¹)	0.119
Diffractometer Type	Bruker Kappa Axis Apex2
Scan Type(s)	phi and omega scans
Max 2 θ for data collection, °	72.822
Measured fraction of data	0.999
Number of reflections measured	115194
Unique reflections measured	9118
<i>R</i> _{merge}	0.0995
Number of reflections included in refinement	9118
Cut off Threshold Expression	$I > 2\sigma(I)$

Structure refined using	full matrix least-squares using F^2
Weighting Scheme	$w=1/[\sigma^2(F_o^2)+(0.0638P)^2+4.2041P]$ where $P=(F_o^2+2F_c^2)/3$
Number of parameters in least-squares	233
R_1	0.0566
wR_2	0.1645
R_1 (all data)	0.0743
wR_2 (all data)	0.1721
GOF	1.103
Maximum shift/error	0.001
Min & Max peak heights on final ΔF Map ($e^-/\text{\AA}$)	-0.385, 0.497

Where:

$$R_1 = \sum (|F_o| - |F_c|) / \sum F_o$$

$$wR_2 = [\sum (w(F_o^2 - F_c^2)^2) / \sum (w F_o^4)]^{1/2}$$

$$GOF = [\sum (w(F_o^2 - F_c^2)^2) / (\text{No. of reflns.} - \text{No. of params.})]^{1/2}$$

AA Table 3 Summary of crystal data for **23**.

Formula	$C_{38}H_{65}ClSi_2$
Formula Weight (g/mol)	613.53
Crystal Dimensions (mm)	$0.370 \times 0.318 \times 0.226$
Crystal Color and Habit	colourless prism
Crystal System	monoclinic
Space Group	$P 2_1/n$
Temperature, K	110
a , \AA	13.389(5)
b , \AA	16.659(7)
c , \AA	16.955(7)
α , $^\circ$	90
β , $^\circ$	101.200(11)
γ , $^\circ$	90
V , \AA^3	3710(3)
Number of reflections to determine final unit cell	9832

Min and Max 2θ for cell determination, °	4.96, 63.68
Z	4
F(000)	1352
ρ (g/cm)	1.099
λ, Å, (MoKα)	0.71073
μ, (cm ⁻¹)	0.191
Diffractometer Type	Bruker Kappa Axis Apex2
Scan Type(s)	phi and omega scans
Max 2θ for data collection, °	70.038
Measured fraction of data	0.999
Number of reflections measured	277282
Unique reflections measured	16343
R _{merge}	0.0630
Number of reflections included in refinement	16343
Cut off Threshold Expression	I > 2sigma(I)
Structure refined using	full matrix least-squares using F ²
Weighting Scheme	w=1/[sigma ² (Fo ²)+(0.0603P) ² +1.1508P] where P=(Fo ² +2Fc ²)/3
Number of parameters in least-squares	544
R ₁	0.0404
wR ₂	0.1094
R ₁ (all data)	0.0567
wR ₂ (all data)	0.1208
GOF	1.030
Maximum shift/error	0.002
Min & Max peak heights on final ΔF Map (e ⁻ /Å)	-0.572, 0.629

Where:

$$R_1 = \sum | |F_o| - |F_c| | / \sum F_o$$

$$wR_2 = [\sum (w(F_o^2 - F_c^2)^2) / \sum (w F_o^4)]^{1/2}$$

$$GOF = [\sum (w(F_o^2 - F_c^2)^2) / (\text{No. of reflns.} - \text{No. of params.})]^{1/2}$$

AA Table 4 Summary of crystal data for **25**.

Formula	C ₃₈ H ₆₅ BrSi ₂
Formula Weight (g/mol)	657.99
Crystal Dimensions (mm)	0.371 × 0.204 × 0.074
Crystal Color and Habit	colourless plate
Crystal System	monoclinic
Space Group	P 2 ₁ /c
Temperature, K	110
<i>a</i> , Å	43.354(11)
<i>b</i> , Å	9.7127(19)
<i>c</i> , Å	18.647(4)
α, °	90
β, °	101.658(8)
γ, °	90
<i>V</i> , Å ³	7690(3)
Number of reflections to determine final unit cell	9056
Min and Max 2θ for cell determination, °	4.76, 49.58
<i>Z</i>	8
F(000)	2848
ρ (g/cm)	1.137
λ, Å, (MoKα)	0.71073
μ, (cm ⁻¹)	1.154
Diffractometer Type	Bruker Kappa Axis Apex2
Scan Type(s)	phi and omega scans
Max 2θ for data collection, °	51.392
Measured fraction of data	0.998
Number of reflections measured	163154
Unique reflections measured	14597
R _{merge}	0.0972
Number of reflections included in refinement	14597
Cut off Threshold Expression	I > 2sigma(I)
Structure refined using	full matrix least-squares using F ²
Weighting Scheme	w=1/[sigma ² (Fo ²)+(0.0482P) ² +88.7

	225P] where $P=(F_o^2+2F_c^2)/3$
Number of parameters in least-squares	777
R_1	0.0869
wR_2	0.2028
R_1 (all data)	0.0973
wR_2 (all data)	0.2084
GOF	1.109
Maximum shift/error	0.001
Min & Max peak heights on final ΔF Map ($e/\text{\AA}$)	-1.383, 2.828

Where:

$$R_1 = \sum | |F_o| - |F_c| | / \sum F_o$$

$$wR_2 = [\sum (w(F_o^2 - F_c^2)^2) / \sum (w F_o^4)]^{1/2}$$

$$GOF = [\sum (w(F_o^2 - F_c^2)^2) / (\text{No. of reflns.} - \text{No. of params.})]^{1/2}$$

AA Table 5 Summary of crystal data for 27.

Formula	$C_{38}H_{65}ISi_2$
Formula Weight (g/mol)	704.98
Crystal Dimensions (mm)	$0.203 \times 0.114 \times 0.067$
Crystal Color and Habit	colourless prism
Crystal System	triclinic
Space Group	P -1
Temperature, K	110
a , \AA	9.034(3)
b , \AA	11.457(4)
c , \AA	18.695(6)
α , $^\circ$	93.904(12)
β , $^\circ$	99.636(6)
γ , $^\circ$	96.122(10)
V , \AA^3	1889.6(11)

Number of reflections to determine final unit cell	9281
Min and Max 2θ for cell determination, °	4.6, 62.72
Z	2
F(000)	748
ρ (g/cm)	1.239
λ, Å, (MoKα)	0.71073
μ, (cm ⁻¹)	0.934
Diffractometer Type	Bruker Kappa Axis Apex2
Scan Type(s)	phi and omega scans
Max 2θ for data collection, °	64.178
Measured fraction of data	0.999
Number of reflections measured	13171
Unique reflections measured	13171
R _{merge}	0.0792
Number of reflections included in refinement	13171
Cut off Threshold Expression	I > 2sigma(I)
Structure refined using	full matrix least-squares using F ²
Weighting Scheme	w=1/[sigma ² (Fo ²)+(0.0315P) ² +0.76 32P] where P=(Fo ² +2Fc ²)/3
Number of parameters in least-squares	388
R ₁	0.0306
wR ₂	0.0685
R ₁ (all data)	0.0376
wR ₂ (all data)	0.0707
GOF	1.062
Maximum shift/error	0.001
Min & Max peak heights on final ΔF Map (e ⁻ /Å)	-0.734, 0.562

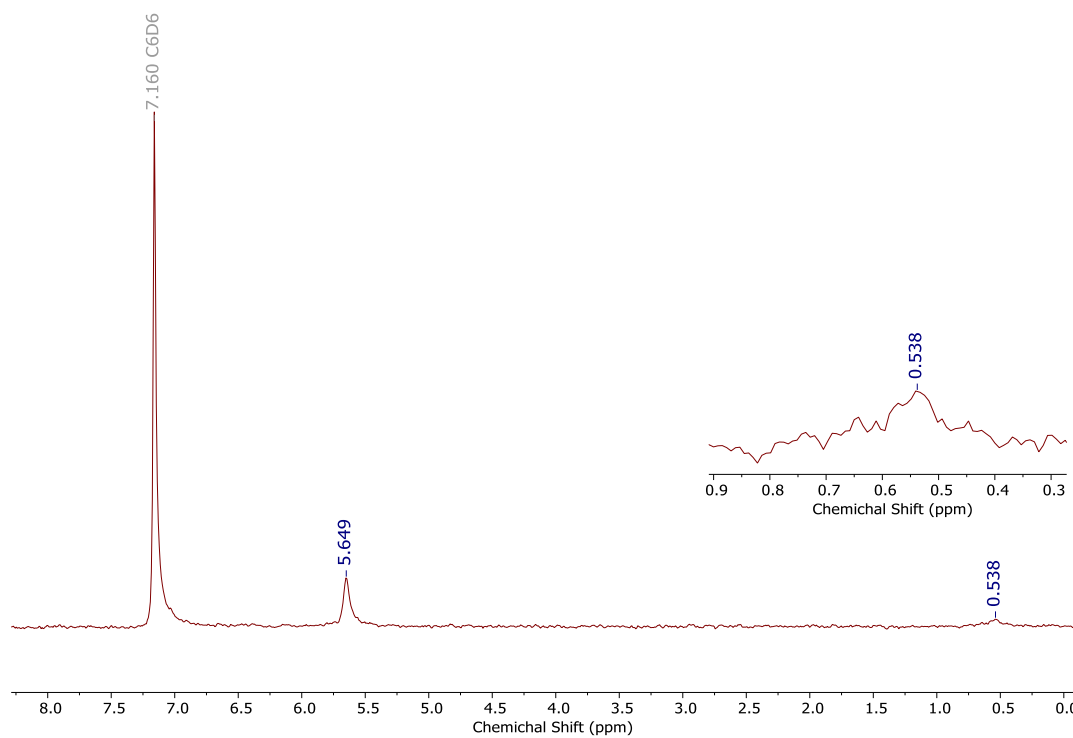
Where:

$$R_1 = \frac{\sum | |F_o| - |F_c| |}{\sum F_o}$$

$$wR_2 = \left[\frac{\sum (w(F_o^2 - F_c^2))^2}{\sum (w F_o^4)} \right]^{1/2}$$

$$GOF = \left[\frac{\sum (w(F_o^2 - F_c^2))^2}{(\text{No. of reflns.} - \text{No. of params.})} \right]^{1/2}$$

5.4 Appendix B: Supplementary Material for Chapter 3



AB Figure 1 ^2H $\{^1\text{H}\}$ NMR spectrum (92 MHz, C_6D_6) of **29**.

Curriculum Vitae

Post-secondary Education and Degrees

The University of Western Ontario
London, Ontario, Canada
2016-2020 B.Sc, Honour Specialization in Chemistry
Thesis Project: Solubilizing Polyferrocenyl - Silver Dithiolates with NHCs
Dr. John F. Corrigan

The University of Western Ontario
London, Ontario, Canada
2020-Present M.Sc in Chemistry expected fall 2022
Thesis Project: The Stereochemistry of the Addition of Ammonia to
Disilenes
Dr. Kim Baines

Related Work Experience

Teaching Assistant
The University of Western Ontario
2020 fall - 2022 winter

Research Assistant
The University of Western Ontario
2020 fall - present

Lab Manager
The University of Western Ontario
2022 fall

Presentations

“Solubilizing Polyferrocenyl - Silver Dithiolates with NHCs” 48th SOUSCC,
June 15th, 2020
19th - ISOS (International Symposium On Silicon chemistry), Poster - July
2021

50th Physical Organic Minisymposium (POMS), Poster - November 2021

51st IUPAC General Assembly and 48th World Chemistry Congress, 104th
CCCE (Canadian Chemistry Conference and Exhibition), Poster - August
2021

Dalton Trans RSC IISER desktop seminar, Poster - May 2022

CSC, CCCE: Canadian Chemistry Conference and Exhibition, Diversity and
Innovation in Chemistry, Poster - June 2022

53rd IDW: Inorganic Discussion Weekend, Oral presentation - November
2022

Courses TA	CHEM 2213A - Organic Chemistry for Life Sciences, Laboratory - 2020 fall virtual, 2021 fall in-person
	CHEM 2213A - Organic Chemistry for Life Sciences, OWL - 2022 winter
	CHEM 2223B - Organic Chemistry of Biological Molecules Laboratory - 2020 winter virtual
	CHEM 3370B - Organic and Inorganic Structure Elucidation OWL - 2022 winter in-person
Course Report	CHEM 9513S - INTRO. PHYSICAL ORGANIC CHEM - 82%
	CHEM9555T - ORGANIC PHOTOCHEMISTRY - 85%
	CHEM 9603R - ADV. NMR. SPEC. II - 81%
	CHEM9507Q - ADVANCED CHEM COMMUNICATIONS - 88%
Awards	19 th - ISOS (International Symposium On Silicon chemistry), Poster Award - July 2021
	Dalton Trans RSC IISER desktop seminar, Poster Award - May 2022
	53 rd IDW: Inorganic Discussion Weekend, Oral presentation, The Dalton Transaction Award - November 2022